# DESIGN OF A THREE PHASE FOUR QUADRANT VARIABLE SPEED DRIVE FOR PERMANENT MAGNET BRUSHLESS DC MOTORS

JONAS DON-YELEE DAKORA
Student Number: 21242393

A thesis submitted in fulfilment of the requirements for the
Master of Engineering Degree
in the
Faculty of Engineering and the Built Environment
Department of Electronic Engineering
Durban University of Technology

I undertake that all the material presented in this thesis is my own work and has not been written for me, in whole or in part by any other person. I undertake that any quotation or paraphrase from the published or unpublished work of another person has been duly acknowledged in the work which I now present for examination.

_____

Student: Jonas Don-yelee Dakora

Approved for Final Submission

_____ _____

Supervisor: Dr. Poobalan Govender Co-Supervisor: Mr. Nelendran Pillay

Durban, 25 February 2016

# ACKNOWLEDGEMENTS

I would like to thank my supervisor, Dr Poobalan Govender and my co-supervisor, Nelendran Pillay for their academic, encouragement and enthusiasm to complete this project. Thanks to them for all their motivation, suggestions and corrections.

Thank you to the Department of Electronic Engineering at Durban University of Technology for the financial support and an office with all hour's access. The financial assistance of the Centre for Research Management and Development at the Durban University of Technology is hereby acknowledged.

I also wish to express my sincere appreciation to the Optimization and Energy Studies Group at the Durban University of Technology for the use of the post graduate control system laboratory.

# DEDICATION

This thesis is dedicated to my son, Benedict Dakora and my brother, Samuel Dakora. May you live to fulfill the destiny of the Tampaa Dakora family. God richly bless you.

# ABSTRACT

The aim of this research project is to design a three phase four quadrant variable speed drive (VSD) for a permanent magnet brushless direct current motor (PMBLDC) that can be applied to an electric bicycle (e-bike). The design is confined to PMBLDC motors with a maximum power rating of 1.5kW. The speed controller operates in current mode at a maximum voltage and current rating of 50V and 30A, respectively. The VSD has the ability to smoothly control the current delivered to the DC motor and therefore controls its torque. The motor's current is limited in all four quadrants of operation, and its speed is limited in the forward and reverse directions. The performance of the proposed DC motor VSD system is tested on an electric-bicycle.

The PMBLDC motor has three hall sensors embedded into the stator to determine rotor position. A phase switcher module interprets the position signals and produces a switching pattern. This effectively transforms the BLDC motor into a direct current (DC) brushed motor. The unipolar switching scheme used ensures that current flows out of the battery only for motoring operation and into the battery during regenerative braking. The current and torque are directly proportional in a BLDC motor. Torque control is achieved in the BLDC motor using a single channel current controller. The phase switcher current is monitored and used to control the duty cycle of the synchronous converter switches.

The proposed e-bike speed control system provides efficient control in all four quadrants of operation and it is a suitable alternative for a low cost transportation mode.

# TABLE OF CONTENTS

# LIST OF FIGURES

# LIST OF TABLES

# NOMENCLATURE

| Abbreviation | Meaning |
|---|---|
| AC | Alternating current |
| ADC | Analog to digital converter |
| BL | Brushless |
| BLDC | Brushless direct current |
| CCM | Continuous current mode |
| cf | Refer to |
| CMOS | Complementary metal oxide semiconductor |
| CPLD | Complex programmable logic devices |
| DCB | Direct copper bonding |
| DC | Direct current |
| DCM | Discontinuous current mode |
| DSP | Digital signal processors |
| E-bike | Electric bicycle |
| EMF | Electro-motive force |
| EMI | Electromagnetic Interference |
| EV | Electric vehicle |
| FPGAs | Field-programmable gate arrays |
| JFET | Junction gate field effect transistor |
| HEV | Hybrid electric vehicles |
| $I_{arm}$ | Armature current |
| IC | Integrated circuit |
| LT | Linear Technology |
| MOSFET | Metal oxide semiconductor field effect transistor |
| Pa, Pb, Pc | Motor phases |
| $\mu$Ps | Micro-processors |
| PCB | Printed circuit board |
| PI | Proportional integral |
| PM | Permanent magnet |
| PMBL | Permanent magnet brushless |
| PMBLDC | Permanent magnet brushless direct current |
| PMDC | Permanent magnet direct current |
| PWM | Pulse width modulation |
| SMPS | Switched mode power supply |
| SMD | Surface mounted device |
| SPICE | Simulation Program with Integrated Circuit Emphasis |
| $V_{arm}$ | Armature voltage |
| VSD | Variable speed drive |

# CIRCUIT NOMENCLATURE

| Abbreviation | Meaning |
|---|---|
| AH | High output side for phase A |
| AL | Low output side for phase A |
| GND | Ground |
| HINA | High input for phase A |
| LINA | Low input for phase A |
| HS1 | Hall sensor 1 |
| HS2 | Hall sensor 2 |
| HS3 | Hall sensor 3 |
| $I_{bldc}$ | BLDC motor current |
| $V_{bus}$ | Battery voltage |

# CHAPTER1

# INTRODUCTION

## 1.1 BACKGROUND TO RESEARCH

With a fast developing world, we have reached a point where efficient and sustainable solutions need to be found to address the issues of transport, pollution, traffic congestion, cost of fuel, cars' high maintenance and insurance cost. Electric drives offer huge potential for energy conservation in transportation. While efforts to introduce commercially-viable Electric Vehicles (EV) continue with progress in battery and fuel cell technologies, hybrid electric vehicles (HEV) are sure to make a huge impact (Teahyung *et* al., 2006). HEV's offer fewer generated emissions and better energy efficiency than internal combustion engine vehicles, making them desirable to implement (Thompson, 2008). Considering the high fuel prices and carbon dioxide emissions, electric bicycles (E-bike), electric vehicles (EV) and motor cycles are some of the potential technologies for three phase four quadrant variable speed drives to improve the lives of people. Electric bicycles in China and India have already demonstrated the ability to offer an inexpensive way to travel the short distances covered in urban areas.

VSD technology spans virtually the entire industrial revolution, from the development of the steam engine to modern microprocessor based electronic motor controllers (George and William, 2000). Refinements of this technology have being fuelled in recent years by improved reliability

and performance of electronic devices and are occurring at a more rapid pace than ever, resulting in greater performance at low cost (Komatsu *et* al., 2010). EVs used as urban commuting vehicles are one way of providing the same level of transportation while eliminating the urban hazardous gas emissions, thus maintaining the standard of life without compromising the environment.

Given the above-mentioned shortcomings, this research offers a further refinement to current VSD technology by proposing the design, construction and testing of a four quadrant DC VSD in current-mode for a PMDC-BL motor drive for a 3 phase brushless DC motor. The proposed VSD must be suitable for a variety of Permanent Magnet Direct Current (PMDC) Brushless (BL) motors suitable for use in E-bikes, EVs, Wheel Chairs and Motor Bikes. The refinement proposed in this research focuses on improved current control in the forward and reverse directions.

Brushless DC motors were chosen for this project because of their improved torque characteristics, higher power and reduced electromagnetic interference characteristics (Janpana *et* al., 2012). By including the four quadrant control methodology, the design makes it possible for the motor to be controlled in the forward and reverse directions. Four quadrant control also makes it possible for the drive to operate the motor in four different modes by changing the polarity of the voltage and the direction of the current. The drive will also consist of a regenerative system to charge batteries during braking.

Brushless dc servo motors have been replacing brushed motors in machine tool and robotics applications (Collins, 2005). When compared to brushed motors, brushless motors are simple and efficient and provide improved reliability, higher power to weight ratios, and are easier to

cool (Bhim and Sanjeev, 2009). Early DC brush motor control systems used analog control circuits and thyristor power switches (Figueroa *et* al., 2003). Present day brushless motor drives utilize high power transistor switches, combined with digital signal processors and processor based digital controllers (Jawad *et* al., 1994).

## 1.2 RESEARCH PROBLEM

There have been many methods of motor control invented over the past years (Salam, 2003). They range from simple rheostat type controllers, which are variable resistor, to voltage-step contactor controls and to the modern electronic versions available today (Thompson, 2008). Most methods of motor control in the application of scooters and bicycles use the two quadrant voltage control method which is inefficient or do not provide smooth operation (Hwang and Chang, 2000). The voltage control method only controls the speed since the voltage is directly proportional to the speed (Taehyung *et* al., 2006). Therefore the motor's torque cannot be controlled at high speed which can lead to fatal accident. In the current state of the technology only two-quadrant voltage mode control is on offer for E-bike applications (Britten *et* al., 2007). The shortcoming of two quadrant control is twofold (Britten *et* al., 2007), namely:

1. Poor torque control leading to an overall poor control performance and
2. Inefficient regenerative braking for energy production.

## 1.3 RESEARCH AIM AND OBJECTIVE

The aim of this project is to design an efficient and economical DC motor speed control system. To achieve this aim, our objective will be the design of an energy efficient drive system that will

use full *four quadrant operation* to operate a three phase permanent magnet brushless DC motor to power an electric bicycle. This research will focus mainly on the design of a three phase four variable speed drives for PMBLDC motors to operate at a maximum voltage and current rating of 50V and 30A in current mode, with the ability to smoothly control the current delivered to the motor. By controlling the current we will be able to achieve the objective of torque control within the systems operating parameters. Torque control is made possible by motor current limiting in all four operating quadrants, and motor speed limiting in forward and reverse will be implemented.

## 1.4 SCOPE OF RESEARCH

The four quadrant current mode motor control system proposed in this work will consist of a power electronic circuit with associated control logic.

The motor VSD system will use digital logic integrated circuits to decode position sensor information. A current sensor will be used to sense the motor current and then amplified using analog comparators and operational amplifiers that will enable control of the BLDC motor line currents. Torque output will be controlled by comparing an input demand signal to the magnitude of the motor current. The torque and current can be positive or negative, which makes motoring and generating possible. The proposed drive also utilizes regenerative braking to store kinetic energy in the form of electrical energy in a battery.

## 1.5 CONTRIBUTION OF THE STUDY

Modern VSD technology requires high efficiency to control power to the motor smoothly and safely (De Vries and Jenman, 2006). The four quadrant current-mode tolerance band control scheme proposed in this project utilises high efficient comparators and high speed power MOSFETs. Full motor torque is available from standstill to high speed, and output torque is relative to the controller command. Therefore, the controller has the ability to fully control the motor's torque at high speed. The VSD is designed to operate at high temperatures and to withstand high levels of electrical noise and mechanical vibrations.

## 1.6 STRUCTURE OF THE THESIS

This document is arranged as follows:

Chapter 1: Introduction;

Chapter 2: Literature Review;

Chapter 3: Current Drive Control Methods;

Chapter 4: Hardware Design;

Chapter 5: Simulation Studies;

Chapter 6: Testing and Performance Evaluation;

Chapter 7: Conclusions and Recommendations.

This page is intentionally blank

# CHAPTER 2

# LITERATURE REVIEW

## 2.1 INTRODUCTION

Modern VSDs have been designed to increase performance and system efficiency (Panel, 2005). There are different techniques of controlling a PMBLDC, depending on its application (Herman and Rajesh, 2006). Motor controller designs are based on power MOSFETs and digital logic components such as $\mu$Ps, DSP, FPGAs and CPLD. Some of these devices consume a lot of power which limits battery usage (Dixon, 2013). Applications where DC motors were dominant are now designed using brushless DC motors due to their simple speed control techniques. PMBLDC motors are electronically commuted, therefore there are no brushes on the rotor and commutation is performed electronically at certain rotor positions.

## 2.2 CONTROLLERS WITH DIFFERENT TECHNIQUES

The control of a BLDC motor consists of a three-phase full bridge power converter and a logic control system. The power converter controls the power flow from the three phase of the motor by using six power MOSFET switches. The power for the control system is provided by batteries with a rating to match the maximum voltage rating of the motor. The PMBLDC motor is

controlled by using hall sensors to determine the rotor position. The VSD controller senses the rotor position and applies the correct voltage pattern to the motor. However, some controllers use the sensorless control scheme to avoid the Hall Effect sensors since they are very sensitive. Advanced technology in digital signal processors and electronics has added more features to VSD systems to make them more efficient and reliable in industrial applications (Bhim and Sanjeev, 2009). Control signals are usually derived from sensors, whose outputs dependent on the control strategy and the application required. The motor only needs rotor-position sensing at the commutation points. The commutation sequence is generated by the controller according to the rotor position which is sensed using Hall sensors or optical encoders (Bhim and Sanjeev, 2009). However, the sensors make it complex to control the PMBLDC motor (Thiyagarajan and Sekar, 2012). Some of the motor control techniques are discussed in the following sections based on the literature.

### *2.2.1 3-Phase BLDC motor control with quadrature encoder using 56F800/E*

Freescale semiconductor (2005) described the software design of a 3-phase BLDC motor drive based on digital signal processor 56F800/E controllers. The application described a speed closed-loop control drive using a Quadrature Encoder. The 56F800/E is a DSP chip which contains PWM module, ADC and Timers which is ideal for motor control. The PWM module has three complementary PWM signal pairs or six independent PWM signals to control the outputs of the power MOSFET drivers. This permits a high efficiency control of the BLDC motor.

The motor control utilizes the complementary PWM mode to generate control signals for all the switches of the power stage with inserted dead time to avoid short circuit (Padmaraja, 2003). The

outputs of the PWM can also be controlled separately by software to enable or disable the control signal.

Efficient operation of a BLDC motor requires the angle between rotor flux and stator to remain close to 90°. The rotor position is detected by Hall sensors and the sensors directly detect the commutation moment. However, this application uses the quadrature encoder to sense the rotor position which makes it very difficult for a six-step control technique to keep a 90° between the rotor flux and the stator flux (Freescale Semiconductor, 2005).

### *2.2.2 Electric bike BLDC hub motor control using the Z8FMC1600 MCU*

Zilog (2008) proposed a VSD drive for a 200 W, 24 V Brushless DC motor used to power an electric bike. The design uses Z8FMC16100 Microcontroller to implement motoring control, regenerative braking, and fault protection. The main features of the controller consist of protection logic for over-voltage, over-current and thermal protection, potentiometer-adjustable motor speed and motor speed measurement. It also has a PWM module with three complementary pairs or six independent PWM outputs and fault protection trip input. This application uses the hall sensor technique to control the motor. The Hall sensor commutation technique is ideal for BLDC motor application which requires high torque at low speed (Zilog, 2008). PMBLDC motor used in an electric bicycle application requires high initial torque which is a perfect application for Hall sensor commutation (Pavel, 2005).

### *2.2.3 Current control of brushless DC motor based on a common DC signal for space operated vehicles*

A simple current controlled modulation technique for brushless dc motors was proposed by Karthikeyan and Sekaran (2011). In most VSD applications, a wide range of speed and torque control of the electric motor is required due to its low inertia, fast response and high reliability (Karthikeyan and Sekaran, 2011).

This application utilizes a current controlled technique based on the generation of quasi-square wave currents using only one controller for the three phases. This current control strategy uses a triangular carrier for the power MOSFETs with the advantage of controlling all the phases and keeping the phase currents at the same magnitude. The best way to control PMBLDC motor is through voltage–source current-controlled inverters (Dixon and Leal, 2002). The inverter must supply a quasi square current waveform whose magnitude is proportional to the machine shaft torque. Therefore, the torque and speed can be varied by controlling the phase-currents.

### *2.2.4 Design of permanent magnet brushless DC motor control system based on the dsPIC30F4012*

Qingping and Wenchao (2012) introduced the principle of PMBLDC motor and digital signal controller (dsPIC30 F4012). This control solution was proposed according to the fans and pumps load requirements of the application. The PMBLDC motor has no commutation spark and reliable, hence, it has been widely used under load condition which requires long-term stable operation of the fan and pump in industrial applications (Qingping and Wenchao, 2012). Microchip Technology Inc has promoted a dsPIC30F digital signal controller with the PIC16 position monolithic integrated circuit as the core PMBLDC motor control areas (Microchip

Technology Inc, 2005). This application implemented a 270V applied on the three-phase full bridge power MOSFET through a filter circuit. The rotor position signal which is produced by Hall sensors is processed by the PICF4012 to produce a PWM control signal (Qingping and Wenchao, 2012).

### *2.2.5 A hybrid controller for the speed control of a permanent magnet synchronous motor drive*

Elmas and Ustun (2007) proposed a hybrid controller which consists of a parallel connected sliding mode controller and a neuro-fuzzy controller for the speed control of a permanent magnet synchronous motor (PMSM) drive. Their aim was to design a controller that provides a fast and smooth dynamic response for the speed control of a PMS motor. An error band method was used to control the sliding mode controller to get a fast dynamic response in transient mode and the neuro-fuzzy controller to get a smooth dynamic response in steady state mode (Elmas and Ustun, 2007). The performance of the proposed controller was verified by computer simulations and experiments.

### *2.2.6 Super-capacitor/battery hybrid powered electric bicycle via a smart boost converter*

Manoj, Dino and Rosalina (2010) implemented a smart boost converter to enable an electric bicycle to be powered by a battery/super-capacitor hybrid combination. A 36V, 250W front hub motor BLDC motor was used to carry out the experiment. They connected a 16.2V, 58F super-capacitor module in parallel with the battery pack through a microcontroller-based boost converter which circulates power between the battery and super-capacitor. The experiment was carried out in up-hill acceleration of the bicycle to indicate the results of the boost converter

being responsive enough to boost the current from the high power complementary super-capacitor module avoiding a quick discharge of the battery. However, recharging the super-capacitor through regenerative braking proved to be very difficult since the boost converter was not designed to be bi-directional (Manoj *et* al., 2010).

### *2.2.7 Simplified sensorless control for BLDC motor, using DSP technology*

A sensorless control of BLDC motor for electric vehicle applications was proposed by Dixon *et* al. (2002). A BLDC motor is controlled by using embedded encoders or hall sensors to sense the rotor position. It is generally required to count with the position sensors because the active inverter phases must be commuted depending on the rotor position. However, these position sensors make the motor design more complicated and mechanically unreliable (Dixon *et* al., 2002). The proposed solution in this application uses a sinusoidal flux distribution to determine the commutation sequence of a BLDC motor. Their method is based on a two phase current sensing and the determination of the back emf. The application uses the information contained in the back emf to calculate the six commutation points required. This method is only applicable when currents are sensed. Therefore, the system was implemented using a digital signal processor (TMS320F241) which is programmed with a closed loop PI current control in order for the motor to produce a constant torque. And a fiber optic link was placed between the controller and the inverter to minimize noise and possibilities of error on commutations. The DSP controls the motor currents by taking the absolute values of two of the three phase currents to calculate the commutation instants based on the slope variations of these currents and evaluate the instantaneous position of the rotor.

## 2.3 SUMMARY AND CONCLUSIONS

This chapter has provided an overview of current available technologies in VSD systems. From the literature, it is evident that VSD control systems are emerging rapidly with more efficient and advanced techniques in EVs and electric bicycles applications. The following chapter will look at motor and VSD design.

This page is intentionally blank

# CHAPTER 3

# PMBLDC MOTOR DESIGN AND DRIVE CONTROL

## 3.1 DESIGN OF A PMBLDC MOTOR

The PMBLDC motor is steadily emerging as the standard drive method for ebikes, scooters, solar cars and electric vehicles (Bhim and Sanjeev, 2009). With a PMBL motor conversion, there is no need for external mounting brackets and drive chains to support a motor and transmission. Instead all of this is contained inside the front or rear wheel of the bicycle.

Electric motors operate by the interaction of two magnetic fields. One is produced by the stator or field and the other one produced by the rotor or armature (Safedrive, 2009). The magnetic fields are produced by either energised windings or permanent magnet. Brushless motors have windings only on the stator. All motors without permanent magnets and brushes like induction motors have currents flowing in their rotors that produce heat in the rotor (Wang, 2012). In the PMBL motor there are no such currents, allowing the PM motor to outperform other motor types in continuous high torque production (Hwang and Chang, 2000). Compared to a DC motor, the BLDC motor uses an electric commutator, replacing the mechanical commutator and making it more reliable. In BLDC motors, rotor magnets generate the rotor's magnetic flux, allowing BLDC motors to achieve higher efficiency (Safedrive, 2009). Therefore,

BLDC motors can be used in home appliances such as refrigerators, washing machines, dishwashers and industrial applications such as pumps, fans, air compressors that require high reliability and efficiency (Padmaraja, 2003).

There are two basic categories of hub motors, namely direct drive and the geared type. For this study, the *direct drive* motor is used. Typically direct drive motors are radial-flux brushless DC (BLDC) machines that have an array of permanent magnets on the inside surface of the hub (Patterson and Spree, 1995). The stator windings for these motors are attached to the axle and the hub is made to rotate by alternating currents through these windings. For the DC hub type direct drive motor, the magnets are on the axle, and the windings are actually spinning on the inside of the hub.

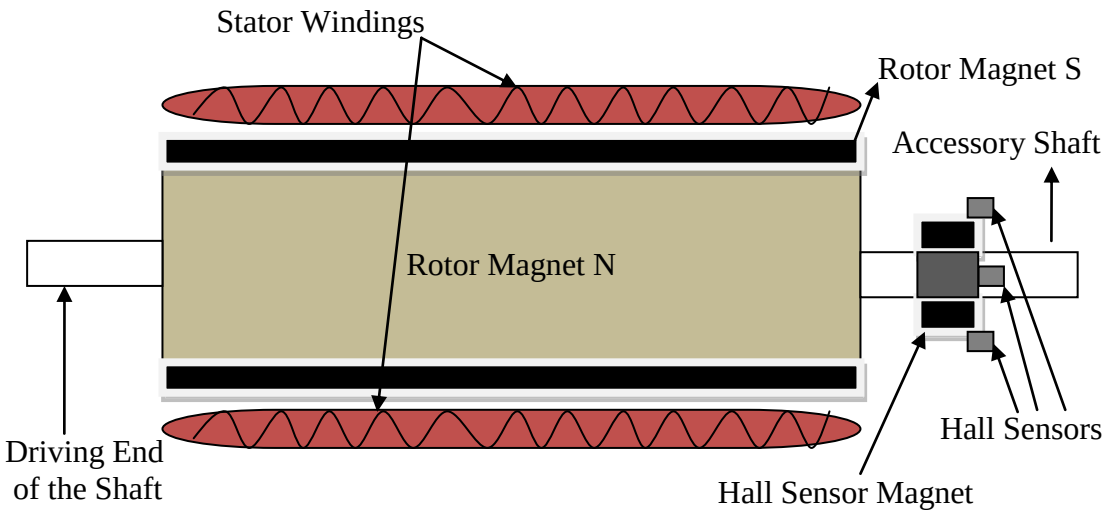


Figure 3.1: Hub-type brushless dc motor (Padmaraja, 2003).

To get maximum power and torque output, the motor has to be large since the power density from an electric motor is directly proportional to the speed between the magnets and the winding (Padmaraja, 2003). With a bulky geared scheme, the motor often rotates at a very high speed, whereas a smaller direct drive motor can deliver the same speed (Wang, 2012). Hub motors for electric bicycles are usually permanent magnet brushed or brushless. PM motors have the highest power density compared to common motor type (de Vries, 2008).

### *3.1.1 The stator*

The stator of a BLDC motor contains a stack of steel laminations with windings placed in the slots that are axially cut along the inner periphery (Patterson and Spee, 1995) shown in Figure 3.2 and Figure 3.3. PMBLDC motors have three stator windings connected in star format. Each winding is constructed by interconnecting numerous coils and distributed over the stator periphery to form an even numbers of poles (Kasei, 2011). Motors with the correct voltage rating are chosen depending on the control power supply. Motors rated at 48V or less are usually used in electric bicycles, automotive robotics and scooters whilst motors with 100V and above are used in high power automation and in industrial applications (Hwang and Chang, 2000).

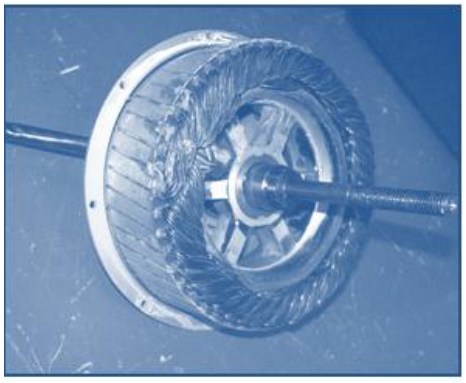

Figure 3.2: Stator of the BLDC motor used in the study with embedded Hall sensors.

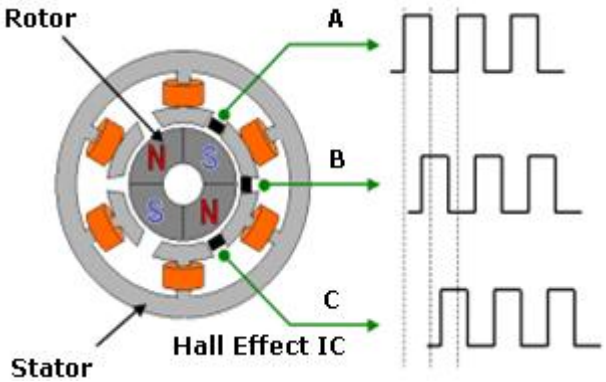


Figure 3.3: Cross-section of the BLDC motor with embedded Hall sensors (Kasei, 2011).

### *3.1.1 The rotor*

The rotor of BLDC is made of permanent magnet and can vary from two to eight pole pairs (Fadal Machines, 2008). Based on the required magnetic field density in the rotor, the proper magnetic material is chosen to make the rotor (de Vries, 2007). Ferrite magnets are used to make permanent magnets since they are inexpensive but have the disadvantage of low flux density (Fadal Machines, 2008). Alloy also has a high magnetic density that enables the rotor to give the same torque. Alloy magnets have improved advantage of size-to-weight ratio and give higher torque for the same motor size using ferrite magnets (Patterson and Spee, 1995). Some of the alloy magnets used in the construction of BLDC motor rotor are Neodymium (Nd), Samarium Cobalt (SmCo) and the alloy of Neodymium, Ferrite and Boron (NdFeB) (Hwang and Chang, 2000). Figure 3.4 shows a conventional type brushless DC motor and Figure 3.5 indicates the rotor of a PMBLDC motor in a bicycle wheel used in this study.

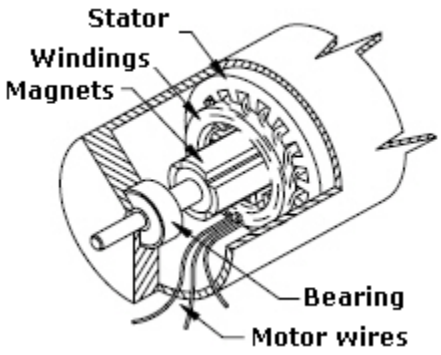


Figure 3.4: A brushless-type DC motor (Fadal Machines, 2008).

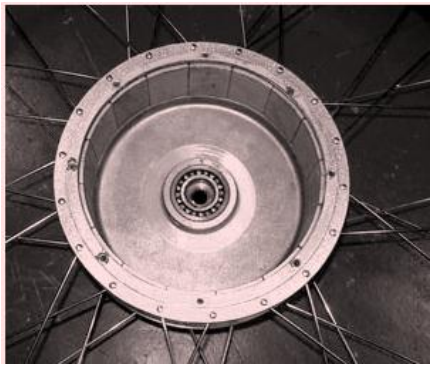

Figure 3.5: The rotor of the PMBLDC motor used in the study.

Comparative analysis for brushless DC and brushed DC motor has been presented in Table 3.1 and Table 3.2. This was done to select a good choice of motor that suits the application. The PMBLDC motor is more suitable for E-bikes, EVs and HEVs and low power applications, due to high torque, high power density, high efficiency and low maintenance (Bhim and Sanjeev, 2009). The motor should have high efficiency, high torque and compactible for high speed applications (de Vries and Jenman, 2006). To run the motor at high speed, the back EMF constant is designed to be smaller to reduce the voltage drop. This causes a low starting torque which is one of the disadvantages of a PMBLDC motor in high-speed applications (Bhim and Sanjeev, 2009). The combinations of unipolar and bipolar techniques are used to utilize the advantage of the large starting torque of a bipolar drive scheme and the high operating speed of a unipolar drive scheme (Microchip Technology, 2003). A DSP/FPGA based controller can be used to drive the PMBLDC motor with the bipolar or unipolar method and to switch from one method to the other at any speed (Janpana *et* al., 2012).

Table 3.1: Comparison of the performance characteristics of a brushless DC motor to that of a brushed DC motor (Microchip Technology, 2003**)**

| **Feature** | **BLDC Motor** | **Brushed DC Motor** |
|---|---|---|
| Control | Complex and expensive. | Simple and inexpensive. |
| Commutation | Electronic commutation based on Hall position sensors. | Brushed commutation. |
| Control Requirements | Controller is required to run the motor. The same controller can be used for variable speed control. | Controller is required only for variable speed. No controller required for fixed speed. |
| Speed Range | Has high speed range. | Low due to mechanical limitations by the brushes. |
| Rotor Inertia | Low due to permanent magnets on the rotor which improves the dynamic response. | High rotor inertia which limits the dynamic characteristics. |
| Electric Noise Generation | Low. | Arcs in the brushes generate noise causing EMI in nearby equipments. |
| Maintenance | Less maintenance required due to absence of brushes. | Periodic maintenance is required. |
| Speed/Torque Characteristics | Straight which enables operation at all speeds with rated load. | Moderately flat which increase brush friction at higher speeds, reducing useful torque. |
| Output Power/Frame Size | High power and small size due to superior thermal characteristics. BLDC has the windings on the stator which is connected to the case, thus heat dissipation is better. | Moderate power and bigger size. Heat produced by the armature is dissipated in the air gap, thus increasing the temperature in the air gap. |
| Cost of Building | High due to permanent magnets | Low. |
| Efficiency | Higher. There is no voltage drop across brushes. | Moderate. |
| Life | Longer. | Shorter. |

Table 3.2: Comparison of performance characteristics of BLDC Motor to that of an AC Motor (Padmaraja, 2003)

| Feature | BLDC Motor | AC Induction Motor |
|---|---|---|
| Slip | No slip is experienced between stator and rotor frequencies | The rotor runs at a lower frequency than stator by slip frequency and slip increases with load on the motor. |
| Starting Current | No special starter circuit required. | Approximately up to seven times of rated Starter circuit rating should be carefully selected. Normally uses a Star-Delta starter. |
| Control Requirements | A controller is always required to keep the motor running. The same controller can be used for variable speed control. | No controller is required for fixed speed; a controller is required only if variable speed is desired. |
| Speed Range | Higher. No mechanical limitation imposed by brushes/commutator. | Lower due to mechanical limitations by the brushes. |
| Rotor Inertia | Low. | High due to poor dynamic characteristics. |
| Electric Noise Generation | Low. | Arcs in the brushes generate noise causing electro-magnetic interference (EMI). |
| Maintenance | Regular maintenance | Less maintenance is required. |
| Speed/Torque Characteristics | Straight which enables operation at all speeds with rated load. | Nonlinear causing lower torque at lower speeds. |
| Output Power/Frame Size | High power due to permanent magnets on the rotor and smaller size. | Moderate because both stator and rotor have windings making it bulky. |
| Cost of Building | Higher due to permanent magnets. | Low. |
| Efficiency | High. There is no voltage drop across brushes. | Moderate. |
| Life | Shorter. | Longer. |

## 3.2 POWERING OF A PMBLDC MOTOR

A generic E-bike controller schematic is given in Figure 3.6. The power source represents the supply voltage from the battery which energizes the power MOSFETs to control the motor phases. The sensors and the logic control unit controls the hall sensors for commutation.

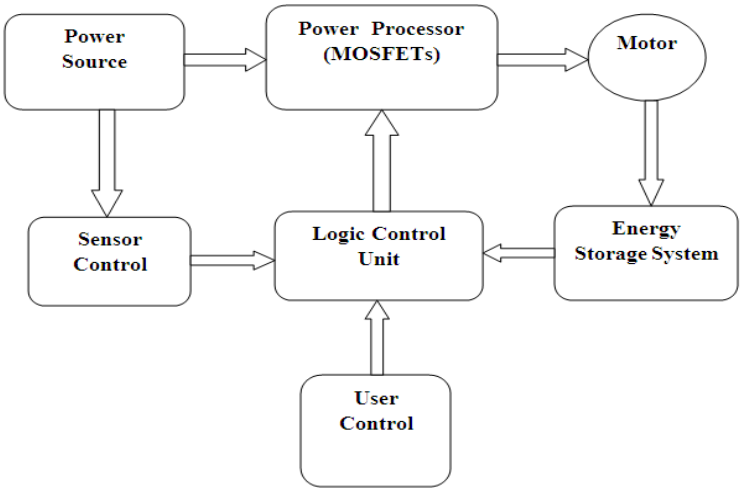


Figure 3.6: Schematic of a DC VSD system.

3-phase BLDC motors are switched using a combination of six independently switched power MOSFETS (cf. Figure 3.7) (cf. Pavel, 2005; Wang, 2012; Freescale semiconductor, 2005). There are two basic types of power transistor switching, namely *independent switching* and *complementary switching* (S.T. Microelectronics, 2007). The power MOSFETs may be switched independently or in complementary mode (S.T. Microelectronics, 2007). Figure 3.8 shows typical voltages applied to a BLDC motor (Free scale semiconductor, 2005). The lower voltage is generated using a PWM technique as indicated in Figure 3.9.

Only two MOSFETs are switched on when the current is conducted from the power supply to the phase of the BLDC motor in independent switching. All the MOSFETs are switched off during freewheeling. In the independent switching scheme, the current continues to flow in the same direction through freewheeling diodes and decay to zero. Whilst in complementary switching, the MOSFETs are switched on during freewheeling, so the current is able to flow in the opposite direction (S.T. Microelectronics, 2007). Both switching modes can work in bipolar

or unipolar scheme. This application utilizes the independent unipolar PWM scheme as shown in Figure 3.9.

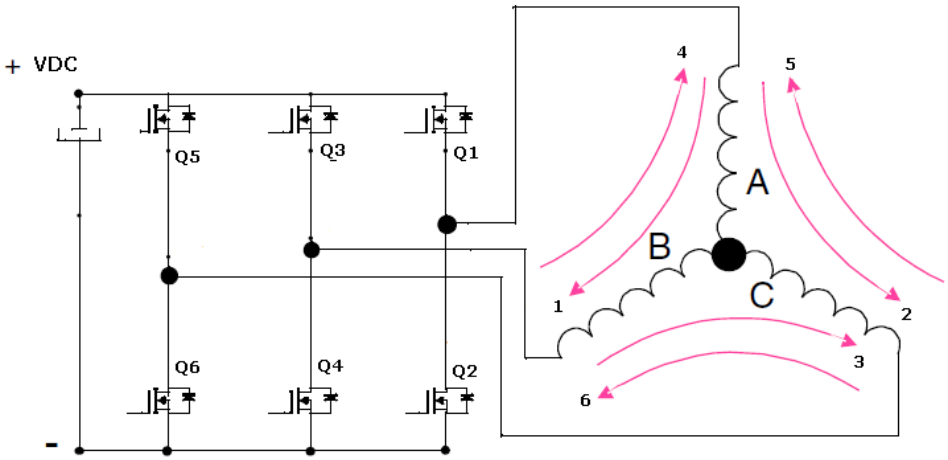


Figure 3.7: A typical 3-phase MOSFET power stage showing its 6 switched voltage vectors (S.T. Microelectronics, 2007).

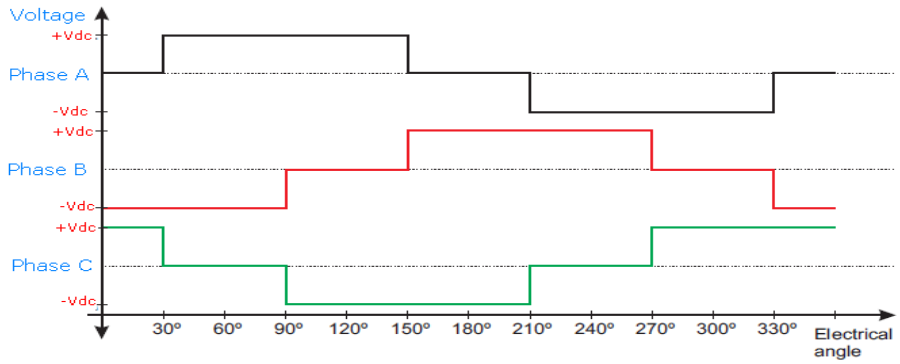


Figure 3.8: SPICE simulated phase voltages switched to a 3-phase PMBLDC motor (S.T. Microelectronics, 2007).

.

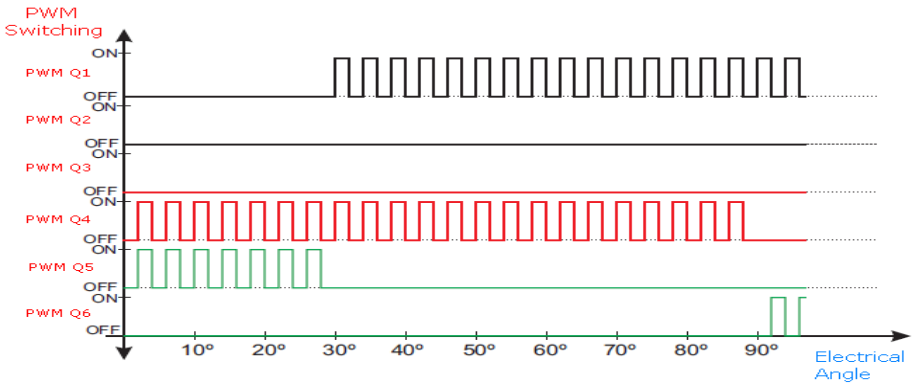


Figure 3.9: SPICE simulated PWM switching signals for power MOSFET drivers . (S.T. Microelectronics, 2007).

### *3.2.1 Commutation*

Commutation creates a rotation field. Proper operation of a BLDC motor requires the angle between stator and rotor flux to remain close to 90° (Freescale Semiconductor, 2005). Six-step control yields a total of six possible stator flux vectors. The stator flux vector must be changed at a certain rotor position. The rotor position is usually detected by Hall Sensors. The Hall Sensors directly detect the commutation moment. The application presented uses the hall sensors to sense rotor position. The electrical revolution can be divided into six sectors. Each sector corresponds to a certain stator flux vector as illustrated in Figure 3.10. The actual rotor position in Figure 3.11 corresponds to the sector ABC [binary pulse 110]. Phase A is connected to the positive DC bus voltage by the MOSFET Q1, Phase C is connected to the ground by MOSFET Q6 and Phase B is floating. The six-step control technique varies from an angle of 60° to 120° between the rotor flux and the stator flux. The commutation is repeated every $60^0$. The commutation process is critical for its accuracy because any deviation can cause torque ripples and therefore, speed variation. Each commutation sequence has one of the windings energized to positive power, the second winding is negative and the third winding is non-energized. Torque is produced due to

the interaction between the magnetic field generated by the stator coils and the permanent magnets. Ideally, the peak torque occurs when these two fields are at 90° to each other and falls off as the fields move together (Lee and Eshsani, 2001). To keep the motor spinning, the magnetic field produced by the windings should shift position with the movement of the rotor to catch up with the stator field.

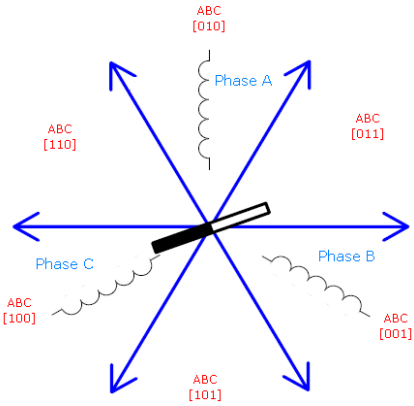


Figure 3.10: Stator flux vectors under 6-Step control (Freescale Semiconductor, 2005).

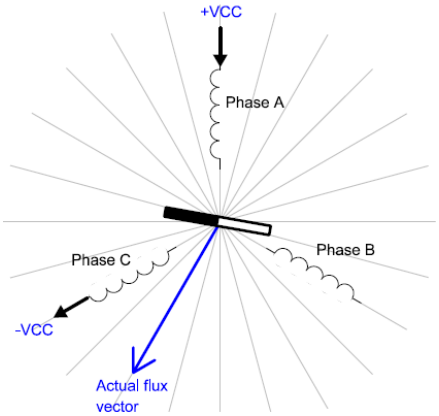


Figure 3.11: Rotor position at a binary pulse 110 (Freescale Semiconductor, 2005).

The PMBLDC motor uses two pair conduction controls for the phase shift. Table 3.3, Table 3.4, Figure 3.12 and Figure 3.13 show the sequence in which these power switches should be switched based on the Hall sensor inputs labeled A, B and C. The switching sequence in Table 3.3 corresponds with the clockwise rotation of the motor in Figure 3.12. And Table 3.4 corresponds with the counter clockwise motor rotation in Figure 3.13. When deriving a controller for a particular motor, the sequence defined by the motor manufacturer should be followed. To vary the speed, these signals should be Pulse Width Modulated (PWM) at a much higher frequency than the motor frequency. When the duty cycle of PWM is varied within the

sequences, the average voltage supplied to the stator reduces, thus reducing the speed (MSK Corp., 2011). Another advantage of having PWM is that if the DC bus voltage is much higher than the motor rated voltage, the motor can be controlled by limiting the percentage of PWM duty cycle corresponding to that of the motor rated voltage. This makes it flexible for the controller to operate motors with different rated voltages.

Table 3.3: Switching sequence for forward direction rotation DIR = 1 (DIR = 1 indicates forward direction)

| **Signal from Hall sensor** | | | **Figure 2.7 MOSFET switching** | | | | | | **Motor phases** | | | **Rotation direction** |
|---|---|---|---|---|---|---|---|---|---|---|---|---|
| **A** | **B** | **C** | **Q1** | **Q2** | **Q3** | **Q4** | **Q5** | **Q6** | **Pa** | **Pb** | **Pc** | **DIR** |
| 1 | 0 | 1 | on | off | off | off | off | on | H | L | - | 1 |
| 1 | 0 | 0 | on | on | off | off | off | off | H | - | L | 1 |
| 1 | 1 | 0 | off | on | on | off | off | off | - | H | L | 1 |
| 0 | 1 | 0 | off | off | on | on | off | off | L | H | - | 1 |
| 0 | 1 | 1 | off | off | off | on | on | off | L | - | H | 1 |
| 0 | 0 | 1 | off | off | off | off | on | 0n | - | L | H | 1 |

Table 3.4: Required Switch regime for reverse direction DIR = 0 (DIR = 0 indicates reverse direction rotation)

| **Signal from Hall sensor** | | | **Figure 2.7 MOSFET switching** | | | | | | **Motor phases** | | | **Rotation direction** |
|---|---|---|---|---|---|---|---|---|---|---|---|---|
| A | B | C | **Q1** | **Q2** | **Q3** | **Q4** | **Q5** | **Q6** | **Pa** | **Pb** | **Pc** | **DIR** |
| 1 | 0 | 1 | off | off | on | on | off | off | L | H | - | 0 |
| 1 | 0 | 0 | off | off | off | on | on | off | L | - | H | 0 |
| 1 | 1 | 0 | off | off | off | off | on | on | - | L | H | 0 |
| 0 | 1 | 0 | on | off | off | off | off | on | H | L | - | 0 |
| 0 | 1 | 1 | on | on | off | off | off | off | H | - | L | 0 |
| 0 | 0 | 1 | off | on | on | off | off | off | - | H | L | 0 |

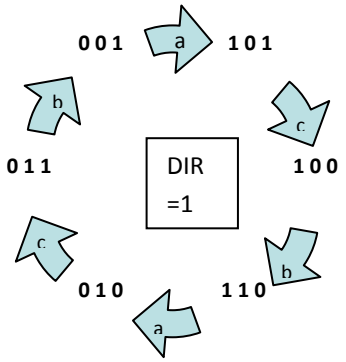


Figure 3.12: Forward direction binary sequence based on Table3..3

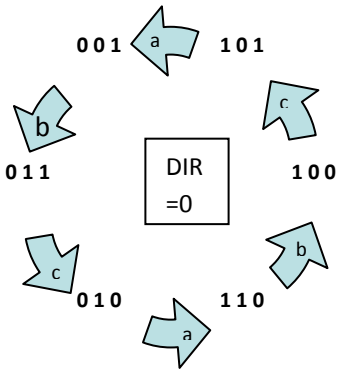


Figure 3.13: Reverse direction binary sequence based on Table3.4.

Figure 3.14 shows an example of Hall sensor signals with respect to back EMF and the phase current. This is an example of Hall sensor signals having a $120^0$ phase shift with respect to each other. One of the Hall sensors changes state at every $60^0$ of rotation. Therefore it takes six steps to complete one electrical cycle. The number of electrical cycles to be repeated to complete a mechanical rotation is determined by the rotor pole pairs. One cycle is completed for each rotor pole pair. Therefore the number of rotations equals the rotor pole pairs.

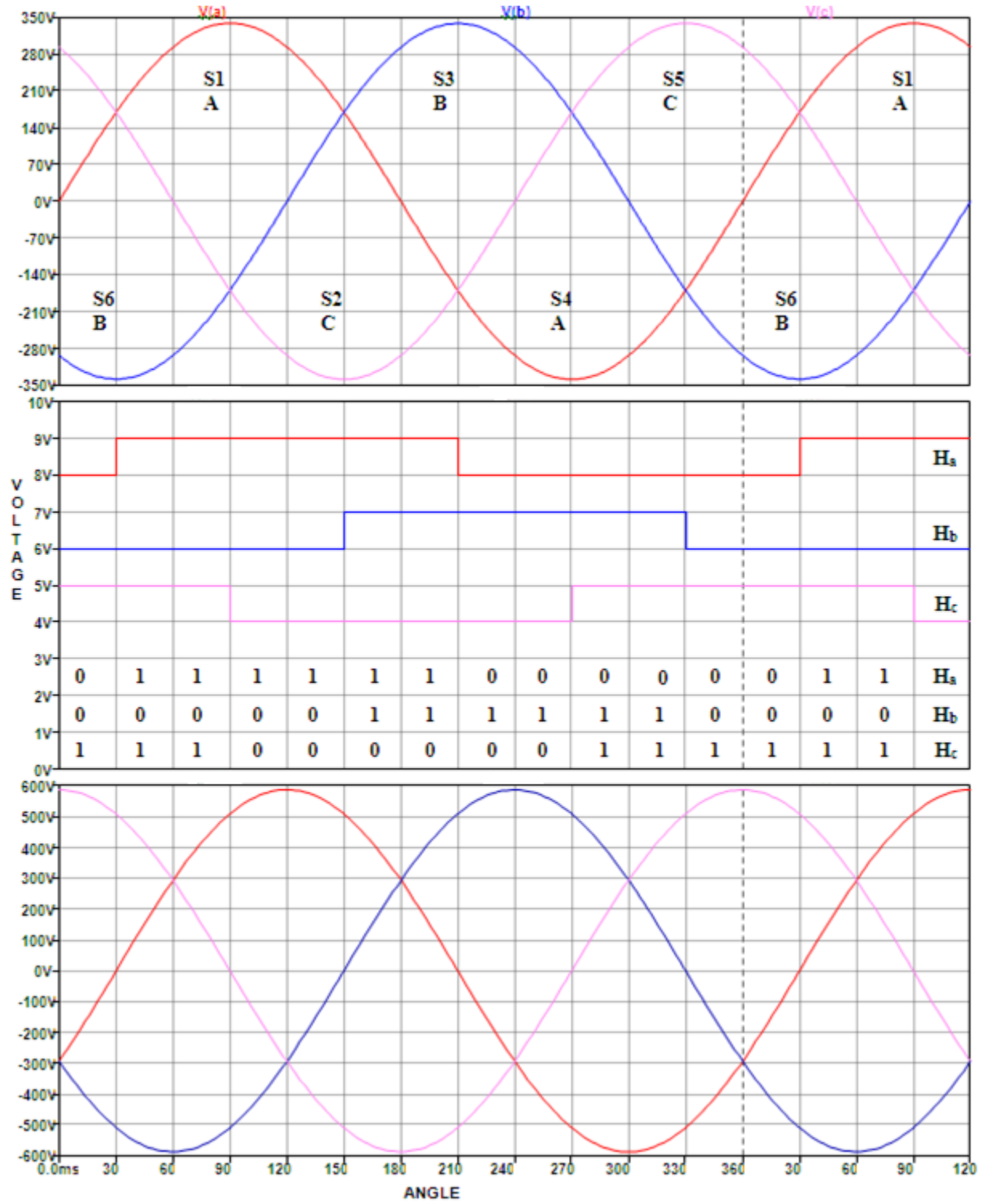


Figure 3.14: SPICE simulation of phase voltages with Hall sensors at 120°.

### *3.2.2 Back EMF*

When a BLDC motor rotates, each winding generates a back EMF. The polarity of this back EMF is in opposite direction of the energized voltage. When the motor is at steady state, this voltage closely matches the supply voltage applied to the motor (Pavel, 2005). When the motor is spinning and the load is increased its speed will drop therefore causing the back EMF to also drop and hence the current drawn by the motor will increase. By Ohm's Law, the current drawn by the motor is given by the equation:

$$I = \frac{Supply\ Voltage - back\ EMF}{Motor\ resistance} = \frac{V-(K_e \Phi \omega)}{R_t} \qquad \text{(Equation 3.1)}$$

$$Back\ EMF = (E) \propto NlrB\omega \qquad \text{(Equation 3.2)}$$

With regards to equation 3.1 and equation 3.2, V is the supply voltage, $K_e$ is the motor back EMF constant, $\Phi$ is the field strength, $R_t$ is the motor resistance, N is the number of winding turns per phase, $l$ is the length of the rotor, $r$ is the internal radius of the rotor, B is the rotor magnetic field density and ω denotes the motor's angular velocity.

The rotor magnetic field and the number of turns in the stator windings remain constant in the BLDC motor. The only factor that governs the back EMF is the angular velocity or speed of the rotor and as the speed increases, the back EMF also increases (Hemanand and Rajesh, 2006). The motor technical specification gives the back EMF constant that can be used to estimate the back EMF for a given speed. The potential difference across a winding can be calculated by subtracting the back EMF value from the supply voltage. PMBLDC motors are designed with a back EMF constant such that when the motor is running at the rated speed, the potential difference between the back EMF and the supply voltage will be sufficient for the motor to draw

the rated current and deliver the rated torque (Tashakori and Ektsesabi, 2012). If the motor is driven beyond the rated speed, back EMF may increase substantially, thus decreasing the potential difference across the winding, reducing the current drawn which results in dropping torque curve.

### *3.2.3 Torque*

The torque produced by a PMBLDC motor is directly proportional to the motor current. Therefore to effectively control the torque, a sensor is used to sense the motor current. The motor current is amplified using operational amplifiers. The peak or maximum torque required for the application can be calculated by summing the load torque, torque due to inertia and the torque required to overcome the friction (Padmaraja, 2003). There are other factors such as the resistance in the air gap which contribute to the overall peak torque requirements (Tshikawa and Slemon, 2012). The torque produced by a permanent magnet motor is given by the equation (Salam, 2003):

$$T = K_e \Phi i_a \qquad \text{(Equation 3.3)}$$

With regards to equation 3.3, $T$ is the torque, $K_e$ is the EMF constant for the motor, $i_a$ is the armature current and $\Phi$ represents the field strength.

### *3.2.4 Speed control*

The speed is directly proportional to the supply voltage in the BLDC motor. The commutation ensures the proper rotation of the BLDC motor, while the motor speed depends only on the

amplitude of the supply voltage. This amplitude can be controlled by the PWM technique. The technique to BLDC commutation is to sense the rotor position, then energize the phases that will produce maximum torque. The rotor travels $60^0$ per commutation step. The appropriate stator current path is activated when the rotor is $120^0$ from alignment with the corresponding stator magnetic field (Chengang and Yaochun, 2010). The stator current is deactivated when the rotor is $60^0$ from alignment at which time the next phase is activated and the process repeats. Commutating the electrical connections through the six possible combinations will pull the rotor through one electrical revolution. The speed can be expressed by the given equation:

$$\omega = \frac{V_a}{K_v I_f} \qquad \text{(Equation 3.4)}$$

With regards to equation 3.4, $\omega$ is the motor speed, $K_v$ is the motor voltage constant, $V_a$ is the armature voltage and $I_f$ denotes the field current.

### *3.2.5 Power efficiency*

The power drawn by a motor from the supply is given by:

$$P_{in} = VI = \frac{V^2}{R} \qquad \text{(Equation 3.5)}$$

The mechanical power produced by the motor is given by:

$$P_{out} = T\omega \qquad \text{(Equation 3.6)}$$

From equation 3.5 and equation 3.6:

$$efficiency = \frac{P_{out}}{P_{in}} = \frac{T\omega}{VI} \times 100 \qquad \text{(Equation 3.7)}$$

## 3.3 DC-DC LEVEL SHIFTER OPERATION

A DC-DC level shifter allows DC voltages to be raised or lowered similar to how a transformer does with AC voltages. DC-DC conversion became very popular with the advent of power transistors, and since then many circuits have been invented (Mohan et *al*., 2003). The simplest types of converter are the non-isolated buck and boost converters. Other types include the Buck-Boost converter as well as isolated designs such as the forward converter and fly-back converter.

### *3.3.1 Boost converter*

The boost converter is used to step-up the motor voltage to charge the batteries when the circuit is operating in the regenerative mode. It has a high speed switching MOSFET (Q), a flywheel diode (D), an inductor (L) and an output filter capacitor (C) as illustrated in Figure 3.15. The output voltage is monitored and maintained at a desired level by a control circuit which switches Q on and off at a set frequency but with a varying duty cycle. The duty cycle of the high speed switch controls the output voltage. The circuit boosts the voltage using energy stored in the inductor. When the switch is turned on, current flows from the supply through the inductor and energy is stored in the inductor's magnetic field. At this stage there is no current through the diode. Therefore the load current is supplied only by the charge in the capacitor. When the switch is turned off, the inductor opposes the change in current by reversing its voltage. In trying to maintain the current flow, the inductor voltage rises so that the inductor voltage adds to the

source voltage. Current due to this boosted voltage flows from the source through L1, D1 and the load R1, recharging C as well. Figure 3.16 indicates the output voltage, output current and the gate pulse of the boost converter circuit in Figure 3.15. The output voltage is related to the duty cycle by:

$$V_{out} = \frac{V_s}{(1-D)}$$

(Equation 3.8)

With regards to equation 3.8, $V_{out}$ is the output voltage, $V_s$ is the supply voltage and D represents the duty cycle.

With an input of 5V to give an output of 12V/1A; $V_{out} = \frac{Vo - Vin}{(1-D)}$

$$D = \frac{V_o - V_{in}}{V_o}$$

$$D = \frac{12[V]-5[V]}{12[V]} = 58\%$$

For a switching frequency of 20 kHz at a voltage ripple of 240mV and inductor ripple current of 1.5A;

$$T = \frac{1}{f} = \frac{1}{20\times10^3[\text{Hz}]} = 50\mu s$$

$$i = C\frac{dv}{dt} \therefore C1 = \frac{25\times10^{-6}[\text{s}]}{240\times10^{-3}[\text{V}]} \times 1[\text{A}] = 104.17\mu\text{F}$$

For practical purpose, a100μF capacitor is used.

$$\therefore L1 = \frac{V_{in}\times(V_{out}-V_{in})}{\Delta I_L \times f_s \times V_{out}} = \frac{5[V]\times(12[V]-5[V])}{1.5A\times20\times10^3[\text{Hz}]\times12[\text{V}]} = 97\mu\text{H}$$

For practical purpose, a100μH inductor is used.

$$R_1 = \frac{V_{out}2}{P_{out}} = \frac{12^2[\text{V}]}{12[W]} = 12\Omega$$

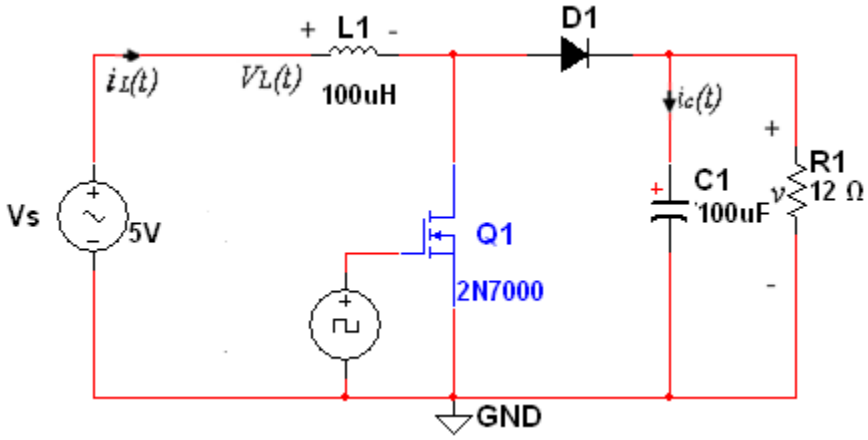


Figure 3.15: Circuit of a boost converter.

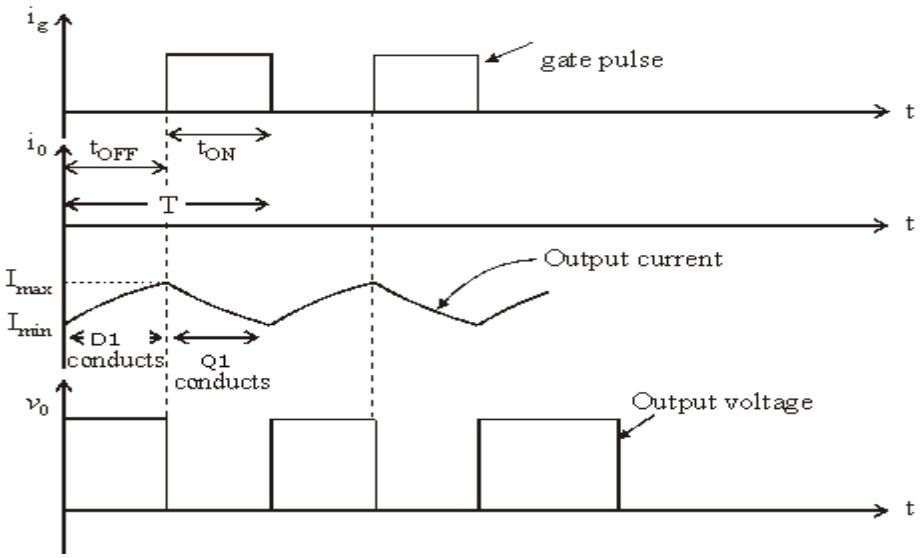


Figure 3.16: Voltage and current waveforms of a boost converter (Mohan et *al*., 2003).

### *3.3.2 Two quadrant operation*

From the literature (cf. Britten et *al.*, 2007), the two quadrant of motor operation only covers the following modes as illustrated in bold in Figure 3.17:

*Operating mode 1*: Forward motoring that generates a positive voltage and a positive current.

*Operating mode 2:* Forward regeneration that generates a positive voltage and a negative current.

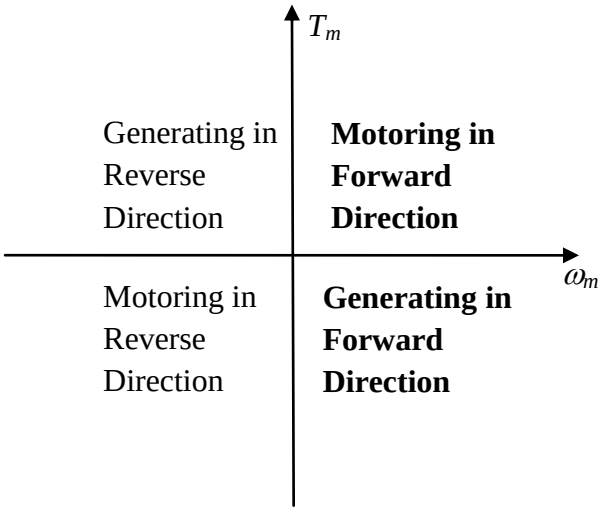


Figure 3.17: Two quadrants of motor operation (the quadrants where motoring and generation in forward direction occurs are indicated in bold).

The VSD puts the BLDC motor into generating mode when the throttle detects a negative current. The motor has to be moving to convert mechanical energy to electrical energy. Active braking zone in the generating quadrant is unreachable for the VSD designed for two quadrants in the same mechanical direction (Britten et *al.*, 2007). The controller can only short the motor terminals, causing a maximum negative current that is proportional to the speed. This is the case for a BLDC motor with a two quadrant drive as illustrated in bold in Figure 3.17 (Salam, 2003). The measurements of torque were not very accurate and prevented meaningful analysis of efficiency (Britten et *al.*, 2007).

The two quadrant operation uses the half bridge configuration as shown in Figure 3.18. The PWM technique is used to control the switches in the half bridge circuit to vary the power delivered to the motor. $Q_1$ and $D_2$ form a step down converter that can reduce the voltage to the motor. Current flows from the battery to the motor when $Q_1$ switches on, therefore causing the

motor to rotate as illustrated in Figure 3.19. When $Q_1$ is turned OFF, energy stored in the inductance ($L$) of the motor forces current to flow through the diode $D_2$ and the output voltage becomes zero. Thus, varying the duty cycle of $Q_1$ will control the motor in the motoring mode.

Applying the PWM control signal to $Q_2$ allows the motor to be controlled as a generator. When $Q_1$ is ON (cf. Figure 3.19), the load current is positive and the output voltage is equal to the supply voltage received by the load. When $Q_2$ is triggered, the voltage $V_a$ forces current to flow in opposite direction through motor (cf. Figure 3.20). Therefore the output voltage becomes zero. When $Q_2$ switches OFF, the energy stored in the inductance drives current through diode $D_1$ to the source. The power MOSFETs $Q_1$ and $Q_2$ should not be turned ON simultaneously as it would result in short circuiting the supply**.** In forward motoring which is the first quadrant operation, $Q_1$ and $D_2$ conduct (cf. Figure 3.19). When $Q_1$ is on, the supply voltage is connected to the motor terminal and when it switches off, the current freewheels through $D_2$. Therefore the motor speed ($V_a$) is determined by the duty ratio. Figure 3.21 indicates the corresponding output voltage and current waveforms of the H-Bridge circuit.

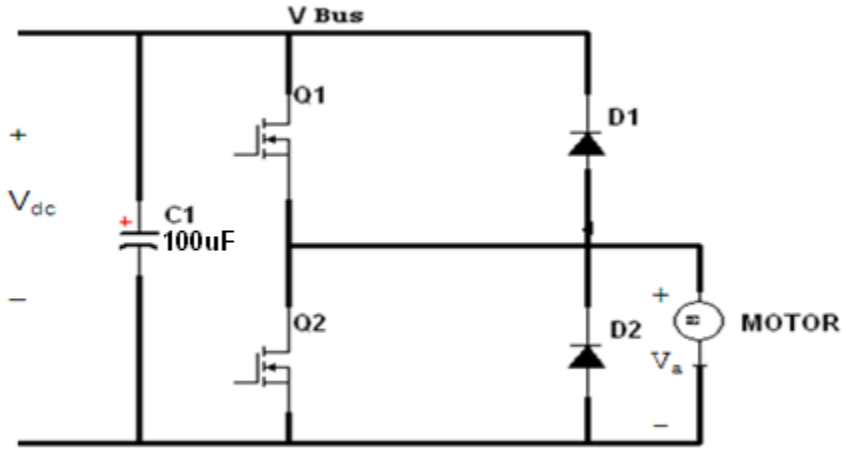


Figure 3.18: Half bridge circuit configuration (single H configuration) for two quadrant operation.

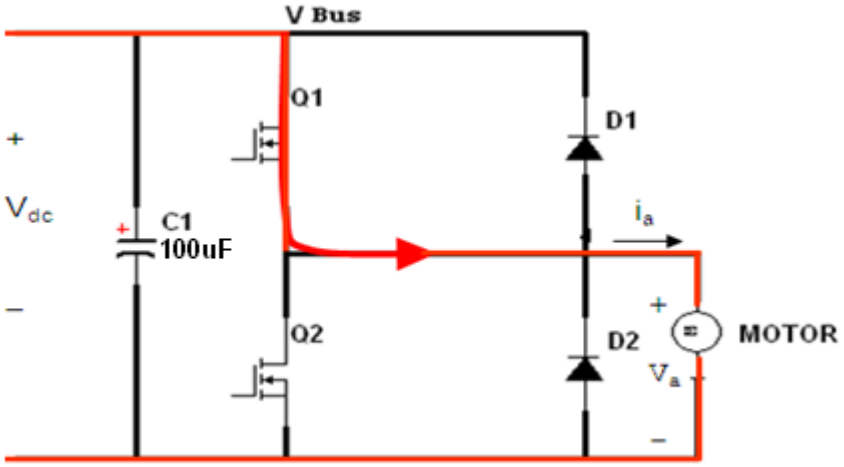


Figure 3.19: Forward motoring when $Q_1$ is conducting: $v_a = V_{dc}$
$D_2$ conducts $\rightarrow$ $v_a = 0$.

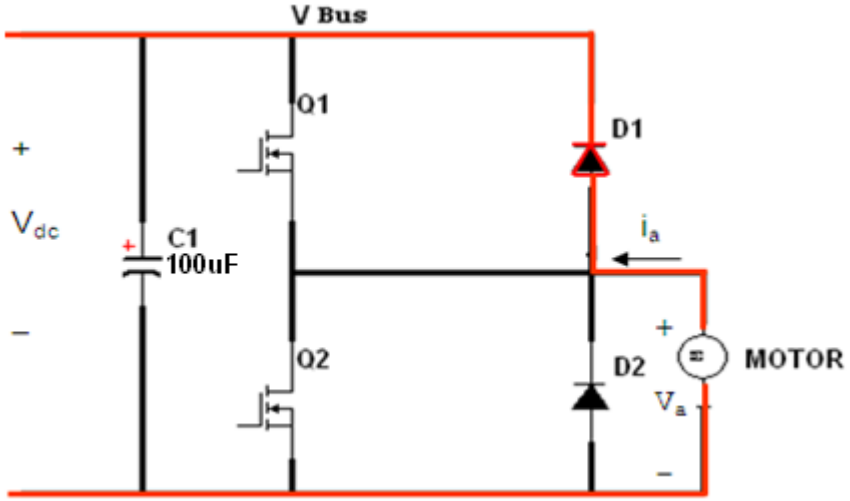


Figure 3.20: Regeneration when $D_1$ is conducting: $v_a = V_{dc}$
$Q_2$ conducts $\rightarrow$ $v_a = 0$.

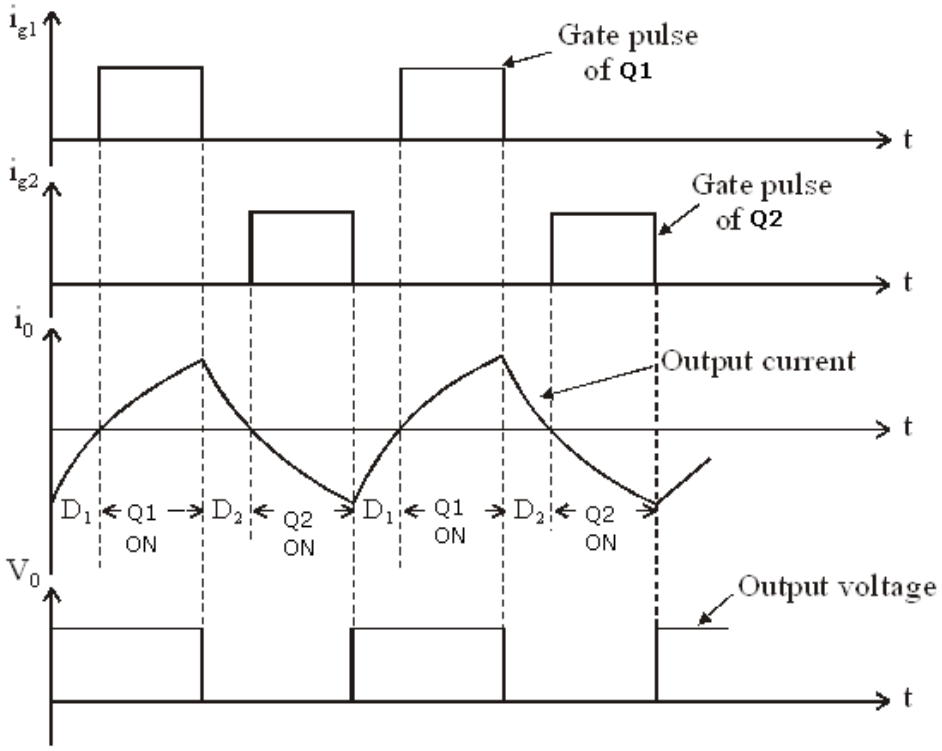


Figure 3.21: Measured output voltage and current waveforms of the H-bridge circuit (Mohan et *al*., 2003).

## 3.4 SUMMARY AND CONCLUSIONS

This chapter has discussed the basic BLDC motor theory, system design concepts and hardware implementation. From the literature and based on personal experience, BLDC motors have advantages over brushed DC motors and induction motors. They have better speed versus torque characteristics, high dynamic response, high efficiency, long operating life, noiseless operation, higher speed ranges and low maintenance. Also, torque delivered to the motor size is higher, making it useful in applications where space and weight are critical factors. With these advantages, BLDC motors find wide spread applications in automotive, appliance, aerospace, instrumentation and automation industries. The next chapter will discuss a variant of 4 quadrant operation which was used for the drive system proposed in this study.

This page is intentionally blank

# CHAPTER 4

# HARDWARE DESIGN FOR THE PROPOSED 4-QUADRANT VARIABLE SPEED DRIVE

## 4.1 INTRODUCTION

This chapter discusses the *author's original design* for the four quadrant speed control system. It discusses the various parts, design and their respective functions in the control system. The PMBLDC motor is a perfect choice with simple drive requirements for this application. Thus FDP3632 MOSFET's, LM5101 drive, GWM100-01X1 three phase full bridge, ATmega328 or CPLD and SG3524 were chosen as the main components. The design accommodates the following practical specifications: 36V-DC battery, 500W trapezoidal back EMF BLDC motor, 3 Hall effect rotor position sensors, arranged in a $360^0$ configuration and a control input or throttle signal that is derived from an angular position sensor that produces a 1VDC to 5VDC signal.

## 4.2 FOUR QUADRANT OPERATION

The 4- quadrant drive control system proposed in this study (cf. Figure 4.1) utilises the following 4 operating modes:

*Operating mode 1*: Forward motoring that generates a positive voltage and a positive current.

*Operating mode 2:* Forward regeneration to generate a positive voltage and a negative current.

*Operating mode 3:* Reverse motoring that generates negative voltage and negative current.

*Operating mode 4:* Reverse regeneration to generate a negative voltage and a positive current.

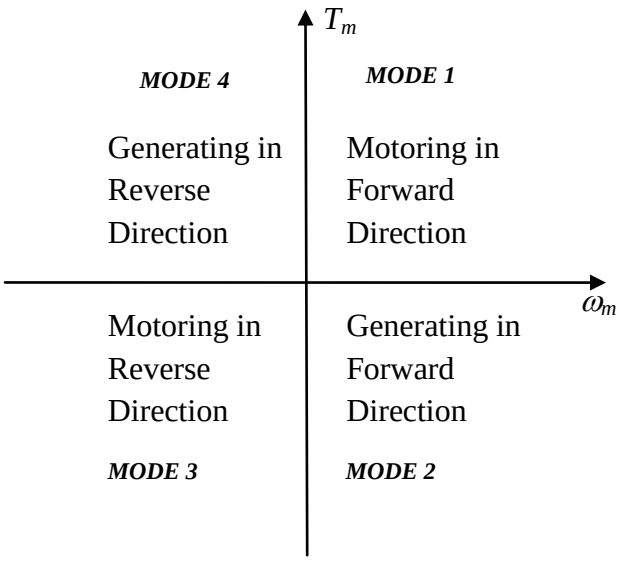


Figure 4.1: The four quadrants of motor operation.

The four quadrant drive uses the simplest logic function while regenerating electrical energy from the PMBL motor. As an added economic advantage, the method for regenerating electrical energy can reduce brake pad wear and thus brake pad replacement frequency. With the ability to return energy to the energy storage devices (battery-capacitor technology), the proposed VSD can also be used as an emergency low power generator. Regeneration takes place in the energy storage system and user control represents the throttle. The benefits of using 4 quadrant current-mode motor control are (Salam, 2003):

- The ability to smoothly control the current delivered to the motor, thus controlling its torque and speed.

- All operating modes are achieved, including forward, reverse and regenerative braking.
- High efficiency and power losses is minimized and an efficiency of 90% is easily achievable.
- Implemented into digital circuits, allowing high levels of torque control.

A full bridge configuration is used to control a PMBLDC motor in four quadrants operation. Four power MOSFETs which are connected in H-Bridge configuration to form a full bridge is used to control the motor to operate in all four quadrants as shown in Figure 4.2. Switching on $Q_1$ and $Q_4$ will supply voltage across the motor in one polarity, and $Q_3$ and $Q_2$ will give the opposite. Operation between the quadrants is as follows:

*Quadrant 1:* $Q_1$ and $Q_4$ are triggered (cf. Figure 4.2), the output current $i_O$ flows in a positive direction through them and the output voltage $V_O = V_{dc}$.

*Quadrant 4:* $Q_1$ and $Q_4$ are OFF, the energy stored in the motor inductance drives the output current through $D_2$ and $D_3$ in the same direction, but the output voltage becomes negative ie.

$V_O = -V_{dc}$.

*Quadrant 3:* When $Q_2$ and $Q_3$ are switched ON simultaneously, the load current $i_O$ flows in the opposite direction and the output voltage remains negative ie. $V_O = -V_{dc}$ as illustrated in Figure 4.3. Since both output voltage and output current are negative, the motor operates in third quadrant.

*Quadrant 2:* When both $Q_2$ and $Q_3$ are switched OFF, the load current continues to flow in the same direction through $D_1$ and $D_4$ and the output voltage becomes positive with a negative output current.

Bipolar switching and unipolar switching are used to control the average voltage in a DC converter that supplies bi-directional currents and voltages to the load.

*Bipolar Switching:* In bipolar switching, Q1 and Q2 (cf. Figure 4.2) operate in a complementary manner such that when Q1 is turned on, Q2 is turned off and vice versa. Q1 and Q4 are switched ON, with Q2 and Q3 switched off therefore connecting the Positive side to $V_{bus}$ and the Negative side to $V_{gnd}$. Q1 and Q4 are turned off when Q2 and Q3 are turned on; connecting the Positive side to $V_{gnd}$ and the Negative side to $V_{bus}$.

Both load and the supply experience large ripple currents during bipolar switching (Tshikawa and Slemon, 2012). The load swings between $+V_{bus}$ and $-V_{bus}$ as shown in the results in Figure 4.4. This makes the load current to change at a high rate. The current supplied from $V_{bus}$ will also swing between $+I_{LOAD}$ and $-I_{LOAD}$.

*Unipolar Switching:* For the unipolar modulation scheme, all 4 MOSFETS switch simultaneously (cf. Fig. 4.2). The scheme uses two sine waves of the same frequency and magnitude but are $180^0$ anti-phase (Namboodiri and Harshal, 2014). Therefore the output voltage switches between either zero and +Vdc during the positive half cycle or between zero and –Vdc during negative half cycle of the fundamental frequency (Namboodiri and Harshal, 2014). This technique involves a condition where the terminals of the load are connected together so that for a positive load current the supply only experiences a unidirectional current draw. Therefore the supply current ripple is reduced to half as illustrated in the results in Figure 4.5. The load ripple current is also reduced because the full supply voltage is only applied to the load for half cycle.

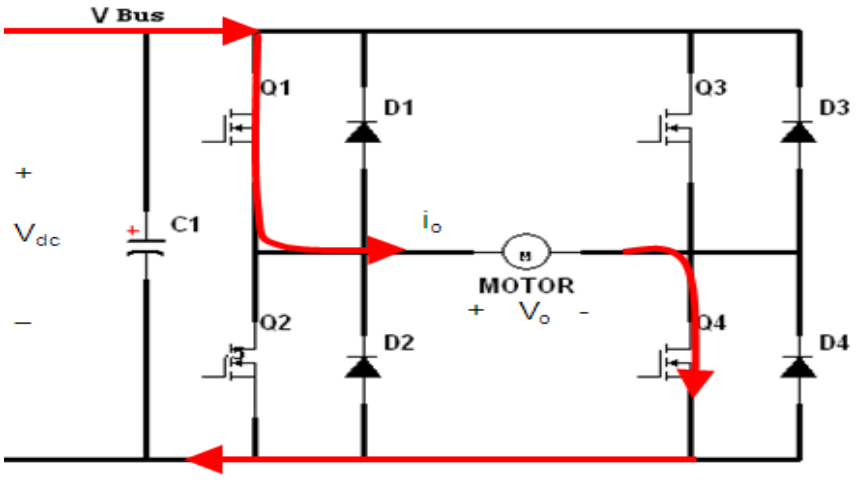


Figure 4.2: Full bridge configuration (double H) with positive current: when $Q_1$ and $Q_4$ are ON $V_o = V_{dc}$, $D_3$ and $D_2$ are ON $V_o = -V_{dc}$.

*Regenerative Braking:* Regenerative braking occurs when the voltage across the motor is greater than the battery voltage. For this reason, a boost converter is included in the design. During regenerative braking, the current flows out of the motor into the batteries. With regards to Figure 4.3, the motor acts as a generator when $Q_2$, $D_4$ and $D_1$ are simultaneously commutated into the saturation region. With $Q_2$ and $D_4$ simultaneously on, the motor experiences a short-circuit condition which gives rise to a large current and voltage to build up within the motor loop. The large currents flow through high speed switching diodes $D_4$ and $D_1$ to charge the batteries as shown in Figure 4.3**.**

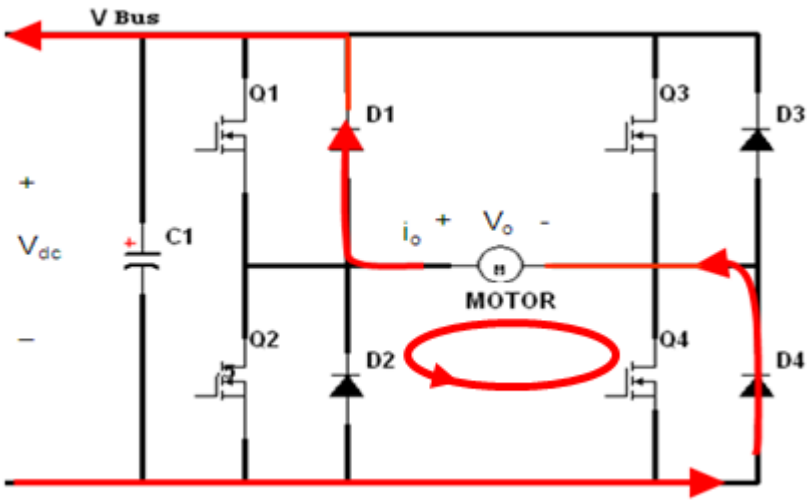


Figure 4.3: Full bridge configuration with negative current: when $D_1$ and $D_4$ are ON $V_o = V_{dc}$, $Q_3$ and $Q_2$ are ON $V_o = -V_{dc}$.

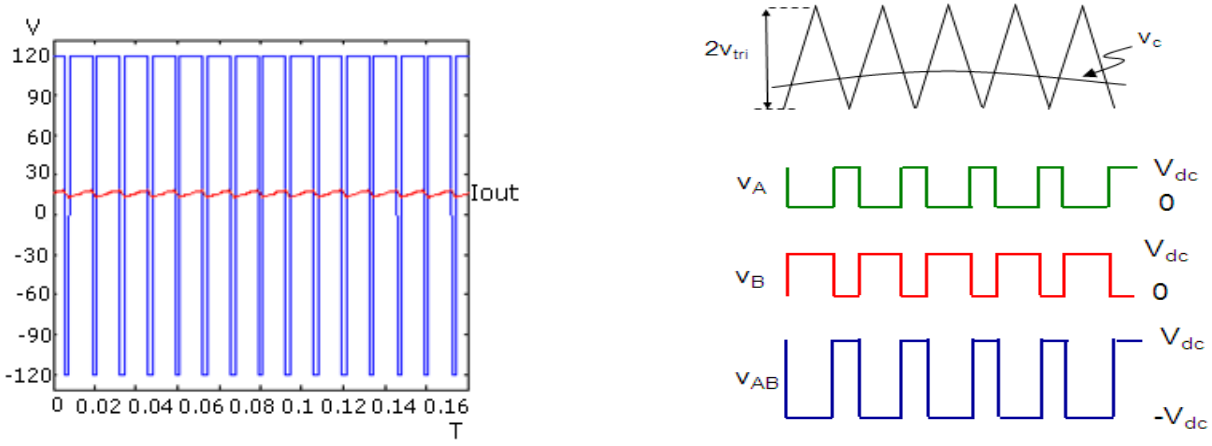


Figure 4.4: SPICE simulation of 4-quadrant bipolar switching (output swings between $V_{DC}$ and $-V_{DC}$).

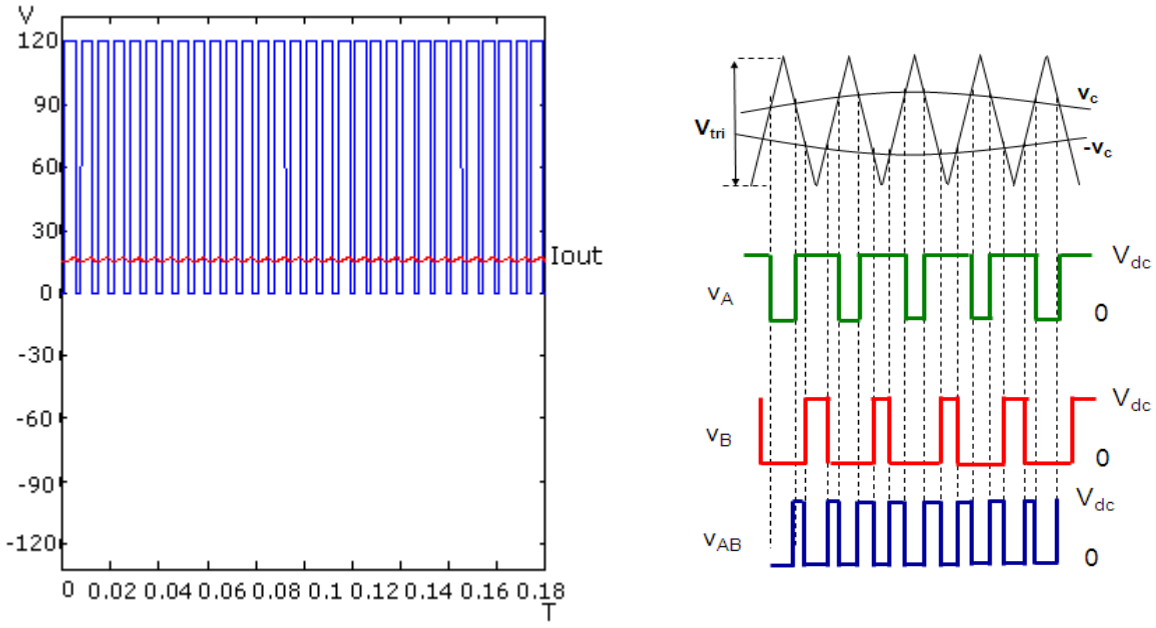


Figure 4.5: SPICE simulation of $V_{bus}$ and $I_{load}$ of unipolar switching scheme.
The ripple current is smaller and the frequency is doubled.

## 4.3 DESIGN OF THE PROPOSED VSD SYSTEM

Figure 4.6 shows the schematic design of the four quadrant variable speed drive (VSD) proposed in this study. The system essentially consists of a current controller and a phase switcher, together with other ancillary circuits. With regards to Figure 4.6:

*Current Controller:* The current controller block gets feedback from the current sensor which is positioned to detect the effective motor current, $I_{BLDC}$.

*Phase Switcher:* The phase switcher directs the current supplied by the previous stage into the correct motor phases based on the information provided by the rotor position sensors. The MOSFET driver power supply is shared by the current controller and the phase switcher modules. The MOSFET driver requires a supply voltage of 12VDC and the logic and analog components are separately supplied with 5VDC. The current controller and the phase switcher

are isolated from each other. A detailed description of the proposed four quadrant speed control system follows.

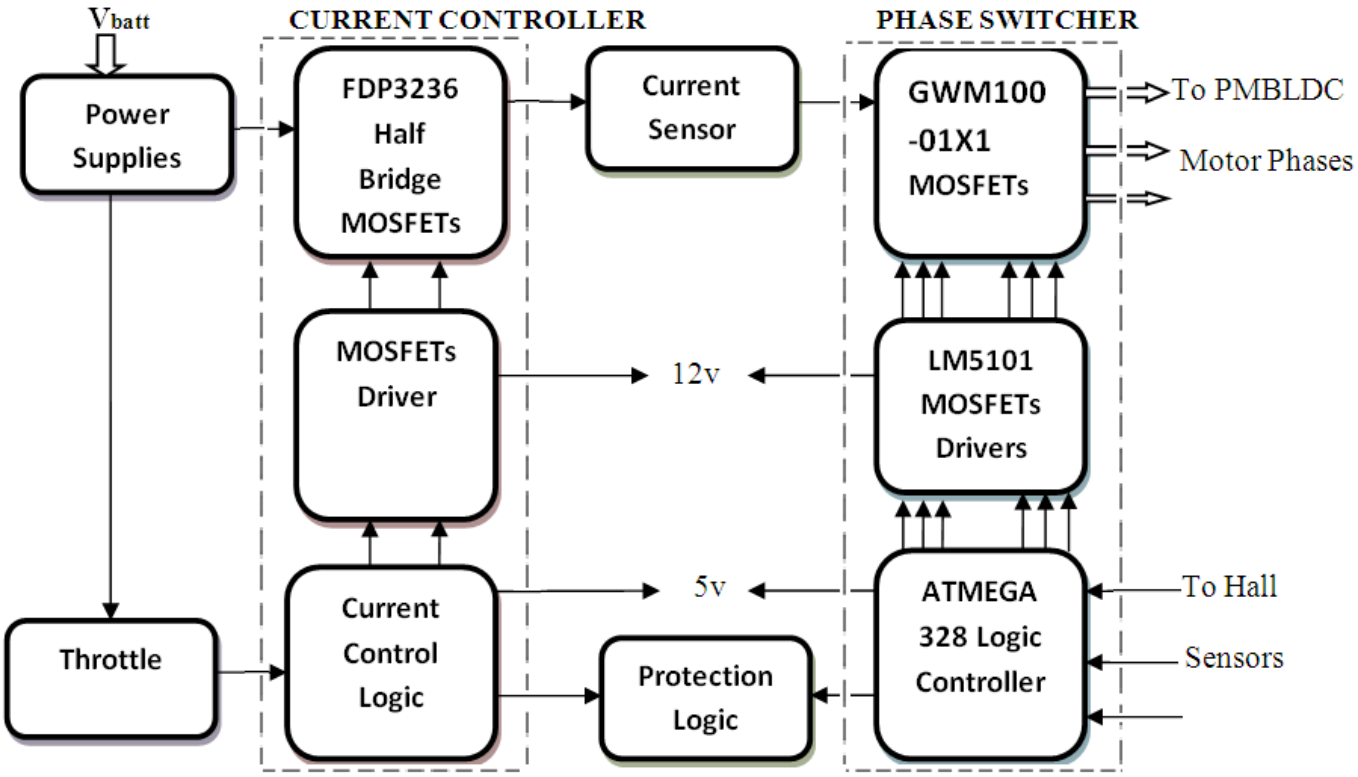


Figure 4.6: Four quadrant control system.

### *4.3.1 Three phase switcher design*

The GWM100-01X1 is a three-phase full bridge circuit with an isolated high voltage and current package. The bridge system has six temperature regulated trench MOSFETs in direct copper bonding (DCB) for driving the three phases of the BLDC motor as shown in Figure 4.8. It has a voltage and current rating of 100V and 90A, respectively and a switching frequency of 20 kHz (IXYS, 2009), and is suitable for a wide range of applications in automobiles and industrial vehicles where high power and torque are necessary. The phase switcher module of the VSD is

required to accept the inputs from the Hall-effect position sensors and use that information to effectively transform the BLDC motor into its DC motor equivalent. Figure 4.7 illustrates the schematic diagram of a complete phase switcher design. For this project, the DC bus voltage is maintained at 36V, and is the same as the voltage rating of the BLDC motor. The DC bus voltage is monitored with a protection logic controller.

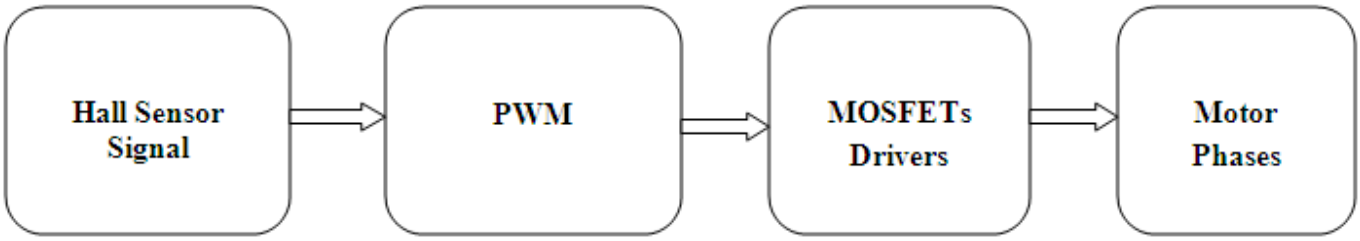


Figure 4.7: Phase switcher schematic.

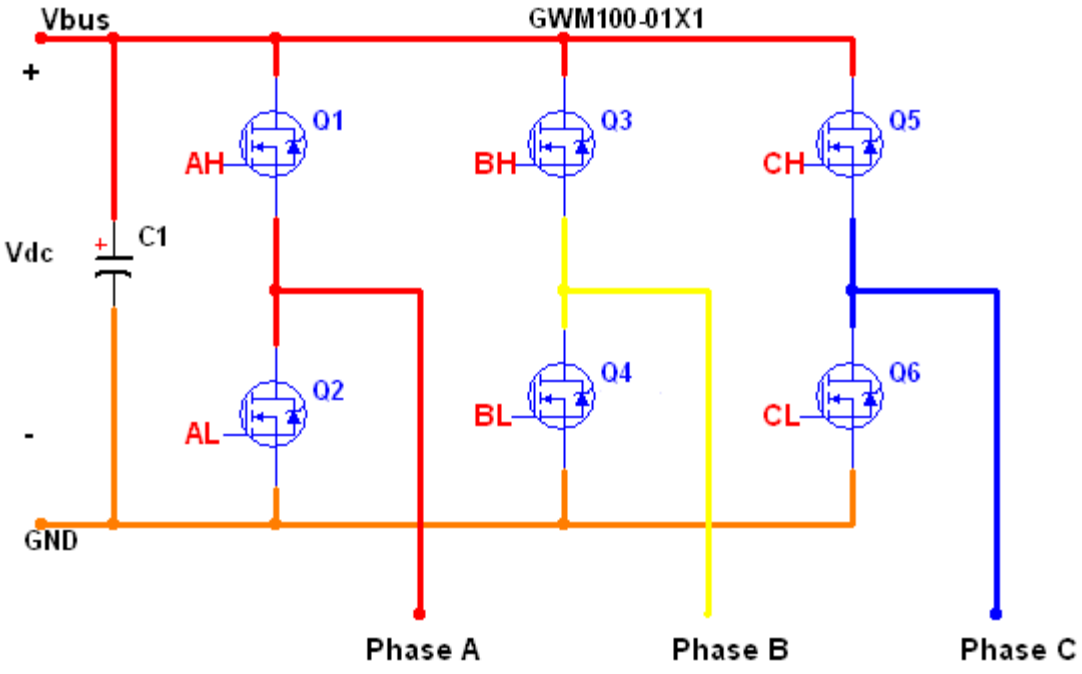


Figure 4.8: GWM100-01X1 – full bridge phase switcher.

### *4.3.2 Power MOSFET drivers*

A MOSFET driver is a power amplifier that accepts a low-power input from a controller IC and produces the appropriate high-current gate drive for a power MOSFET. The MOSFET gate driver is used when the pulse width modulation (PWM) controller cannot provide the output current and voltage required to drive the gate capacitance of the associated MOSFET. To fully turn these MOSFETs on, their gate voltage must be higher than the voltage at the source terminal. This voltage is easily provided for the low side switch (Q2) (cf. Figure 4.9). For the high side MOSFETs gate (Q1) the voltage must be 10V greater than the source terminal. This is achieved including an external bootstrap capacitor. Most of the half or full bridge drivers ICs have these circuits built in.

Three LM5101 MOSFET drivers provide six analogue outputs plus six PWM inputs and are used to drive the phase switcher. The MOSFET drivers switch at high speed whilst consuming low power (National Semiconductor, 2007). Bootstrap capacitors provide power to the upper switches of the half-bridge system. The outputs can be independently controlled according to the inputs from the Hall sensors. The inputs from the Hall sensors determine the sequence in which the three-phase bridge MOSFET is switched. The duty cycle of the PWM is directly proportional to the torque potentiometer input. The change in the duty cycle controls the current through the motor winding, thereby controlling the motor torque.

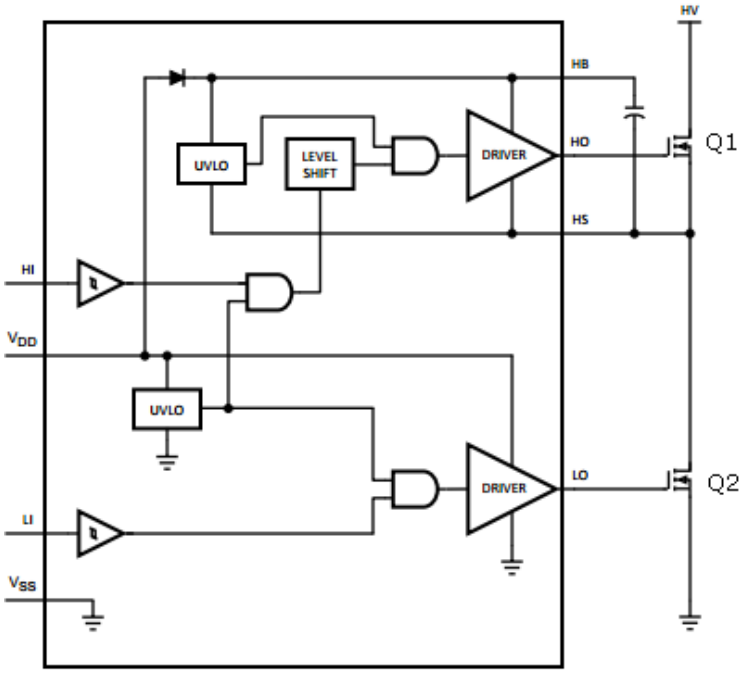


Figure 4.9: Schematic diagram of LM5101 MOSFET driver (National Semiconductor, 2007).

The MOSFET driver IC is designed to drive both the high side (Q1) and the low side (Q2) N-Channel MOSFETs in a half bridge configuration as shown in the schematic in Figure 4.9 and in the design in Figure 4.10. The drain of the high-side driver can operate with supply voltages up to 100V. It can provide currents up to 3A to drive the high speed power MOSFET. An integrated high voltage diode is provided to charge the high side gate drive bootstrap capacitor. A robust level shifter operates at high speed while consuming low power and providing accurate level transitions from the control logic to the high side gate driver. Under-voltage protection is provided on both the low side and the high side. Figure 4.10 shows the half-bridge for a single phase and all three phases will each utilize a similar circuit.

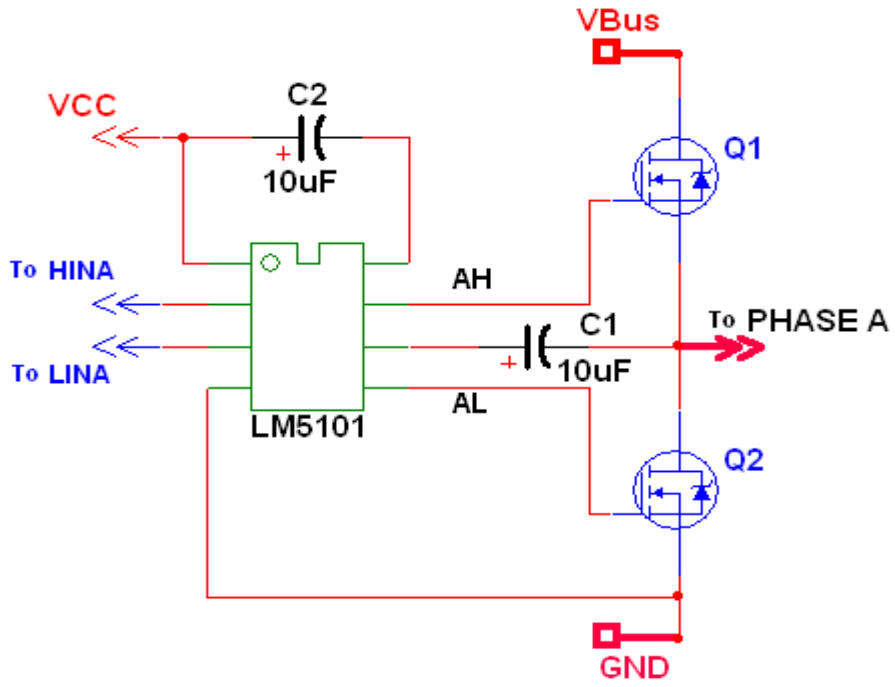


Figure 4.10: Half-bridge LM5101 MOSFET driver circuit.

### *4.3.3 Protection logic control*

To avoid both the high and low side MOSFETs switching on at the same time, a time delay logic control is implemented to control the PWM signal to operate only one half of the bridge at any one time. This prevents the occurrence of a short circuit condition which would destroy the power MOSFETs. The circuit shown in Figure 4.11 is constructed using a LM347 op-amp comparator. The comparator provides three input signals, the PWM signal and two signals for the high side or low side MOSFETs. These devices are low-cost, high-speed and JFET-input operational amplifiers. They require low supply current yet maintain a large gain-bandwidth product and a fast slew rate. In addition, their matched high-voltage JFET inputs provide very low input bias and offset current (Texas Instruments, 2005). This IC is used to create two

inverted signals with a rising edge delay time between the high side and the low side MOSFET gates. Some care must be taken to avoid a *current shoot-through* during the transition period where one switch is turned on while the other is turned off. The current shoot-through is avoided with the introduction of dead time using diodes. During the period of the dead time, the current circulation is through the body diode.

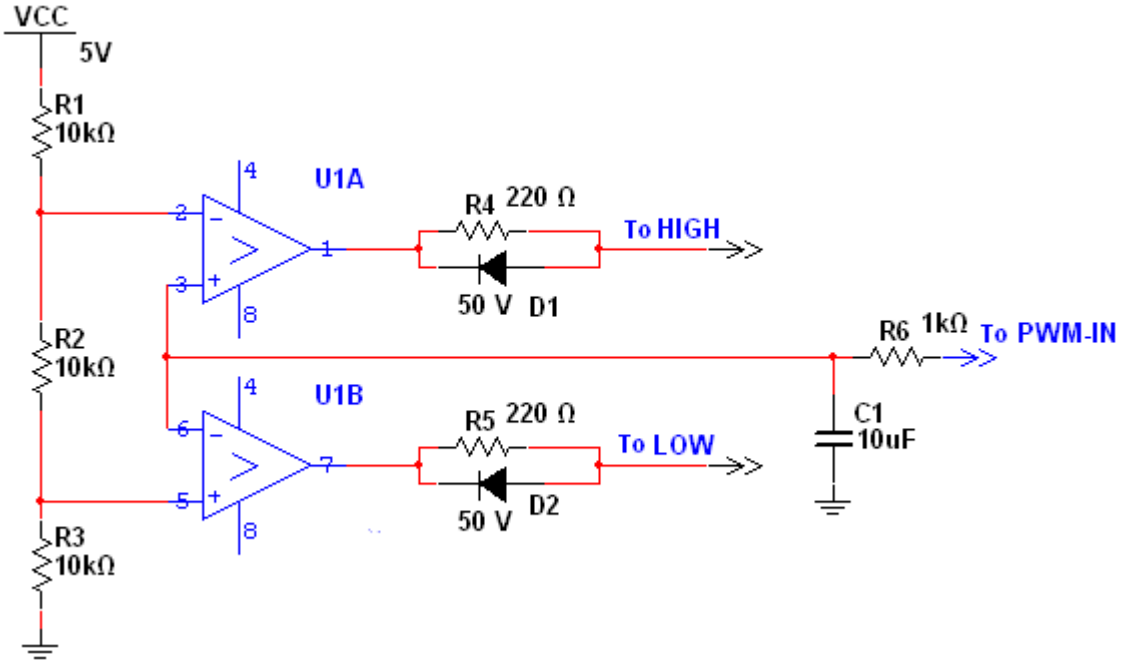


Figure 4.11: Protection logic control with dead time (The Hall effect sensors used in the motor requires pull up resistors of 10kΩ since they have open collector outputs. The resistor size affected the power consumption of the position sensor system and the signal to noise ratio. R4, R5, D1 and D2 were selected to match the application of the LM347 datasheet).

.

### *4.3.4 The ATMEGA328 Microcontroller*

The ATMEGA328 is a high performance controller used to control the rotation sequence of the motor. The device is a low power CMOS 8-bit microcontroller and has bi-directional I/Os ports with internal pull-up resistors (ATMEL, 2009). It also has 14 digital I/O pins, six of which are used as PWM outputs and six as analogue inputs with a 16 MHz crystal oscillator as illustrated in Figure 4.12. The controller is easy to programme as it takes basic logic instructions and

therefore, was programmed using PIC BasicPro compiler as shown in the coding in Appendix B. The rationale used for the software design is given in the flowchart shown in Figure 4.13. The logic circuit for forward and reverse control is given in Figure 4.14. The motor has three Hall sensors embedded into the stator, spaced $120^0$ apart. Each Hall sensor provides either a high or low signal based on the magnetic polarity closest to it. When the rotor passes near the Hall sensors, only two MOSFETs switch on to indicate the phase shift. The microcontroller generates a sequence control signal when the Hall sensors detect a new position. The rotor position is determined by analyzing the outputs of all three Hall devices.

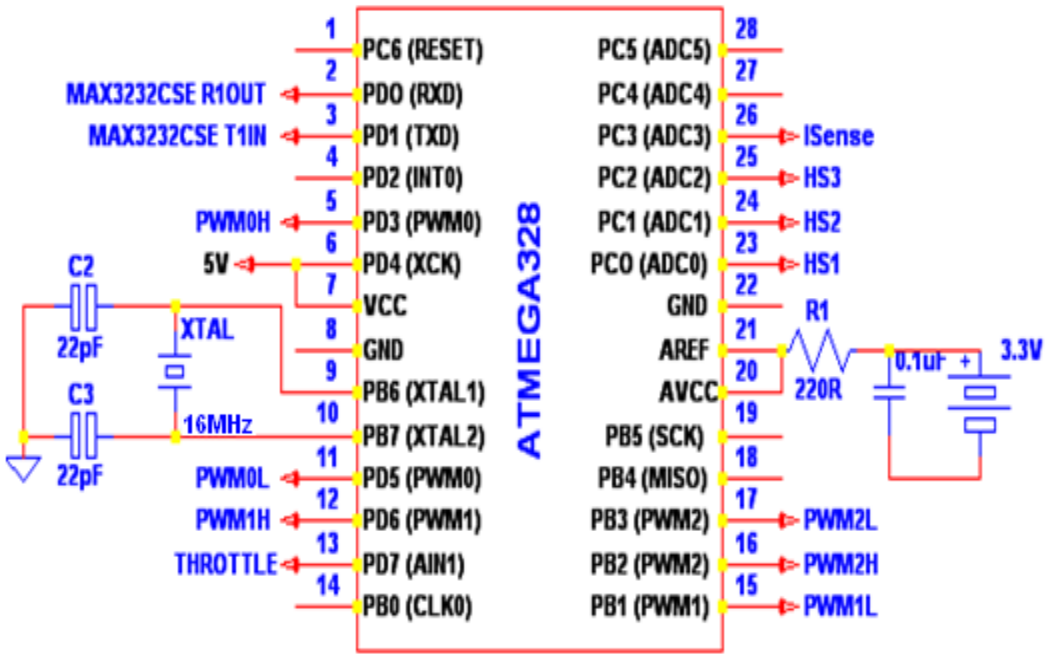


Figure 4.12: ATMEGA328 microcontroller for the logic control (ATMEL, 2009).

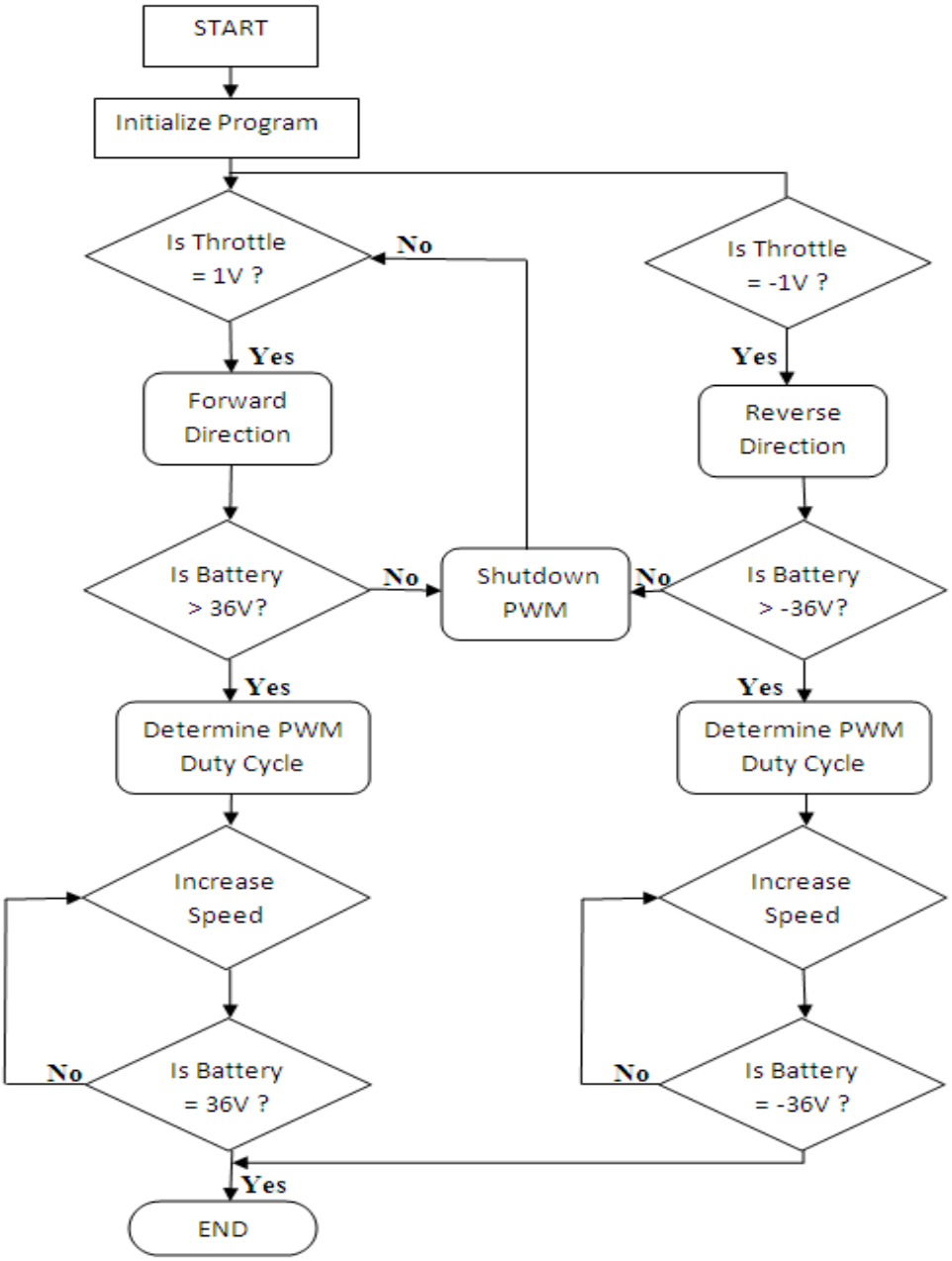


Figure 4.13: Flowchart for the controller.

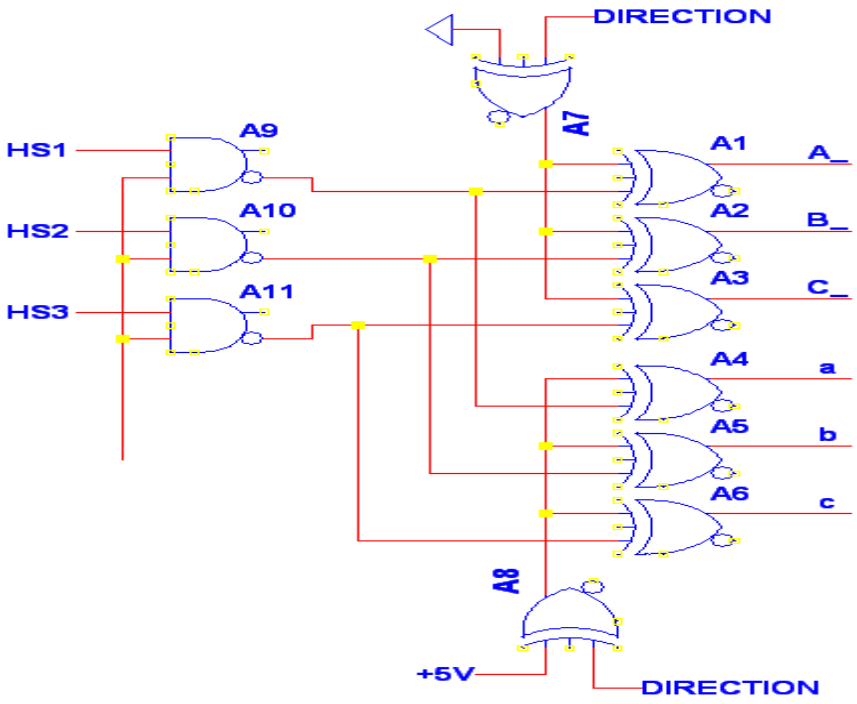


Figure 4.14: Logic control for Forward/Reverse.

### *4.3.5 Pulse width modulation*

The pulse width modulation (PWM) module is another device that is integral to the design. It provides the PWM signal to drive the power MOSFETs. The resolution of the PWM output is the level with which the duty cycle can be varied. It reads the position of the throttle via the ADC and adjusts the PWM duty cycle from 0-100% accordingly. The resistor values were chosen so that the duty cycle can be tuned from 0-100% using potentiometers. The PWM output was monitored by an oscilloscope to ensure that the duty cycle varied according to the position of the throttle. The ATMEGA328P contains a six-channel, 12-bit PWM module configured in this application to run in independent mode. The switching frequency is set to 10 KHz. The output on the individual channels is controlled according to the inputs from the Hall sensors. The inputs

from the Hall sensors determine the sequence in which the three-phase bridge MOSFET is switched. The duty cycle of the PWM is directly proportional to the accelerator potentiometer input. The change in the duty cycle controls the current through the motor winding, thereby controlling the motor torque.

The PWM modulation is performed by a six-channel timer/ pulse-width modulator (PWM) module. The modulation techniques can be determined according to the motor supply voltage or according to the switching of the MOSFETs. *Unipolar control* occurs when the motor detects either the DC bus or zero voltage during one PWM cycle (Narayanan et *al.,* 2006). The ATMEGA328P PWM module can generate any type of PWM modulation technique for this application. Another consideration is the correct back-EMF sensing. One of the requirements for correct back- EMF sensing is that the back-EMF voltage is sensed when both semiconductor switches are conducting (Trzynadlowski and Legowski, 1994). The ATMEGA328P is capable of handling BLDC motor control with Hall sensors. There is a special mode in the capture and compare mode that handles the commutation logic with minimal software. It can handle motors with Hall sensors positioned $60^0$ or $120^0$ apart.

The trapezoidal control of a BLDC means that, at any time only two of the three phases are energized whilst the other phase is kept floating (Kang and Sul, 1995). The slow decay method is the usual modulation method where during the off period of the PWM, the load current is allowed to circulate in the bottom switches. The fast decay method is when all the switches are off during the off period of the PWM. To improve the efficiency of the system, the synchronous rectification method can be used during high load. Instead of letting the load current circulate in the body diode during the off PWM period; it is more efficient to let the current circulate in the

switch itself **(**Thiyagarajan and Sekar, 2012**)**. This means that both the top and bottom switches of the same bridge need to be modulated instead of just the top switch. Figure 4.15 is used to implement this. There is also the fault detection capability of the controller where the output to the three-phase drivers can be immediately turned off when a fault is detected. The ADC conversions can be automatically triggered by the timers. It can be set to perform conversions at the ends of the ON or OFF periods of the PWM. If the conversion needs to be performed at another point of the PWM, another timer can be configured in the single shot mode to start counting at the beginning of every PWM.

In a PWM converter, the output is usually derived from a voltage source that is switched on and off very quickly and then filtered to produce a steady voltage or current at the output. In the case of the current controller the motor inductance can be used as the filter element. The current controller utilizes this to reduce the number of components in the VSD. Choosing a tolerance band for the current signal requires the switching frequency of the current controller. The rate of change of current in an inductor is determined by its inductance and the voltage across the inductance. The time between each current controller switching event can be deduced from:

$$V_L = \mathrm{L} \times \frac{\Delta \mathrm{I_L}}{\Delta \mathrm{t}} \ \therefore \ \Delta \mathrm{t} = \mathrm{L} \times \frac{\Delta \mathrm{I_L}}{\mathrm{V_L}} \qquad \text{(Equation 4.1)}$$

With regards to equation 4.1, $\Delta I_L$ is the magnitude of the tolerance band of the current controller, L is the inductance, $V_L$ is the voltage across the inductor and $\Delta t$ is the change in time.

For a 12V PWM with a rise time of 40μs and a fall time of 10μs, the period (T) = 50μs.

$$\therefore Duty\ Cycle = \left(\frac{\mathrm{t_{on}}}{\mathrm{T}}\right) \times 100\% = \left(\frac{40\mu s}{50\mu s}\right) \times 100\% = 80\% .$$

Therefore, the switching frequency: $f_s = \frac{1}{50\mu s} = 20\mathrm{kHz}$ and the average voltage:

$$V_{ave} = 12 \times 0.8 = 9.6V$$

For a 50% duty cycle: $V_O = \frac{1}{2}V_{in} = \frac{1}{2} \times 12V = 6V$

Therefore to achieve 5V required for the voltage reference:

$$V_o = \left(1 + \frac{R1}{R2}\right) \times V_{ref} = \left(1 + \frac{10 \times 10^3}{10 \times 10^3}\right) \times 2.5V = 5V$$

The current ripple was chosen to be 1A due to the increasing motor core losses and torque ripple. The maximum switching frequency of the tolerance band was around 10kHz. The 100kΩ resistors are connected to $V_{cc}$ where it combines with the 10kΩ resistors to form thevenin equivalent voltage of:

$$V_{Thevenin} = 12V \times \frac{\frac{100 \times 10}{100 + 10}}{100 + \frac{100 \times 10}{100 + 10}} = 999.99mV$$

The comparators are configured to produce a low output when the current sensor signal leaves the tolerance band. These signals then propagate through the inverter to generate MOSFET gate signals Hin and Lin.

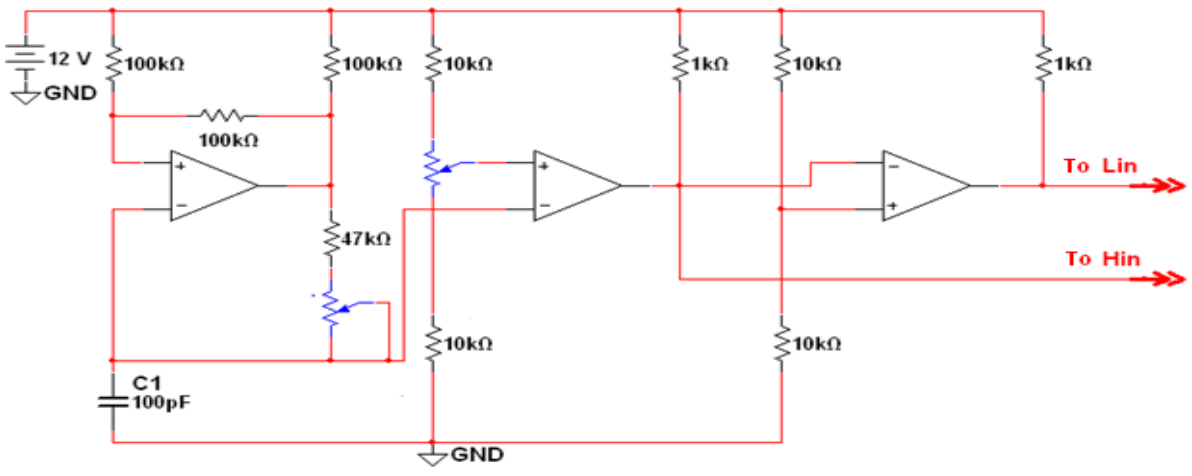


Figure 4.15: Pulse width modulation control circuit.

### *4.3.6 Current controller*

The brushless DC motor with trapezoidal torque characteristic is used in this application. It has high permeability permanent magnets on the rotor and a 3-phase, star-connected stator winding, which derives its power from a standard 3-phase pulse width modulated (PWM) inverter. The current controller controls the commutation of current from one motor phase to another, based on rotor position information. The current during an active phase of a BLDC motor is proportional to the torque produced by it. The VSD controls the output torque and therefore the current of the motor in the drive system. In order to maintain high efficiency, a switching converter design is used in the controller which requires an output filter to produce steady currents or voltages. Control of the exact current magnitude is achieved using one of the following three methods:

- Constant-frequency peak detecting, with turn on determine by the clock pulse time.
- Tolerance band control.
- Constant-"off"-time, peak detection control.

Tolerance band current control is used in the design of our current controller in this design. Table 4.1 compares the three current control schemes with the requirements of BLDC motor control. In the above current control schemes, the current can change at a very low rate, which can lead to a large deviation in the precision of switching sequence. The switching pattern can contain a frequency that is undesirable. To alleviate this problem, the current slope compensation technique is used to effectively increase the rate of change of current and restore the precision of switching events. The average current mode control applies the principle behind slope compensation to obtain better performance over a wide range of current.

Table 4.1: Comparison of Different Current Control Methods (Dake and Ozalevli, 2008)

| METHOD | ADVANTAGES | DISADVANTAGES |
|---|---|---|
| **Tolerance band control.** | • Easy to achieve 100% duty cycle.<br>• Fastest possible response.<br>• Always using actual current for decisions.<br>• Can detect loss of control at any time.<br>• Current ripple is constant. | • Wide variation in frequency range. |
| **Constant-"off"-time, peak detection control.** | • Less sensitive to switching events.<br>• Constant frequency operation possible with time-off adjustment. | • Difficult to achieve 0% duty cycle because of the switch on after time off.<br>• Average current is not directly related to the current peak control variable.<br>• Unable to detect loss of current control during time off.<br>• Wide frequency range of operation. |
| **Constant-frequency peak detecting, with turn on at clock pulse time.** | • Easier to design filter elements for constant frequency case.<br>• Less sensitive to switching transients. | • Unable to detect loss of current control during time off.<br>• Duty cycle is not always constant for constant output leading to sub-harmonic oscillation. |

The current control method depends on accurate current sensing to achieve torque control. A *sense resistor* and the *MOSFET's on condition resistance* methods are the easiest methods of achieving current control. However, the variation of resistance of a MOSFET is large and requires compensation to achieve an accurate result (Zhang et *al*., 2004). Accuracy is critical to protect the power MOSFETs from over current which could easily damage them. Current sensing in the motor's power stage can be done using either *current sensing resistor, current transducer or Hall current sensors*.

*Hall-effect current sensors* measure the current flowing through a conductor over a wide frequency range. They can be used to determine the current flowing by measuring the magnetic field created by the flowing current. The Hall sensors lack sensitivity and stability over temperature (Dixon and Leal, 2002). A current transducer is also a form of current sensor with built-in electronic interface that provides a digital or analog output signal. These are very simple to use as there is no need to design interface and op-amp circuits as these are included in one integrated circuit. *Resistor current sensing* is usually used for lower power motor controls. This is the cheapest way of measuring motor current. It is achieved by placing a resistor in series with the current to be measured and reading the voltage developed across the resistor.

The resistance of a current sensor resistor is very low and is usually rated to produce a voltage in millivolts (Karthikegan and Sekaran, 2011). Electromagnetic interference (EMI) and noise can occur due to the low voltage output of the sensor and the high gain amplifier required. Therefore low pass filters can be used in the amplifier design as shown in Figure 4.16. Op-amps are used to amplify the voltage developed across the resistor to the maximum level as indicated in Figure 4.17. The VSD is designed to operate at a maximum of 1.5kW. For a battery voltage of 36V and 50V, the required current capability of the VSD is:

$$I = \frac{\text{maximum controller Power}}{battery\ voltage\ range} = \frac{1500}{35V\ to\ 50V} = \text{30A to 42A} \qquad \text{(Equation 4.2)}$$

For the BLDC motor having a power rating of 500W used in this application, the sensing resistor current will range from of 10A to 14A.

The PMBLDC motor is first connected to the phase switcher module which uses the six power MOSFETs to transform the motor phase connections into DC motor armature connections. The

current sense module is placed after the phase switcher to simplify measurement and interpretation of the current signal. A specialized 5mΩ resistor sensor was used to sense the current flowing through the motor. This single resistor method eliminates the problem of balancing gains experienced with multi-sensor methods. The size advantage makes it an ideal component of controller designed for electric bicycles, robotic or aerospace applications. However, some noise is injected into the current signal and the entire current control requires current filter design to ensure good performance. The current controller module is designed to receive a single voltage signal that represents the current. A 500mA change in motor current should cause a 50mV change in the voltage signal from the sensor (Dake and Ozalevli, 2008). The resistors are chosen to create a potential divider on the non-inverting input of the operational amplifier since the output is in phase with input therefore the XOR is used to invert the output signals and the feedback resistor is used to determine gain of the system. Since the motor control is capable of regeneration, current must be measured in both directions. The maximum power dissipation for a maximum motor current is:

$$P_{\max} = I^2{}_{\max} \times R_{sense} = 30^2\, A \times 5m\Omega \;=\; 4.5W$$

The FDP3632 MOSFETs used have a nominal turn on resistance of 9mΩ which cause them to dissipate twice the power that the sense resistor dissipates at the same current level. The sense resistor had a maximum power dissipation of 5W and the voltage across the resistor per amp is 5mV/A. The amplifier gain Av can then be calculated as:

$$A_v = \frac{50mV}{5\text{mV}} = 10$$

The motor voltage changes from $V_{gnd}$ to $V_{batt}$ rapidly to achieve high efficiency. The MOSFETs used have capacitance between the drain and source which are discharged through the sense resistor, causing a high power current spike each time the motor voltage swings from $V_{gnd}$ to $V_{batt}$ and vice versa. The speed of the current spikes produces frequencies much higher than required for the components of the current signal. Therefore, the low pass filter is designed to reduce the high frequencies. The response of the filter depends on the resonant frequency and the value of the filter resistor for a given filter inductor and capacitor. The resonant frequency was chosen to be around 60kHz, to allow smooth flow of the motor current frequencies. The inductor was chosen to be 15µH and the capacitor 470nF to give a resonant frequency of 59.9kHz.

The resonant frequency is calculated by:

$$f_r = \frac{1}{2\pi\sqrt{LC}} = \frac{1}{2\pi\sqrt{(15\times10^{-6}[\mathrm{H}])\times(470\times10^{-9}[\mathrm{F}])}} = 59.941\mathrm{kHz} \approx 60\mathrm{kHz}$$

$$\therefore R_2 = \sqrt{\frac{4L}{C}} = \sqrt{\frac{4\times(15\times10^{-6}[\mathrm{H}])}{470\times10^{-9}[F]}} = 11.299\Omega \approx 12\Omega$$

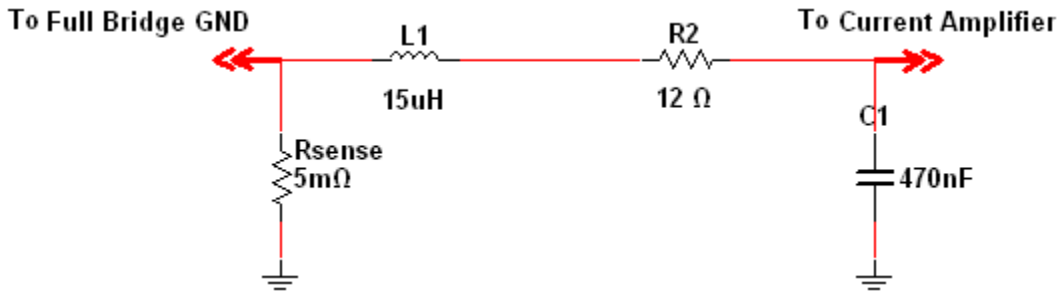


Figure 4.16: Current sense low pass filter.

With regards to Figure 4.17, the current sensor signal is combined with an offset voltage in the amplifier stage. The offset is set by R3 and R4 so that there is equal output swing for positive

and negative currents in sensor. The gain is set by the feedback resistor R6 so that ±30A can be measured by the amplifier. The throttle input used varies from 1V to 5V with higher voltages corresponding to higher or more positive demand torque. Therefore, the amplifier should be able to produce a more positive output for higher machine currents and this requires a non inverting amplifier configuration. The gain of the amplifier should be 10 as calculated. By setting R1 equal to R2, the offset voltage can be calculated as:

$$V_{offset} = \frac{V_{Rsense}}{2} + \frac{V_{cc}}{2} \qquad \text{(Equation 4.3)}$$

The resistors R1 and R2 are made equal to create a thevenin equivalent voltage source with an open terminal voltage of $\frac{V_{cc}}{2}$ and internal resistance $\frac{R_1}{2}$ or $\frac{R_2}{2}$, since R1 = R2.

The comparator uses an external resistor network to achieve Schmitt trigger operation. The strength of the positive feedback in the comparator, configured as a Schmitt trigger determines the difference between the input threshold and the tolerance band. The four quadrant controller has two comparators (cf. Figure 4.17) each managing a pair of thresholds. The $V_{high}$ and $V_{low}$ thresholds are set with R6. The lower resistance R5 increases the difference between the thresholds that comparator switches at, producing $V_{high}$ and $V_{low}$.

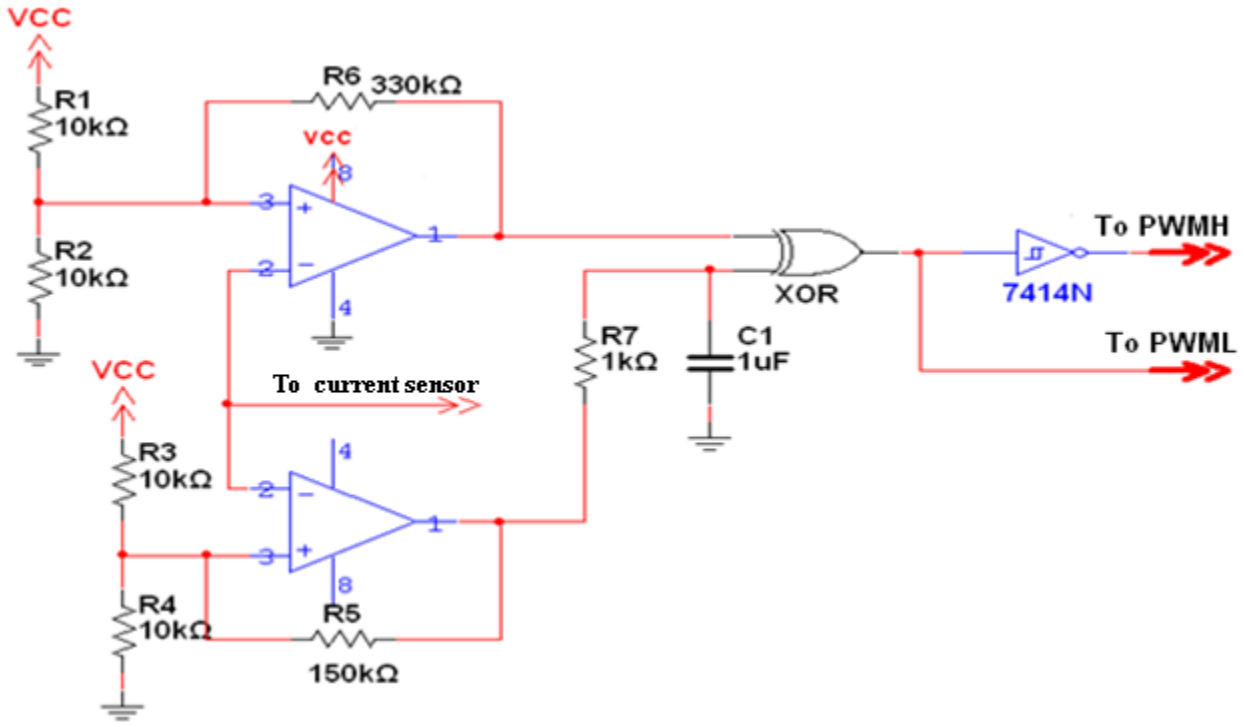


Figure 4.17: Current amplifier (The resistors R1, R2, R3, R4 and C1are typical values selected from the application of the TLV3502 comparator datasheet from Texas Instruments).

The current source half bridge is connected to the phase switcher power stage as shown in Figure 4.18. The sense resistor is positioned so that the load or motor current always flows through it. The half bridge applies $V_{battery}$ or $V_{grnd}$ to the phase switcher to increase or decrease $I_{bldc}$. $V_{bldc}$ is effectively the average value of the half bridge output. The current controller interprets the current sensor signal and the throttle signal to control the MOSFETs QCH and QCL (cf. Figure 4.18). They are used to apply a voltage to the BLDC motor through the phase switcher so that the current in the motor flows to the current demanded by the throttle signal. Figure 4.18 shows the position of QCH and QCL relative to the phase switcher and the supply. The voltage $V_{bldc}$, across the phase switcher is determined by $V_{battery}$ and the state of QCH and QCL.

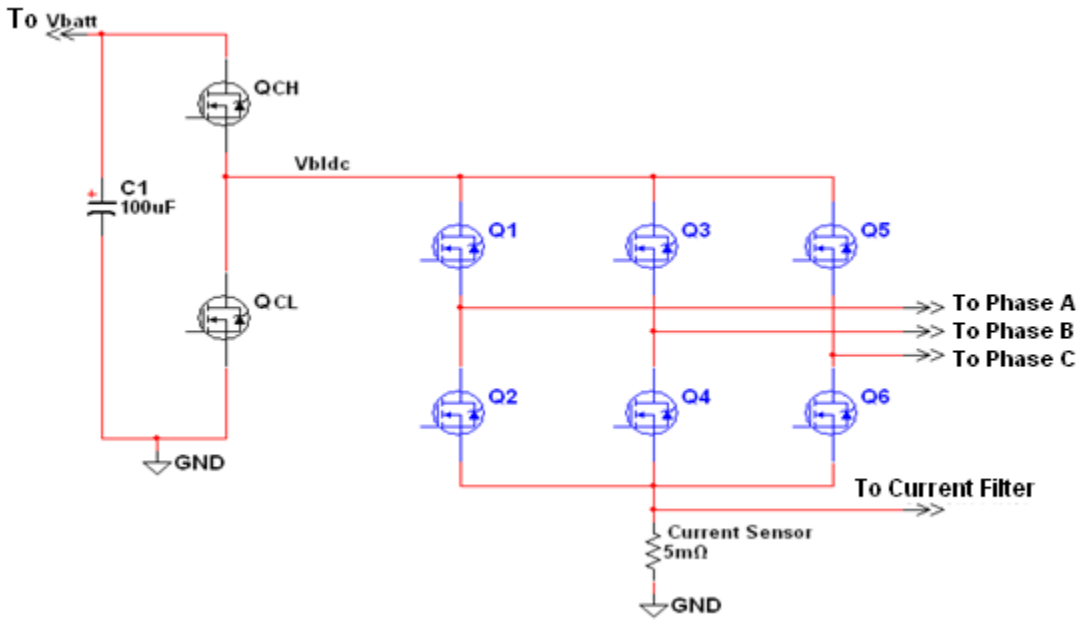


Figure 4.18: Current source half bridge connected to the power stage.

The current controller half bridge is connected to the common drain connections of the phase switcher through $V_{bldc}$. The power to the driver for QCH comes from the battery supply. The current amplifier gate signal generator supplies the high side and low side signals to the LM5101 MOSFET driver.

Figure 4.19 shows the current controller half bridge circuit and how the gate signals for the high side and low side are connected through the LM5101 MOSFET driver to control the switches QCH and QCL respectively. The diode and resistor arrangement on the gate of each MOSFET creates a dead time causing the turn-on of the power MOSFETs to be slower than the turn-off. The FDP3632 is an enhancement mode power MOSFET which only conducts when the gate voltage exceeds a certain threshold. The diode and resistor in parallel ensure that one switch is completely off before the other one turns on, to avoid large flow of current from $V_{batt}$ to $V_{gnd}$

during switching. The FDP3632 MOSFET has a breakdown voltage of 100V, a current rating of 90A, and a turn on resistance of 9mΩ. This gives it approximately a safety factor of two when handling the current and voltage requirements of the controller (Dixon and Leal, 2002). The LM5101 driver matches the breakdown voltage of the FDP3632 and provides up to 3A to drive the MOSFET gate. Suitable resistor and capacitor values are chosen according to the datasheet to create a uniform dead-time between the MOSFETs and the drivers to avoid damaging the MOSFEFs.

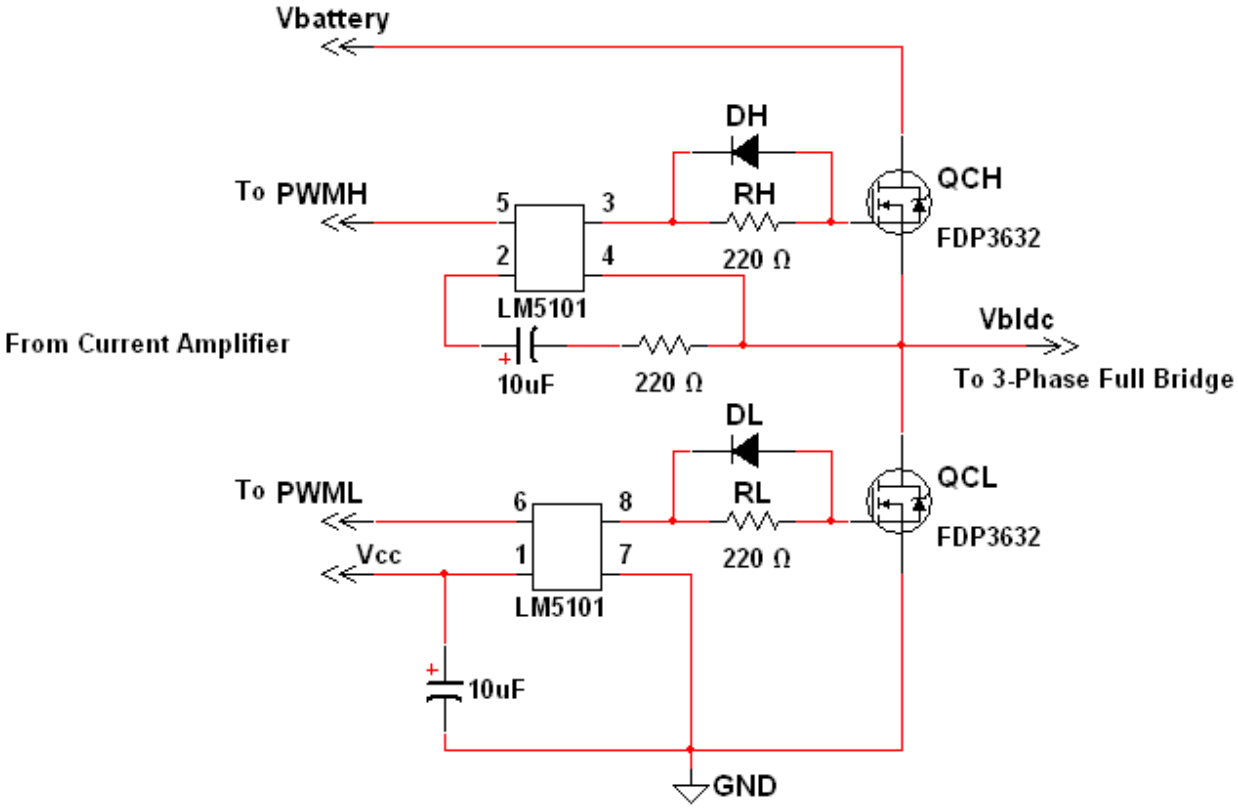


Figure 4.19: Current controller half bridge circuit.

### *4.3.7 Temperature control*

The temperature sensor is required to generate a signal when a certain temperature has been reached. The temperature sensor is implemented to detect excess heat levels from various components. With the circuits attached to the material of the stator, the heat levels in the circuitry and the motor becomes similar (Kim and Doose, 1997). Therefore, to work around this constraint, the temperature sensor design was integrated into the phase switcher circuit. Each phase switcher MOSFET has one logic gate with input signals from two position sensor signals. The temperature cut out circuit shown in Figure 4.20 uses three 1N4154 high speed switching diodes to simulate open collector outputs so that when the temperature threshold is reached all the Hall sensor outputs are driven to logic low.

The temperature control circuit has the effect of switching off all the MOSFETs in the phase switcher and prevents the electric motor from receiving any power from the battery. The temperature sensor is built around the same multi-function gate as the phase switcher logic. The SN74LVC1G58 from Texas instruments has input Schmitt triggers that give the temperature sensor different cut out and re-enable thresholds (Texas Instruments, 2013). The resistance of the thermistor decreases when it heats up causing the voltage at the input of the Schmitt trigger inverter in Figure 4.20 to decrease.

The values of R1 and R2 (cf. Figure 4.20) are calculated for the case of a thermistor that has 10k resistance at $25^0$C. To set the temperature trip points, the input thresholds of the gate and the thermistor resistance at certain temperatures must be known. The temperature cut out point was set at $75^0$C and the re-enable point was set at $40^0$C to ensure that the system had properly cooled

off before attempting operation again. The input thresholds for the logic gate were obtained by information in the data sheet; typical values were estimated to be 0.54Vcc for the rising threshold and 0.37Vcc for the falling threshold. The relationship of temperature to resistance in the thermistor was calculated using the Steinhart-Hart thermistor equation:

$$\frac{1}{T} = A + B \times ln(R) + C \times (ln(R))^{3} \qquad \text{(Equation 4.4)}$$

With regards to equation 4.4, A, B and C are constant coefficients, T is the temperature on the Kelvin scale and R is the resistance of the thermistor in Ohms. At $75^0$C, the resistance of the 10kΩ thermistor was ≈ 1.2kΩ and at $40^0$C the resistance was ≈ 4.3kΩ. The voltage at the input in Figure 4.20 can be calculated using the potential divider equation:

$$\frac{V_{in}}{V_{CC}} = \frac{R_2 + R_{thermistor}}{R_1 + R_2 + R_{thermistor}} \qquad \text{(Equation 4.5)}$$

The temperature cut out point varies from $100^0$C to $60^0$C, while the re-enable temperature varies from $40^0$C to $55^0$C.

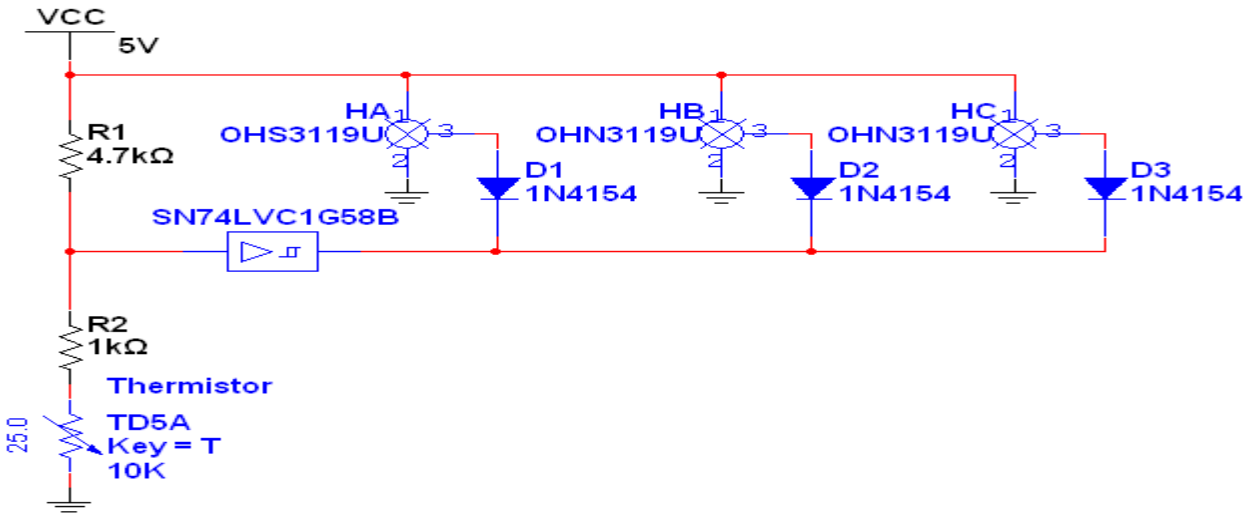


Figure 4.20: The temperature cut-out circuit.

### *4.3.8 Speed limitation*

A speed limiting circuit was designed to limit the motor speed to 500 RPM. This was necessary in order to prevent the controller from being overdriven. Infrared transmitter and receiver sensors were used to detect the number of revolutions per minute. The output from the sensor is a square wave pulse with a frequency proportional to the motor speed. The pulse is fed directly into the microcontroller and the speed is determined by measuring the frequency.

Therefore the LM2917 frequency to voltage converter is used to convert the frequency input into a voltage that can be measured by the microcontrollers ADC. The LM2917 tachometer IC from Texas Instruments is designed for a minimum external part count. The first stage of operation is a differential amplifier driving a positive feedback flip-flop circuit (Texas Instrument, 2013). The input threshold voltage is the amount of differential input voltage at which the output of this stage changes state. The differential input gives the option of setting the input switching level and still have the hysteresis for good noise rejection in any application.

The input stage is the bootstrap capacitor which converts the input frequency to a dc voltage. This requires a timing capacitor, one output resistor, and an integrating capacitor. Change in input state due to a differential voltage input, causes the timing capacitor to charge or discharge linearly between two voltages whose difference is $V_{cc}/2$. Then in one half cycle of the input frequency the change in charge on the timing capacitor is equal to the algebraic product of $0.5V_{cc}$ and C1. If the pulses of current are integrated with the filter capacitor, then:

$$V_{out} = I_c . R_1 = V_{cc} \times f_{in} \times C_1 \times R_1 \times K$$

(Equation 4.6)

With regards to equation 4.6**,** K is the gain constant and $f_{in}$ is the input frequency; $R_1$ and $C_1$ are chosen according to the data sheet for optimum performance. The size of $C_2$ (cf. Figure 4.21) is dependent only on the amount of ripple voltage allowable and the required response time.

The LM2917 has a built in zener diode for applications where an output voltage or current must be obtained independent of supply voltage variations. In this application, the optical sensor on the motor's shaft will produce a pulse for every revolution. For a maximum speed of 500 RPM, this equates to an input frequency of 100Hz. Figure 4.21 is used to convert the square wave signal into a voltage suitable for input into the microcontroller's ADC. The ADC module periodically checks DC bus voltage, DC bus current, and heat sink temperature. If these values go beyond the set limits, the motor is shut down.

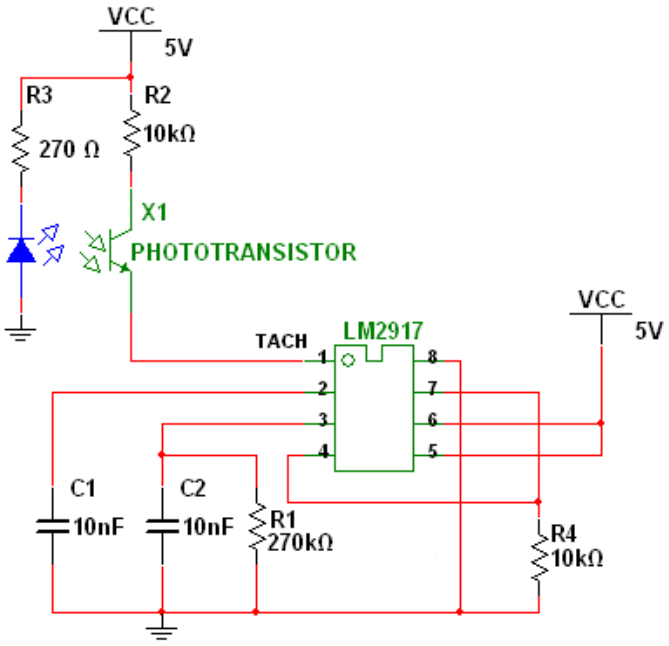


Figure 4.21: The LM2917 circuit.

### *4.3.9 Power supply design*

The power supply required to run the variable speed drive's control circuitry must be obtained from the 36V battery pack. Power supply in the VSD is based on switch-mode regulator approach. The battery voltage is stepped down to the MOSFET driver level by a switching converter and then further reduced by linear regulators to provide power to analog and logic devices. The control circuit requires 12VDC to drive the MOSFET gates and 5VDC for the rest of the circuit with minimum power consumption.

The lead-acid battery pack used in this application has a maximum voltage of 36V when fully charged, therefore the regulator must be able to operate at this maximum voltage level. A switch-mode power supply is used to step the voltage down to 12V with minimal loss. The switch-mode power supply has a low power dissipation compared to conventional linear regulator.

#### *4.3.9.1 MOSFET driver supply*

The MOSFET driver creates a high power gate drive signal from a low voltage input signal. The driver integrated circuit (IC) only operates if the voltage supply to the output buffer is at the maximum level that ensures complete switch ON of the MOSFET. The single chip switch-mode power supply (SMPS) from Texas Instruments was selected to create a 12V supply for the MOSFET drivers because it can operate with high input voltages with a low quiescent current. The LM2576 from Texas Instruments was used to regulate the battery voltage down to the required level for the MOSFET drivers. The LM2576 has an ON/OFF pin used to activate the device. This pin has a Schmitt trigger which is activated by a positive voltage greater than 1.6V (Texas Instruments, 2013) and only deactivated once the voltage at the pin falls 100mV below

the switch ON voltage. In order to protect the battery from excessive discharge the values of R1 and R2 (cf. Figure 4.22) were chosen to cause turn on or off at any voltage level.

This IC has its own bootstrap supply for the power switch and works off input voltages of up to 60V. The LM2576 series of regulators are integrated circuits that provide all the active functions for a step-down (buck) switching regulator, capable of driving 3A load with excellent line and load regulation. Requiring a minimum number of external components, these regulators are simple to use and include internal frequency compensation and a fixed-frequency oscillator. External shutdown is included, featuring 50µA standby current. The output switch includes cycle-by-cycle current limiting, as well as thermal shutdown for full protection under fault conditions (Texas Instruments, 2013).

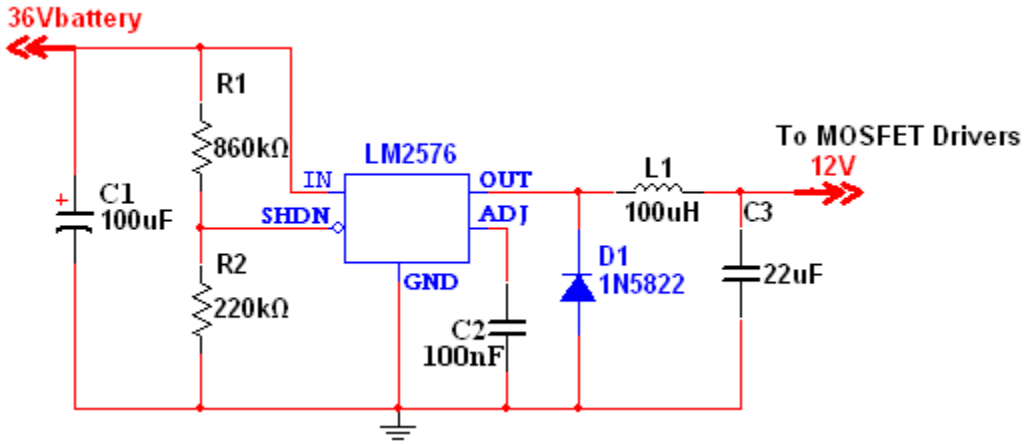


Figure 4.22: LM2576 voltage regulator with an output of 12V for the MOSFET drivers.

### *4.3.9.2 Logic gates and analog supply*

The LM7805 linear voltage regulator IC was used to provide the 5VDC, 1A supply to power the microcontroller and its associated circuits. The controller components are sensitive to power

supply variations especially if there are quick transients as in a switching regulator. The linear regulator from Fairchild semiconductor was chosen for the purpose of powering the more sensitive digital and analog circuitry. The MOSFET driver power supply provided a suitably low voltage to energize the regulator. Figure 4.23 illustrates the circuit diagram of the 5VDC power supply.

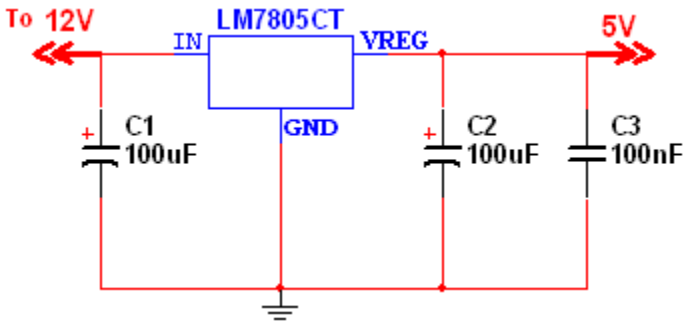


Figure 4.23: 5V Supply using LM7805 voltage regulator.

### *4.3.10 Regenerative braking*

Regenerative braking occurs when the motor operates as a generator. Regenerative braking brakes the motor by converting its mechanical energy into electrical energy and sending it back to the batteries (Britten *et* al., 2007). During braking the PMBLDC motor will generate back EMF which is rectified by the three phase full bridge phase switcher and filtered to DC voltage to charge the battery. The back EMF produced is greater than the DC bus voltage in the second quadrant of operation (Daniel and Patrick, 2012). This causes the current to reverse and oppose the motor torque whilst the motor is running in the forward direction. For current to flow into the battery, the DC bus voltage should be higher than the battery nominal voltage. The battery types chosen for this project are lead acid with a nominal voltage of 12V and a 12AH capacity. Current is usually lost as friction on the bicycle wheel during deceleration (Thiyagarajan and Sekar, 2012) and the current amplifier (cf. Figure 4.17) is used to boost the current for regeneration.

The recovered energy can be stored in an electric energy storage system and subsequently used for the propulsion. This significantly reduces the overall energy consumption of the bicycle and has the potential to minimize exhaust emissions of automobiles powered by internal combustion engines (Zeng *et al*., 2012). A well designed regenerative braking system can increase the driving range of the bicycle and also enhances its safety. The core of the system is represented by a boost converter with FDP3632 power static switches which is connected to the bus voltage as shown in Figure 4.24. The control system measures the battery and the bootstrap capacitors bank voltages, the charging state, the speed and the instantaneous currents on the bootstrap capacitors. The microcontroller then uses these quantities to generate a commutation sequence for controlling the power MOSFET switches.

#### *4.3.10.1 Regenerative braking power status circuit*

This circuit is used to examine the regenerative power status by checking the magnitude of voltage at the output of the circuit. It compares the battery voltage to the back EMF from the motor. The regenerative braking power control circuit operates by transmitting a signal to the boost converter when the output voltage is greater than the input voltage. It only operates when regenerative braking is taking place and switches OFF when the batteries are fully charged. It compares the input voltage with the output voltage and a result of the voltage difference causes control transistor Q1 to turn ON (cf. Figure 4.24). The current driven by the transistor (Q1) passes through R3 and R2 to ignite the gate of the FDP3632 to switch ON whilst D3 and D2 regulate the voltage at the gate to prevent over voltage as shown in Figure 4.24.

#### *4.3.10.2 Boost converter design*

The lack of economically priced energy storage device that provide high power density and high energy density has been the main problem to the acceptance of electric vehicles and bicycles as the main form of private and public transportation (Manoj et *al*., 2010). Therefore, there is a need for an energy management supplementary system to back up the power systems of electric drives. The electric bicycle in this project was powered with the 36V, 12Ah lead acid batteries which require a boost converter to charge the batteries during long distance riding. The required boost converter is shown in Figure 4.25. It can be operated in continuous current mode (CCM) and discontinuous current mode (DCM). This converter function is based on pulse width modulation (PWM). The PWM is sent from a microcontroller in order to control the FDP3632 to switch ON or switch OFF.

When the converter is energized, the FDP3632 will be turned on by setting the PWM to high (cf. Figure 4.25). This results in a positive voltage across the inductor, thus increasing the inductor current linearly. The output capacitor will discharge through the load resistance in order to provide continuous supply to the load. When it de-energizes, the current through the inductor will continue to flow in the same direction and therefore opposes any drop in current by reversing its electromotive force (EMF). Inductor L1 will be treated as a voltage source which is in series with the input voltage. The energy stored in the inductor will add extra voltage to the input voltage to boost the output voltage.

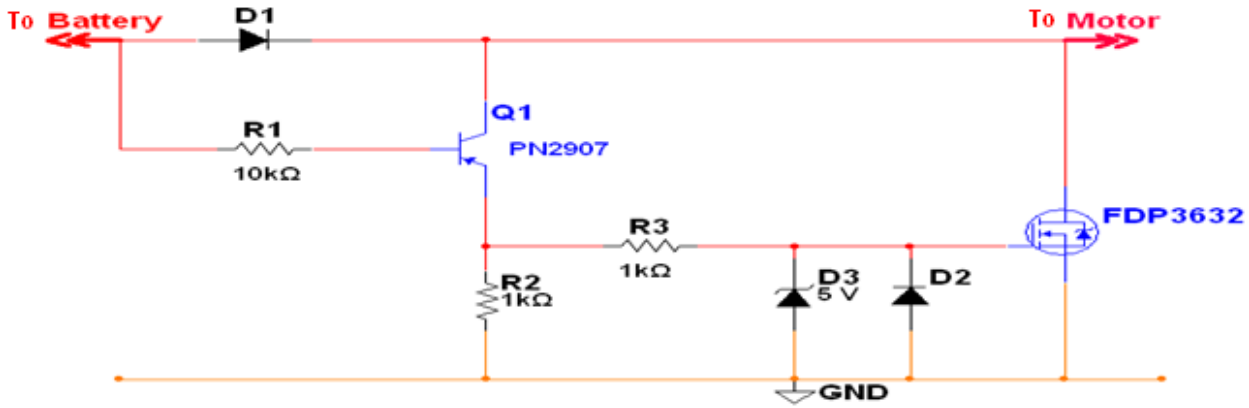


Figure 4.24: Regenerative braking power status circuit.

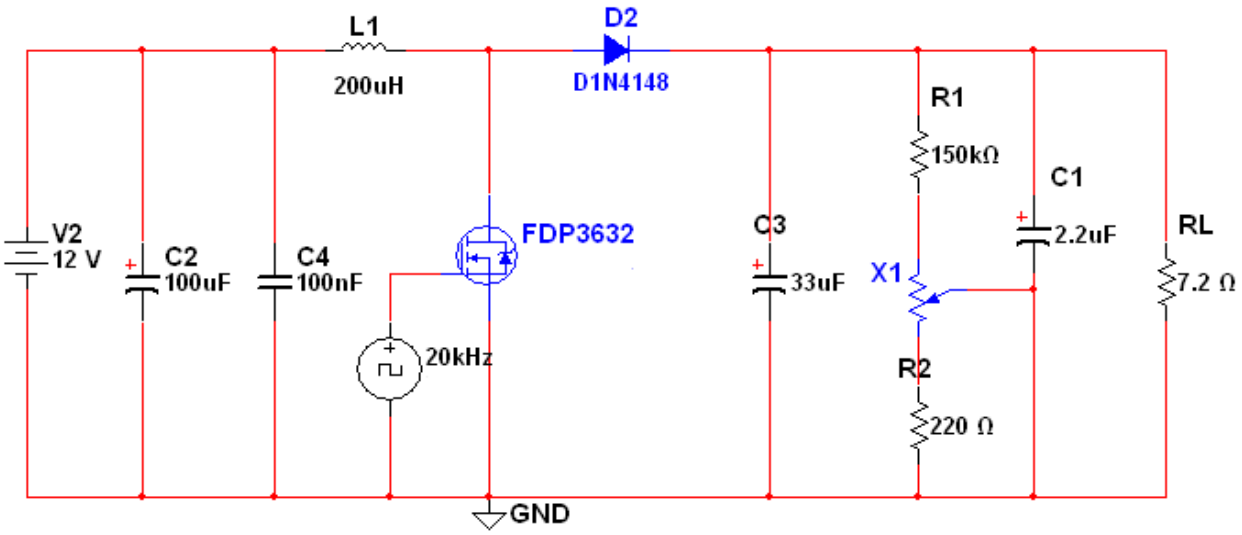


Figure 4.25: Boost converter for regenerative braking.

The Pulse Width Modulated boost converter was designed to operate with an input voltage of 12VDC - 16VDC, to provide an output voltage of 36VDC - 60 VDC. The output power should range from 250W – 500W at a switching frequency of 20 kHz – 100 kHz.

The maximum Duty Cycle at 90% Efficiency is given as:

$$D = 1 - \frac{V_{in}}{V_{out}} \times 90$$

(Equation 4.7)

$$\therefore D = 1 - \frac{12V}{40V} \times 90 \ = 0.7 = 63\%$$

Since the output power is 500W and voltage is 60V, the resistive load can be calculated as

$$R_L = \frac{V_{out}2}{P_{out}} \ = \frac{60^2[\mathrm{V}]}{500[W]} = 7.2\Omega$$

For an estimated inductor ripple current of 2.5A at a switching frequency of 20 kHz;

$$\therefore L = \frac{V_{in} \times (V_{out} - V_{in})}{\Delta I_L \times f_s \times V_{out}} = \ \frac{12[V] \times (60[V] - 12[\mathrm{V}])}{2.5A \times 20 \times 10^3[\mathrm{Hz}] \times 60[\mathrm{V}]} = 192\mu\mathrm{H}$$

(Equation 4.8)

With regards to equation 3.6, $L$ is the inductor, $V_{in}$ is the input voltage, $V_{out}$ is the output voltage, $\Delta I_L$ is the inductor ripple current and $f_s$ is the switching frequency.

At 50 kHz: $$T = \frac{1}{f} = \ \frac{1}{50 \times 10^3[\mathrm{Hz}]} = 20\mu s$$

$$\Delta I_L = \frac{V_{LON} \times T_{ON}}{L} = \frac{6[V] \times 10 \times 10^{-6}[\mathrm{s}]}{192 \times 10^{-6}[\mathrm{H}]} = 313\mathrm{mA}$$

$$V_{Cp-p} = \frac{\Delta I_L T}{8C} \ \ \therefore C = \frac{\Delta I_L T}{8V_{Cp-p}} = \frac{0.313[A] \times 20 \times 10^{-6}[\mathrm{s}]}{8 \times 0.01[\mathrm{V}]} = 78\mu\mathrm{F}$$

At 100 kHz: $$T = \frac{1}{f} = \frac{1}{100 \times 10^3[\mathrm{Hz}]} = 10\mu s$$

$$\Delta I_L = \frac{V_{LON} \times T_{ON}}{L} = \ \frac{6[V] \times 5 \times 10^{-6}[\mathrm{s}]}{192 \times 10^{-6}[\mathrm{H}]} = 156\mathrm{mA}$$

$$V_{Cp-p} = \frac{\Delta I_L T}{8C} \quad \therefore C = \frac{\Delta I_L T}{8V_{Cp-p}} = \frac{0.156[A] \times 10 \times 10^{-6}[\text{s}]}{8 \times 0.01[\text{V}]} = 19.5\mu\text{F}$$

### *4.3.11 Energy storage system*

Most vehicles presently use batteries for energy storage but there are vehicle designs in which ultra capacitors alone or in combination with batteries can increase the efficiency of the vehicle and lead to longer battery cycle life (Andrew *et* al., 2010). Energy storage devices can be compared based on energy and power density, endurance or life time and the cost as indicated in Table 4.2 and Table 4.3. Energy storage devices such as batteries, fuel cells and ultra capacitors are some of the required energy storage system for electric bicycles and vehicles. The energy density is the amount of energy that the device can hold per unit mass or volume which has a critical effect on efficiency and performance of the motor (Burke and Miller, 2009). The power density refers to the amount of instantaneous power that a device can produce consistently (Burke and Miller, 2009). Yen and Patterson (2001) proposed an energy management scheme that combines the super-capacitor with a battery technology to achieve an overall energy supply system with high power ability and high energy density.

For batteries, the input and output power is different depending on the present level of charge and the technology used (Burke and Miller, 2010). The endurance determines how long the device can store and reproduce its energy capacity. The batteries must provide both the energy and power required by the vehicle. In most cases the battery is oversized to store much more

energy than is used by the vehicle in order to achieve long life cycle (Andrew *et* al., 2010). And in some cases, the batteries can be optimized for energy density and life cycle and ultra-capacitors can provide the power both for acceleration and regenerative braking (Burke and Miller, 2009). The high energy and high power density ultra-capacitors are a new technology used in electric vehicles and bicycles. The ultra-capacitor system is comparable to a fossil fuel or fuel cell system in terms of input and out power of the energy storage system.

Battery technologies each have specific charge and discharge characteristics as compared in Table 4.4. The voltage limit for batteries in EV systems should be considered when controlling the output and input power during motoring and regenerative braking (Burke and Miller, 2009). The ultra-capacitor technology is a high density capacitor where charge and discharge rates can be very high and can be repeated often without damaging the device (Yen and Patterson, 2001). There is no conditioning of the input and output energy flow required for this type of energy storage.

Table 4.2: Energy, Power Density, Endurance and Cost of Energy storage System

| **Type** | **Energy** $Wh.kg^{-1}$ | **Power** $W.kg^{-1}$ | **Number of cycles** | **Cost** (as at Aug.2015) |
|---|---|---|---|---|
| Lead Acid battery (Panasonic,2011) | 18 - 40 | 25 - 80 | 200 - 600 | R300 |
| Ultra Capacitors (Maxwell Technology, 2013 | 2-30 | 150 - 5 100 | 200 000 | R1500 |
| Nimh battery (Batteryspace, 2013) | 40 - 85 | 200 - 600 | 2 000 | R 3000 |
| Li-polymer battery (Dixon Batteries, 2013) | 60 - 130 | 300 - 2 800 | 600 | R 2000 |
| $H_2$fuel Cell[2] (Ebay, 2014) | 33 600 | $8.4MW\ell^{-1}\ s^{-1}$ | N/A | R 4 380 |

Table 4.3 Energy storage unit requirements for various types of electric drives (Burkes *et* al., 2010)

| **Type of electric driveline** | **System voltage** | **Useable energy storage** | **Maximum pulse power at 90-95% efficiency kW** | **Cycle life (number of cycles)** | **Useable depth-of-discharge** |
|---|---|---|---|---|---|
| Plug-in hybrid | 300-400 | 6-12 kWh battery 100-150 Wh ultracapacitors | 50-70 | 2500-3500 | 60-80% |
| Electric | 300-400 | 15-30 kWh | 70-150 | 2000-3000 | 70-80% |
| Charge sustaining hybrid | 150-200 | 100-150 Wh ultracapacitors | 25-35 | 300K-500K | 5-10% |
| Microhybrid | 45 | 30-50 Wh ultracapacitors | 5-10 | 300K-500K | 5-10% |

Table 4.4 Comparison of Different Battery Types used in Electric Bicycles (Burke et al., 2009)

| **Battery Type** | **Advantages** | **Disadvantages** |
|---|---|---|
| Lead-Acid (sealed) | • Cheap and simple to manufacture.<br>• Reliable and well known technology.<br>• Low self-discharge<br>• Low maintenance | • Not to be stored in a discharged condition.<br>• Low energy density.<br>• The electrolyte and the lead content can cause environmental damage. |
| Lithium-Ion | • Highest energy density to weight ratio.<br>• Has a better cost-performance ratio.<br>• Li-ion-Cobalt is the most developed Li-ion technology. | • All lithium-ion technologies require a protection circuit to prevent overheating.<br>• Ageing depends on storage conditions.<br>• Can damage easily by over discharge. |
| NiCD | • Has Fast and simple charge<br>• Has good load performance<br>• Cheapest.<br>• Available in a wide range | • Relatively low energy density<br>• The NiCd contains toxic metals.<br>• Has relatively high self discharge. |
| NiMH | • Higher energy densities.<br>• Less prone to memory than the NiCd.<br>• Environmentally friendly | • Limited service life<br>• High self-discharge<br>• Performance degrades at high temperatures.<br>• High maintenance. |

### *4.3.12 Thermal design*

The thermal design section discusses the calculations of power dissipation and losses to ensure the devices operate within specification to maximize reliability. Conduction losses in both the high and low side of the bridge are calculated. Cooling is also implemented with the use of heat-sinks. Heat is the ultimate cause of all power MOSFET failures due to an electrical overstress of the device, extreme temperature and high peak power cycling (Agilent Technologies, 2008). Electrical overstress failures are caused by operating the device outside its safe operating limits. A power cycling failure involves mechanical and thermal stresses on the device experienced due to a low pulse width modulation duty cycle.

Changes in temperature cause materials in the device to expand and contract. Due to the range of materials used in the device, some parts have different coefficients of thermal expansion compared to others. This cyclic expansion and contraction can cause stresses at the interface between two different materials. The faster the change in temperature, the greater will be the stresses. In normal operation, the amount of power lost as heat can be estimated using specifications from the data sheets and this will determine the amount of cooling required.

The heat-sink required is determined by the conduction and switching losses in the power MOSFETs, the maximum junction temperature and power dissipation. The control system steady-state condition was analysed to determine the thermal characteristics of the design. Power dissipation in all the various components was calculated to ensure that the heat generated by the power MOSFETs is equal to the heat absorbed by the heat-sinks. The components data sheets give specifications of the thermal resistance of the semiconductors junction-to-package ($R_{\theta JC}$) which gives the ability of the component to conduct heat away from the junction.

#### *4.3.12.1 Power dissipation calculations*

The conduction loss in the power MOSFET is caused by the drain-to-source ON resistance of the MOSFETs($R_{\mathrm{DS(on)}}$) and switching losses caused by the switching ON and OFF periods of the MOSFETs. The GWM 100-01X1 has a maximum drain-to-source resistance ($R_{DS(on)}$) rating of 8.5mΩ with a minimum of 7.5mΩ. The conduction losses can be calculated by the following formula:

$$P_{\mathrm{D}} = {I_{\mathrm{D}}}^2 R_{\mathrm{DS_{(on)}}} \times D \qquad \text{(Equation 4.9)}$$

With regards to equation 4.9, $P_D$ is the power dissipation, $D$ is the duty cycle of the MOSFET, $I_D$ is the drain current and $R_{DS(on)}$ is the drain-to-source on resistance .

High power dissipation normally occurs when the MOSFETs are driven at 100% duty cycle. The desired maximum current of 30A in motoring mode was used in the final design for the electric bicycle. The maximum conduction losses for the high side MOSFETs at this current with the maximum $R_{DS(on)}$ of 8.5mΩ is shown in equation 4.10:

$$P_{\mathrm{D}} = {I_{\mathrm{D}}}^2 R_{\mathrm{DS_{(on)}}} \qquad \text{(Equation 4.10)}$$

$$= 30^2 A \times 0.0085\Omega$$

$$= 7.65W$$

With the high side of five MOSFETs, each MOSFET will dissipate 1.53W which is within the maximum power dissipation rating of 10W. Each MOSFET carries 6A at the maximum current of 30A which is below the MOSFETs maximum current rating of 90A. The regeneration current will be limited to 15A to protect the batteries from overcharging. The conduction losses in the low side of the full bridge can also be calculated as:

$$P_{\mathrm{D}} = {I_{\mathrm{D}}}^2 R_{\mathrm{DS(on)}}$$

$$= 15^2 A \times 0.0075\Omega$$

$$= 1.69W$$

The low side of the bridge also consists of three MOSFETs which will dissipate 0.56W each. This power is also within the maximum power dissipation of 10W. Since the actual value of $R_{\mathrm{DS(on)}}$ depends on the temperature variation of the device, it is necessary to include the temperature coefficient of $R_{\mathrm{DS(on)}}$ ) in the calculation. Therefore, the equation for conduction losses at a *specific temperature* is given as:

$$P_{\mathrm{D}} = {I_{\mathrm{D}}}^2 R_{\mathrm{DS(on)}}(1 + \delta\Delta_{\mathrm{T}}) \times D \quad \text{(Equation 4.11)}$$

With regards to equation 4.11, $P_D$ is the power dissipation, $I_{\mathrm{D}}$ is the drain current, $\mathrm{R_{DS(on)}}$ is the drain-to-source on resistance, $\delta\Delta_{\mathrm{T}}$ is the temperature coefficient of $R_{\mathrm{DS(on)}}$ in $°C^{-1}$ and $D$ is the duty cycle. The switching losses caused by the rise and fall times of the MOSFET are estimated as follows:

$$t_r = t_f = \frac{Q_G}{I_G} + \frac{L \times I_G}{V_{GS} - V_{TH}} \quad \text{(Equation 4.12)}$$

With regards to equation 4.12, $t_r$ is the rise time, $t_f$ is the fall time, $Q_G$ is the total gate charge, $I_G$ is the gate drive current, $L$ is the inductance of driver to MOSFET connection, $V_{GS}$ is the gate-to-source voltage and $V_{TH}$ denotes the gate turn on threshold (IXYS 2009). The switching losses can be calculated as below if the rise and fall times are known:

$$P_D = \frac{1}{2} I_D V_S (t_r + t_f) f \quad \text{(Equation 4.13)}$$

With regards to equation 4.13, $P_D$ is the power dissipation, $I_D$ is the drain current, $V_S$ is the input source voltage $t_r$ is the rise time, $t_f$ is the fall time and $f$ is the frequency of the PWM signal.

From the data sheet of the GWM 100-01X1 integrated circuit (IXYS, 2009), $I_D$ = 90A, $t_r = 95ns$ and $t_f = 55ns$ . The power dissipation from the 5- MOSFET circuit is:

$$\therefore P_D = \frac{1}{2}\ 90A \times 36V\ (95 \times 10^{-9}[s] + 55 \times 10^{-9}[s])20 \times 10^{3}[Hz]$$

$$= 4.86W$$

This is about 1W per MOSFET due to switching losses. Therefore the total conduction and switching losses is 2.53W (1.53W + 1W) per MOSFET on the high side of the full bridge.

There are also power losses in the freewheeling diodes which occur in the low-side of the full bridge when the circuit is operating at 50% duty cycle at an average current of 15A. The loss can be estimated by the forward voltage drop of the diode and the current flowing through it as follows:

$$P_D = V_{DS} I_D \qquad \text{(Equation 4.14)}$$

With regards to equation 4.14, $V_{DS}$ is the diode forward voltage and $I_D$ is the diode current. In this application, the maximum diode loss is calculated as follows using $V_{DS}$ of 1.2V from the datasheet:

$$P_D = 1.2V \times 15A$$

$$= 18W$$

The three diodes in the low side of the bridge will dissipate 6W each. The loss for the high side diodes also occurs during regeneration with a current of 10A. Therefore the loss is calculated as given below:

$$P_D = 1.2V \times 10A$$

$$= 12W$$

Therefore, the total calculated power dissipation in the switching MOSFETs in the motoring mode when operating at a current limit of 30A is 32.2W (18W + 4.86W + 1.69 + 7.65W). In the regenerating mode the total power dissipation is 12W. The heat-sink chosen easily dissipates this heat and protects the controller.

#### *4.3.12.2 Heat-sink requirements*

Heat transfer in a system can take place through conduction or radiation. The GWM 100-01X1 three phase full bridge is an isolated direct copper bonding package (IXYS, 2009). Therefore interface material is not needed; it is directly mounted onto the heatsink. The type of heatsink depends on the maximum power dissipation and thermal resistance to ensure the junction temperature of the components does not exceed their ratings (Agilent Technologies, 2008). The junction temperature can be calculated using equation 4.15.

$$T_J = P_D \left( R_{\theta JC} + R_{\theta Cs} + R_{\theta sa} \right) + T_a \qquad \text{(Equation 4.15)}$$

With regards to equation 4.15, $T_J$ is the junction temperature, $P_D$ is the maximum power dissipation, $R_{\theta JC}$ is the junction-to-case resistance, $R_{\theta Cs}$ is the case-to-heatsink resistance, $R_{\theta sa}$ is the heatsink-to-air resistance and $T_a$ is the ambient temperature. The value of $R_{\theta JC}$ for the GWM 100-01X1 is given is as 1K/W. The heatsink chosen for this design is able to dissipate sufficient heat to prevent dangerous junction temperatures under all operating conditions. And it is a suitable physical size to mount all the power MOSFETs. The total thermal resistance of the system can be calculated using the maximum desired junction temperature, maximum ambient temperature and the total power dissipation. Therefore the required thermal resistance of the

heat-sink for an estimated maximum power loss of 50W, a maximum ambient temperature of 25°C and maximum junction temperature of 150°C which is the maximum junction temperature of the GWM 100-01X1is given as:

$$R_{\theta TOTAL} = \frac{T_{max} - T_a}{P_D} \qquad \text{(Equation 4.16)}$$

With regards to equation 4.16, $R_{\theta TOTAL}$ is the total thermal resistance, $T_{max}$ is maximum junction temperature, $T_a$ is the maximum ambient temperature and $P_D$ is the power dissipation.

$$R_{\theta TOTAL} = \frac{150°C - 25°C}{50W}$$

$$= 2.5°C/W$$

The thermal resistance is low which requires a quality heat-sink. Therefore the heat-sink chosen for this design is the HS24 TO-3 solderable finish SMD heat-sink from Aavid Thermalloy. The heat-sink is designed with a minimum thermal resistance.

## 4.4 SUMMARY AND CONCLUSIONS

The hardware implementation in this chapter describes the design of a 3-phase BLDC motor drive system based on four quadrant operation method. The design is applicable to a wide range of BLDC motors. Though the design is confined to an E-bike, the control system can be further extended to other application areas which have a broad application prospects such as EV systems. The following chapter will describe the simulation studies that were conducted to assess the design of the proposed motor drive.

This page is intentionally blank

# CHAPTER 5

# SIMULATION STUDIES

## 5.1 INTRODUCTION

The PMBLDC motor and the proposed controller were simulated using the Linear Technology Simulation Program with Integrated Circuit Emphasis (LTspice IV). LTspice IV is a high performance SPICE simulator, schematic capture and waveform viewer with enhanced models for the simulation of switching devices. Linear Technology provides a variety of custom design simulation tools and device models to allow designers to quickly and easily evaluate circuits using high performance switching regulators, amplifiers, data converters and filters. The software was used to predict the operation of the VSD at any time during the control session. The generated voltages of the BLDC motor and the Hall Effect position sensor signals were simulated using periodic waveforms of different frequencies. The speed was varied to obtain results at different speed levels.

## 5.2 VOLTAGE AND CURRENT CONTROL

Voltage control uses PWM of the dc bus voltage ($V_{battery}$) for regulating the duty cycle and the average back EMF of the motor. Current control utilizes tolerance band current control (cf. section 4.3.6) to set the desired current level for the motor. Brushless DC motors with trapezoidal back EMF have concentrated windings, discrete magnets with no skew, and thinner steel which makes the motor inexpensive and easy to control (Colton, 2010).

Six-step commutation is common in controllers that use Hall effect sensors to detect rotor position (Narayanan, et *al*., 2006). For the design, the voltage controller uses six-step commutation to control the power MOSFET switches. The switching period of the motor's back EMF, which is dependent on the rotor's position and velocity, is divided into six $60^0$ segments. Each of these segments corresponds to a different Hall Effect sensor state which in turn switches a different power MOSFET. Figure 5.1 illustrates the trapezoidal back EMF and the motor current in a six-step commutation.

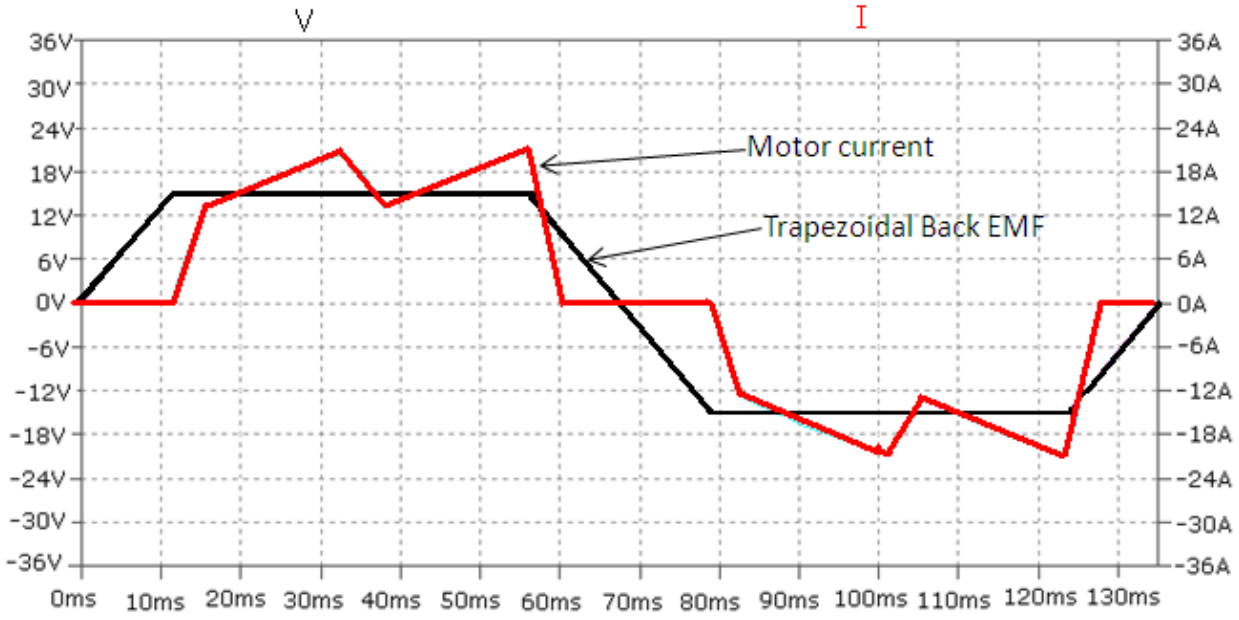


Figure 5.1: LTSPICE simulation of motor current resulting from six-step commutation.

For a 50% duty cycle, the average voltage applied to the motor will be half of the DC bus voltage. The average voltage increases as the duty cycle increases. The amplitude and offset can be controlled within the limits of the DC bus voltage. In Figure 5.2 the average voltage has an amplitude of 22V and an offset of 22V with a 44V DC bus voltage. The motor will operate

within its parameters of maximum speed, torque, voltage and power if all the three phases have the same offset. It will only detect the voltage difference between the phases.

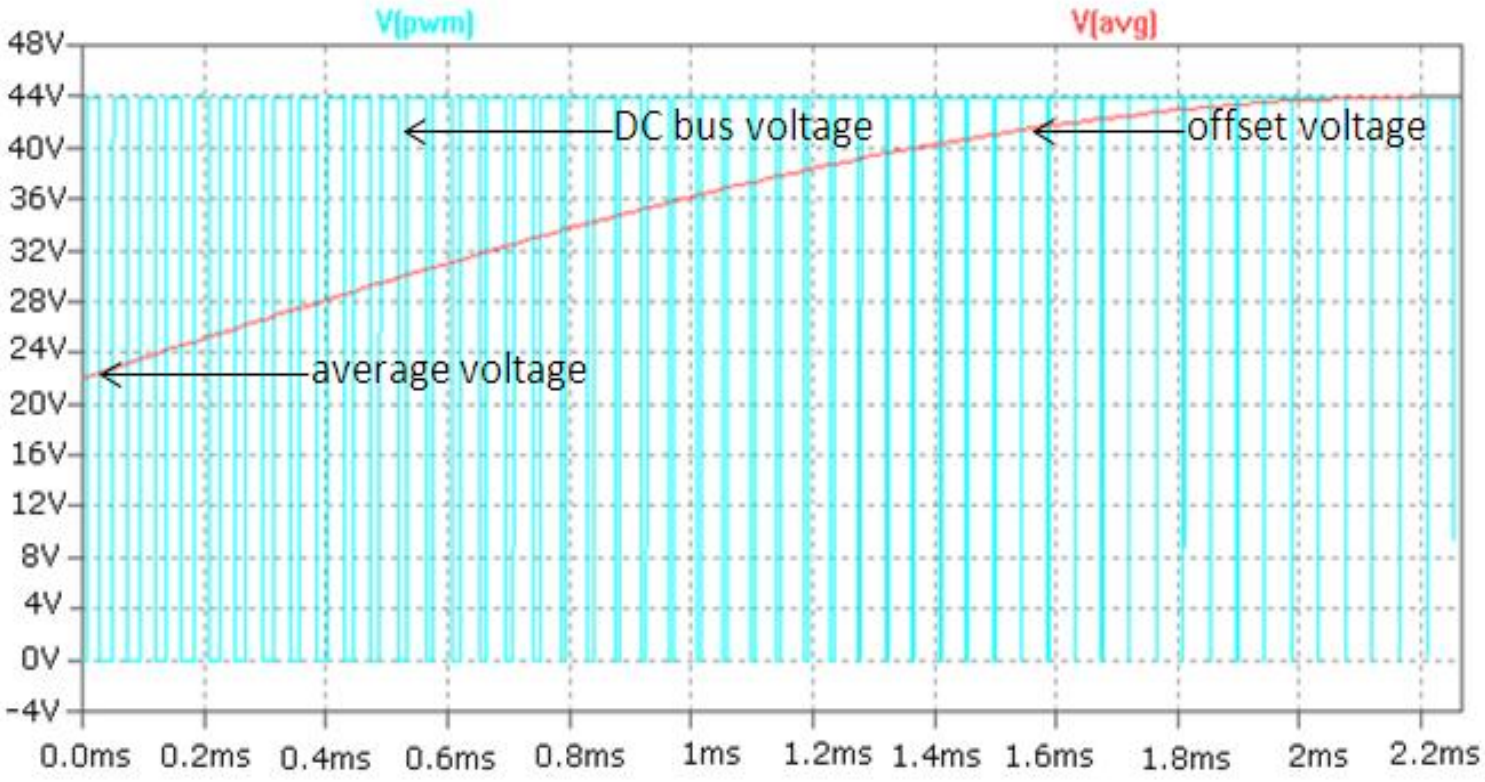


Figure 5.2: LTSPICE simulation of the DC bus voltage and the average voltage at 25 kHz PWM.

The current controller pushes the back EMF to $V_{battery}$ when a commutation occurs so that $I_{phase}$ builds up in the next active phase. Figure 5.3 indicates $I_{phase}$ and $V_{back\ emf}$ for a BLDC motor controlled with a fixed average voltage produced by PWM of $V_{bldc}$ with a constant duty ratio. The torque was varied between the positive and negative maximum voltage in the

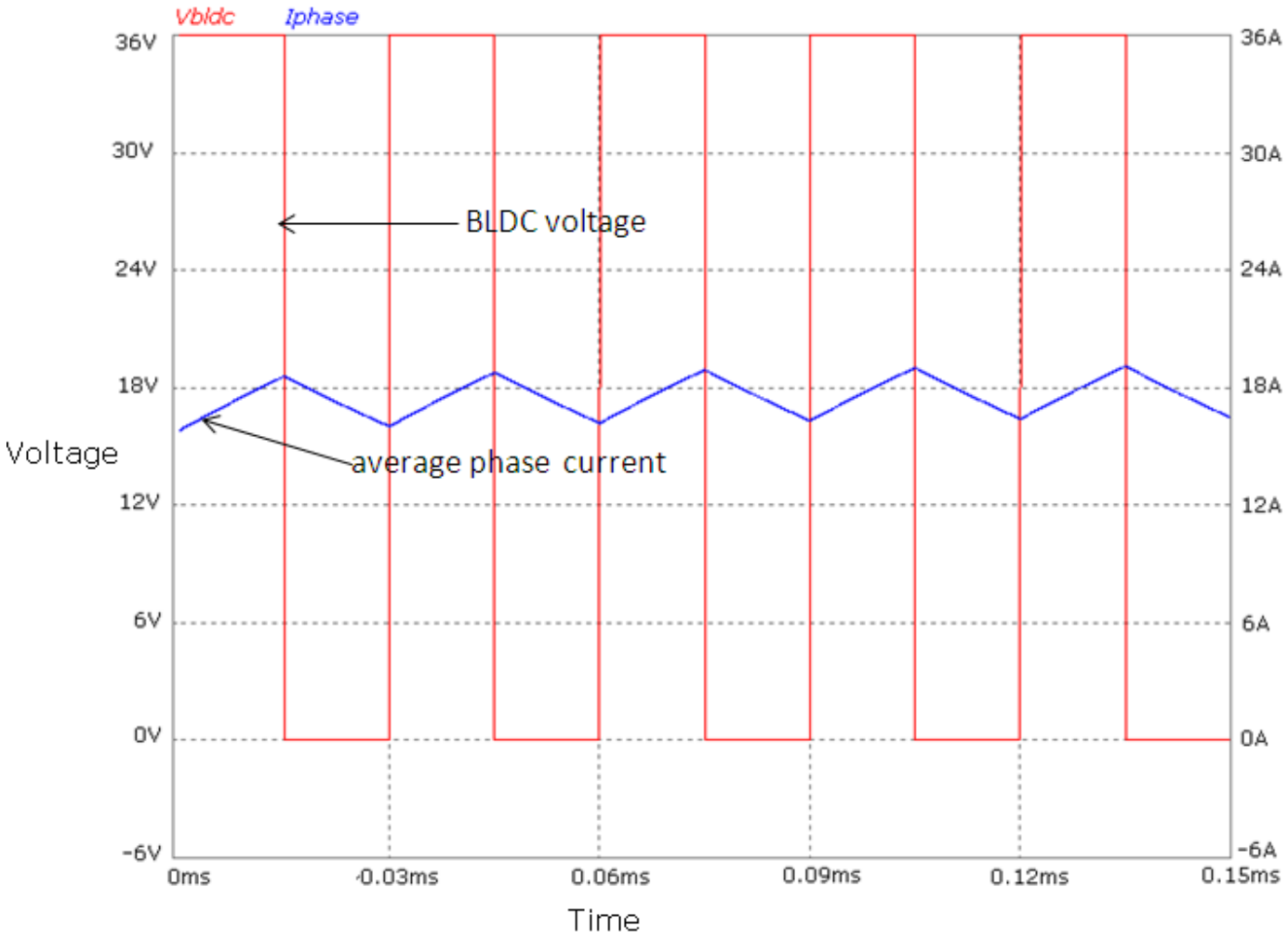


Figure 5.3: LTSPICE simulation of the BLDC voltage and the average phase current.

PMBLDC motor so that the controller can cover active braking zones, and also move from motoring into generating zones. The current was simulated up to the maximum value of ±36A.

Figure 5.4 shows the instantaneous power converted through the back EMF of all the three phases. From Figure 5.4, we observe that the average power output is 270W. The three-phase full bridge has power switches with freewheeling diodes which controls the current flow within the power stage. Therefore current will be pulled through the low side diode from the negative DC voltage if positive current flows through the phase winding. Current will flow through the high side diode into the positive DC voltage if negative current flows (cf. Figure 3.20 and Figure

4.3). This causes power dissipation in the diode voltage drop of approximately 1V at maximum speed as illustrated in Figure 5.5.

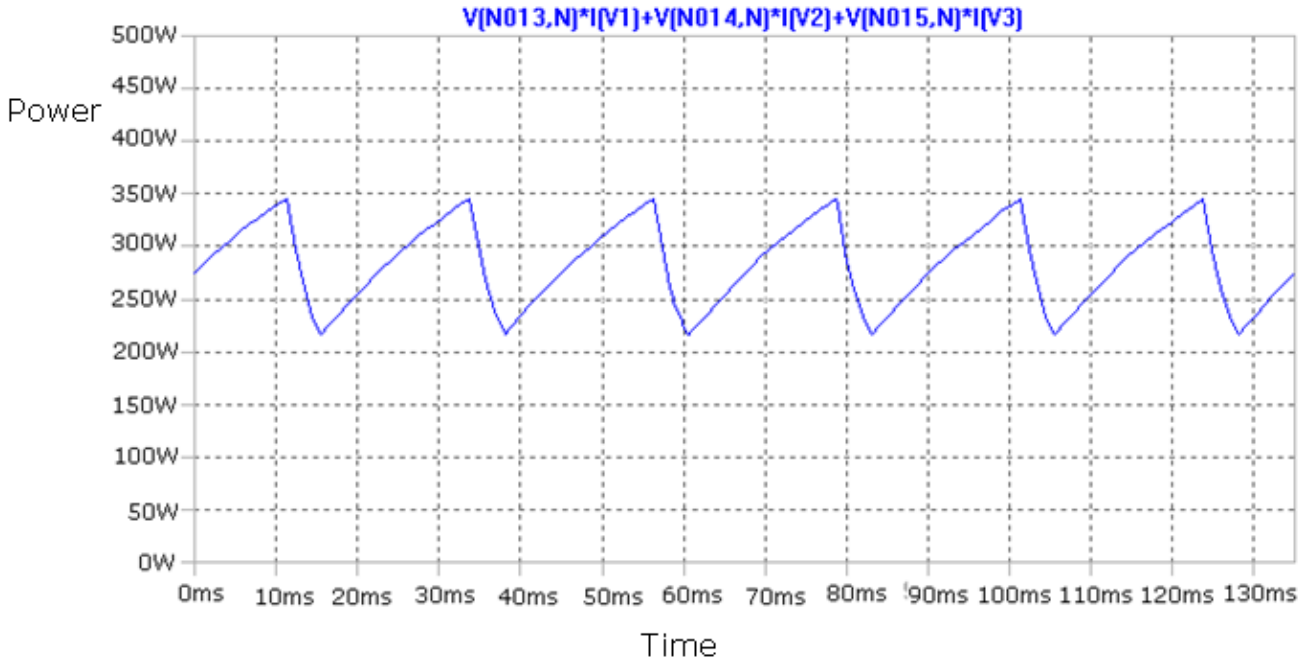


Figure 5.4 LTSPICE simulation instantaneous power converted through the back EMF.

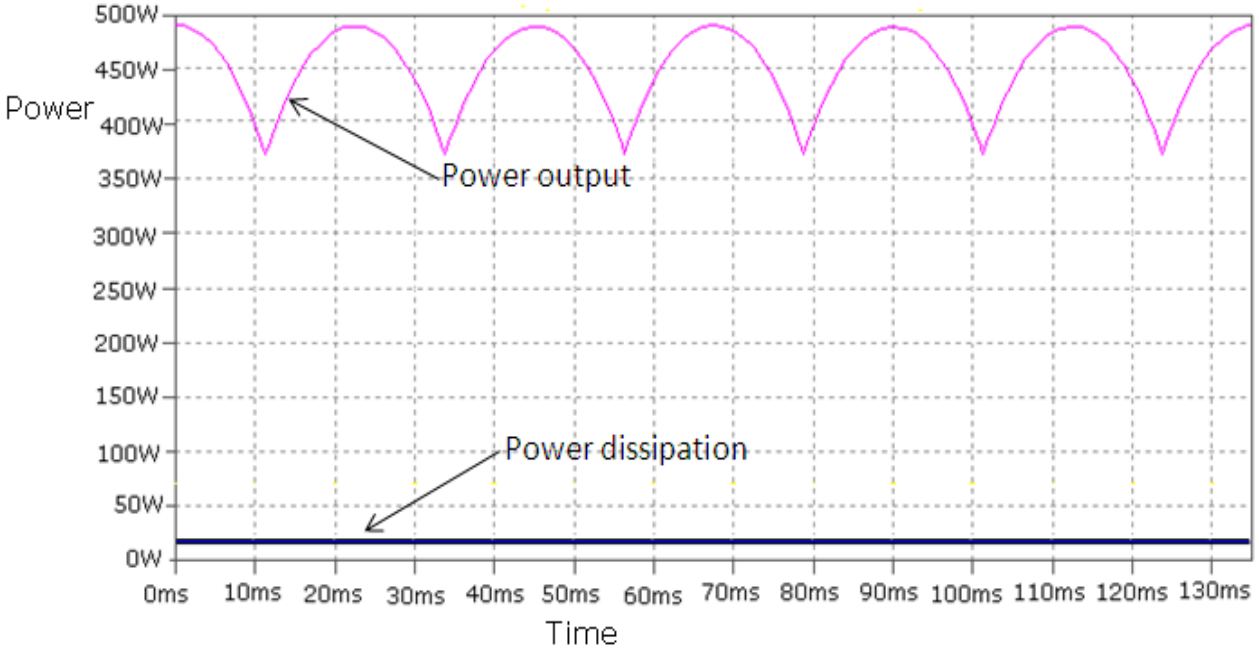


Figure 5.5: LTSPICE simulation of the power output at maximum speed with constant power dissipation.

## 5.3 SUMMARY AND CONCLUSIONS

The chapter has discussed the simulations studies that were performed to assess the design of the proposed E-bike drive speed control system. These simulated results will be confirmed in the next chapter which will provide an analysis of the proposed controller's performance.

This page is intentionally blank

# CHAPTER 6

# LIVE TEST RESULTS

## 6.1 INTRODUCTION AND EXPERIMENT SETUP

This section deals with the practical measurements of the variable speed drive (VSD). These include the motor parameters, simulation and experimental measurements. The four quadrant controller described in Chapter 4 was designed (cf. Appendix A) and built (cf. Figure 6.1) to obtain the experimental results. The simulations were used as a guide for the design of the hardware and the verification of the practical results for the entire design. The motor used in the VSD for testing was a 500W, 36V, 409 hub motor mounted on a DH19 rim. The controller was set up with a hub motor, lead acid battery pack, oscilloscope, multimeter and a throttle (cf. Figure 6.1) to vary the speed for testing at different speed levels.

The controller was set at specific operating parameters which correspond with the PWM outputs to test the various limits. Tests were conducted to ensure that the PWM signal output was correct and varied in accordance with the position of the throttle when no current, speed or voltage limits were exceeded. The throttle was varied from standstill to maximum speed and different measurements were taken at different speeds. The currents and phase voltages were measured at different operating points to ensure that the controller was safely operating in all four quadrants.

The duty cycle of the controller was set at 100% which makes the high side power MOSFET of the current controller to be switched on permanently through the bootstrap MOSFET driver. Testing of the protection logic was undertaken to ensure that only the low side received the PWM signal during regeneration, and only the high side during motor operation. The throttle signal was kept constant while the speed of rotation was allowed to vary over the whole range of speeds where the current could be controlled. Different constant currents were set up by varying the throttle in various positions with a digital multimeter connected in series with the motor.

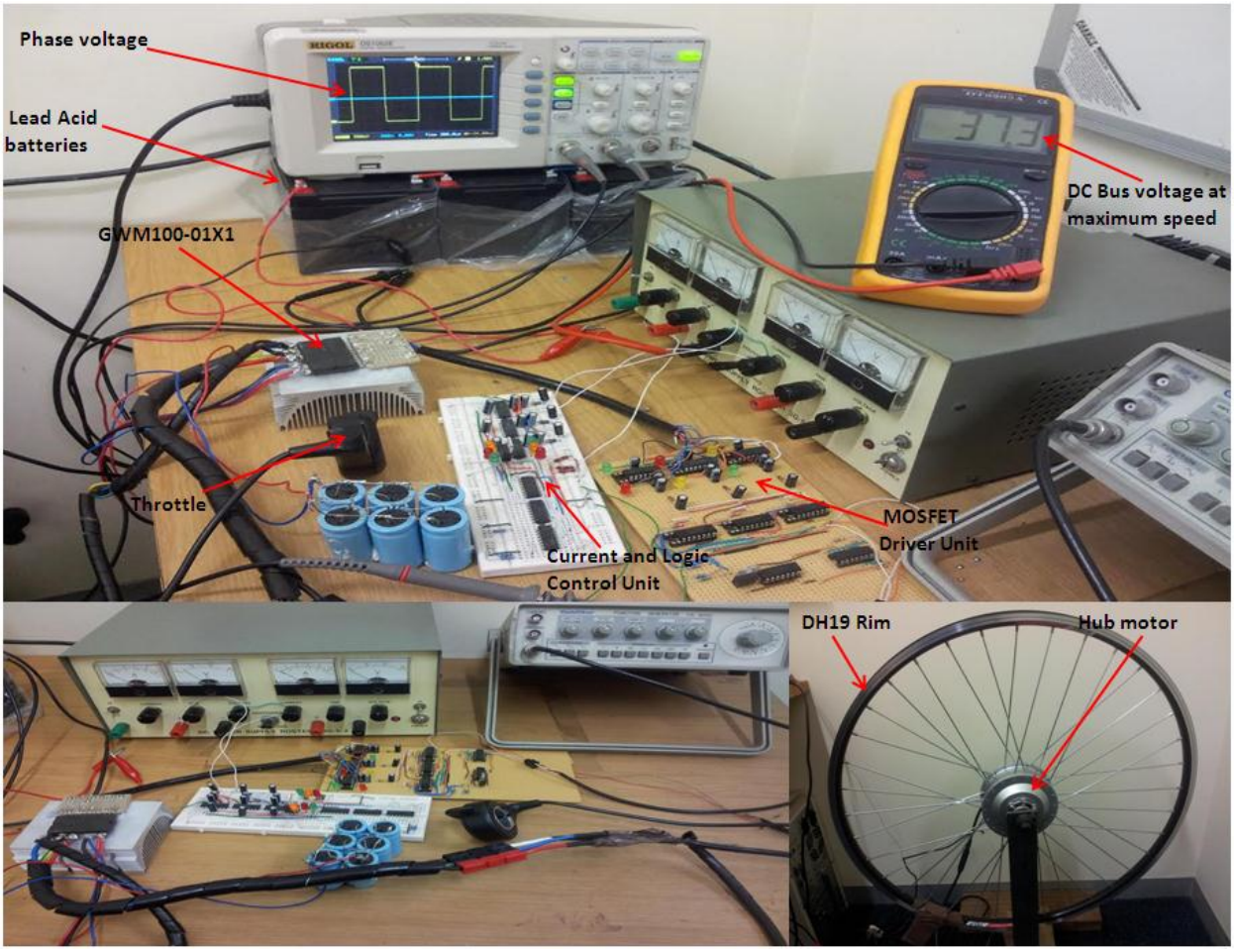


Figure 6.1: Test bench.

## 6.2 EXPERIMENTAL RESULTS

The test results are given in Figure 6.2 to Figure 6.15.

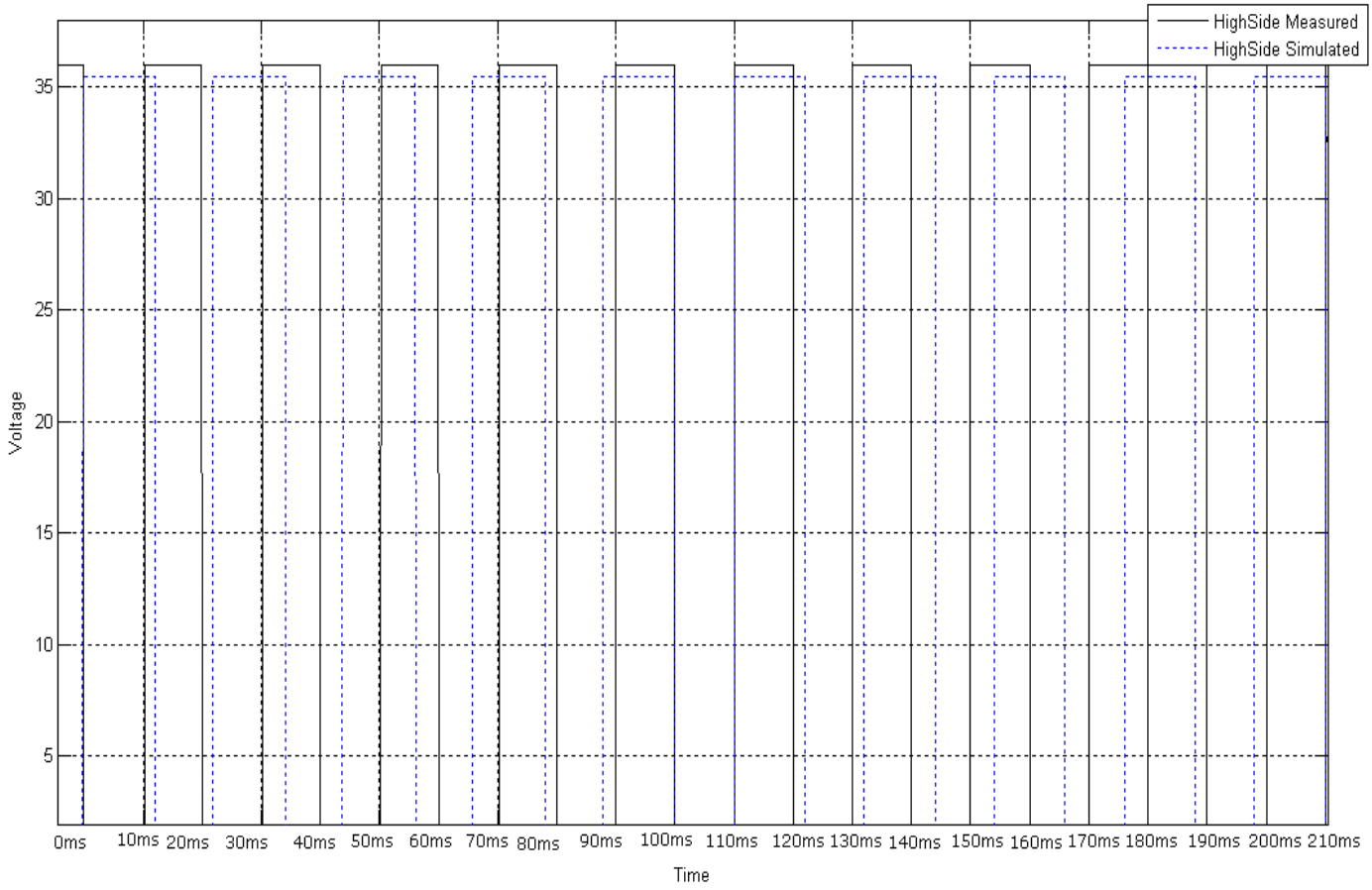


Figure 6.2: Measured and Simulated high side phase voltage at 500rpm (cf. Figure 4.8).

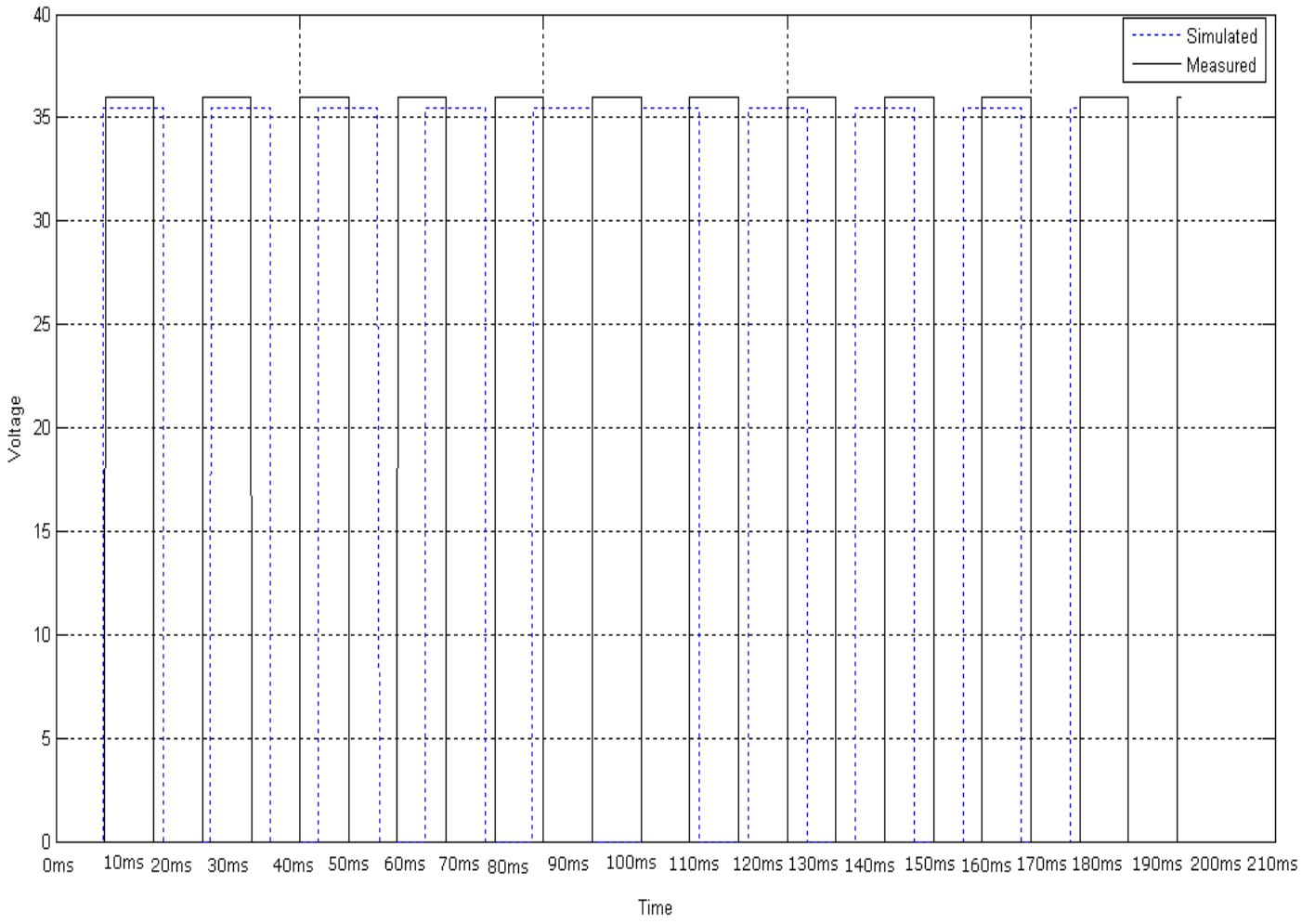


Figure 6.3: Measured and Simulated low side phase voltage at 500rpm (cf. Figure 4.8).

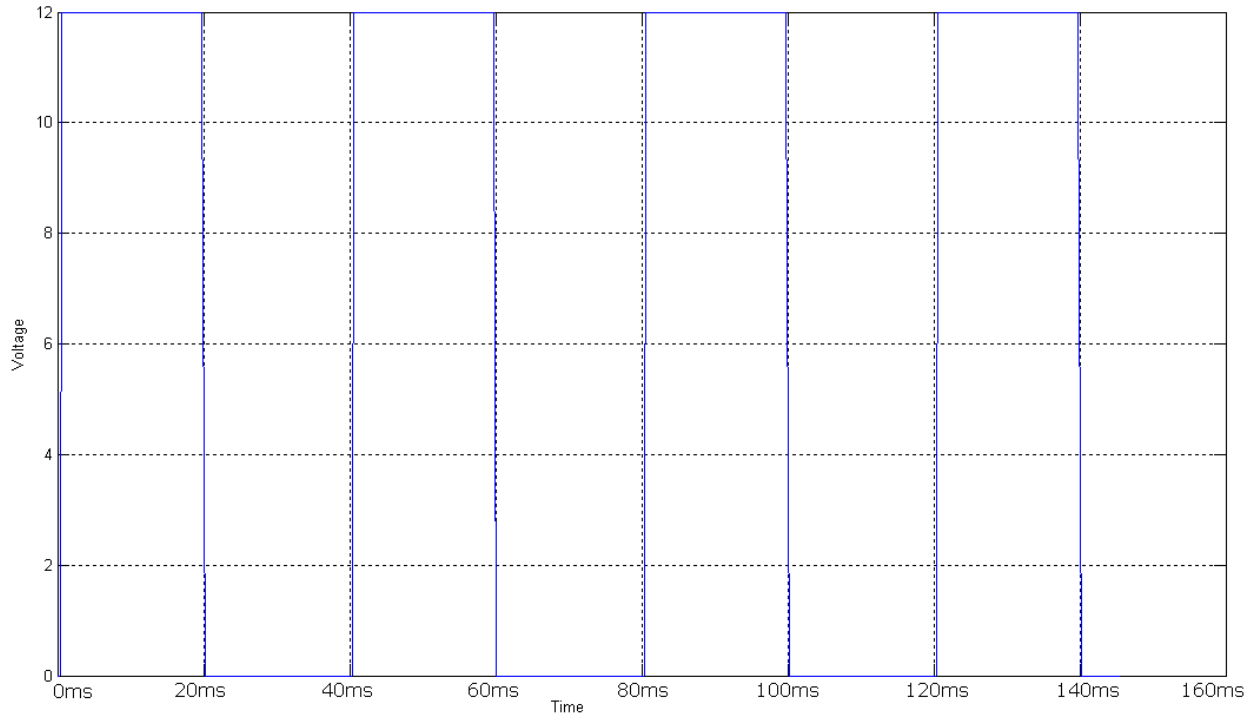


Figure 6.4a: Simulated high side PWM output for each phase (cf. Figure 4.15).

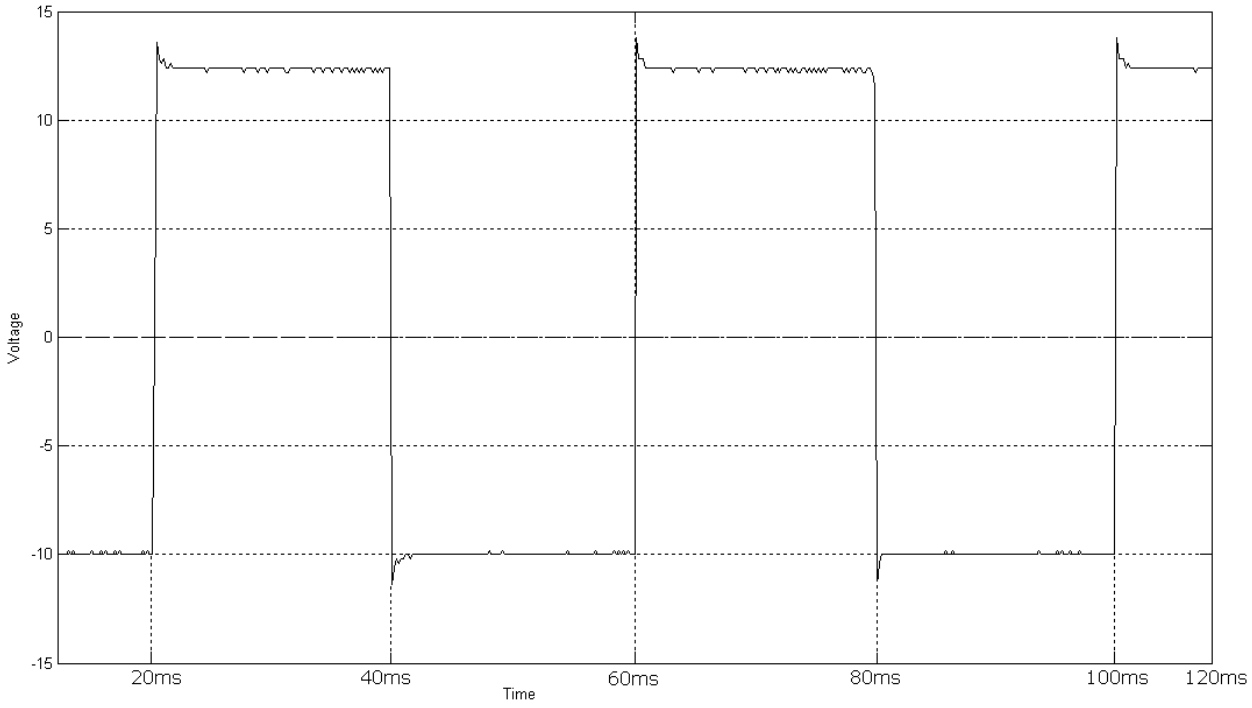


Figure 6.4b: Measured high side PWM output for each phase (cf. Figure 4.10).

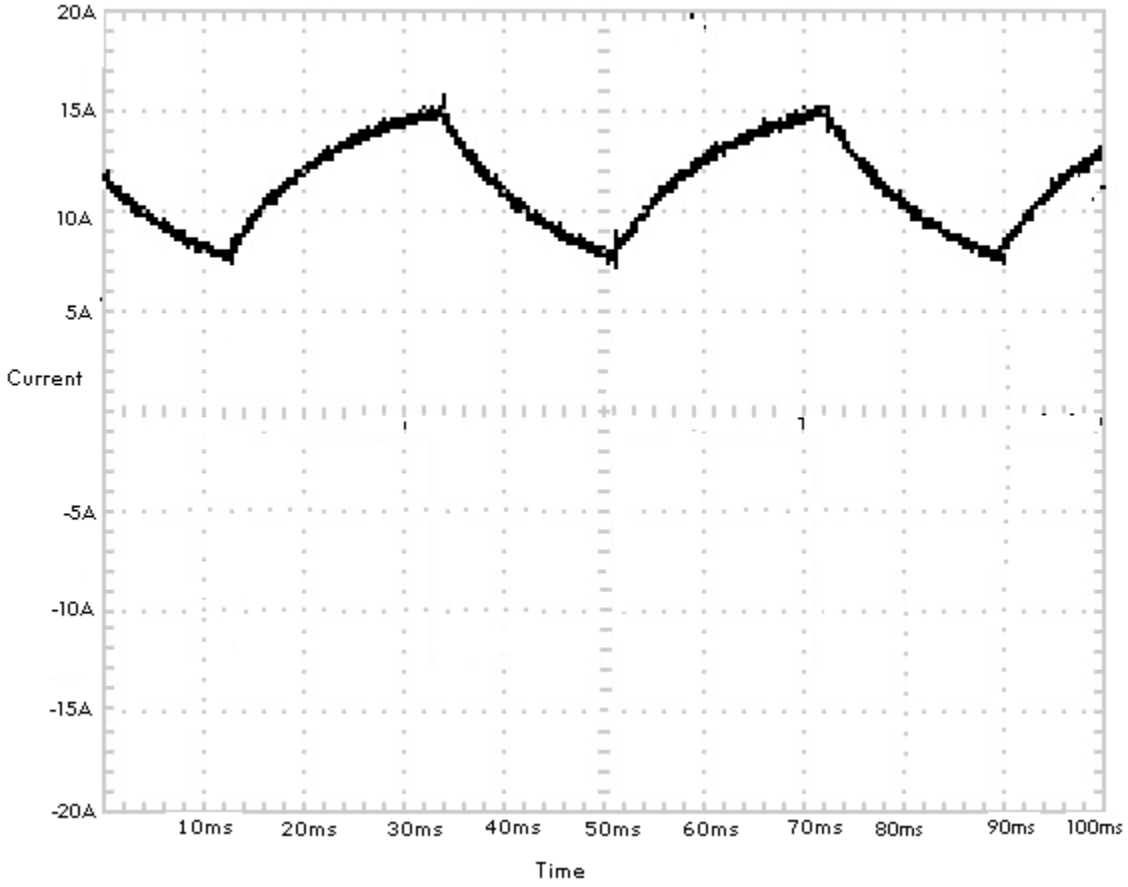


Figure 6.5a: Measured phase current at 500rpm (cf. Figure 4.18).

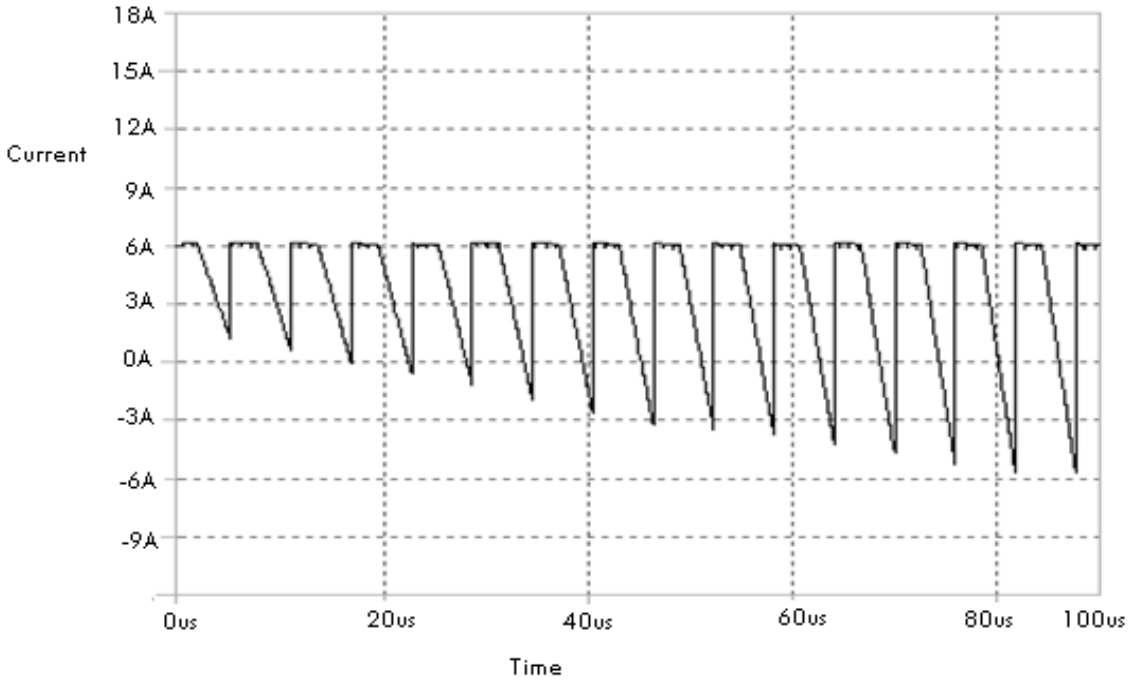


Figure 6.5b: Simulated phase current at 200rpm (cf. Figure 4.18).

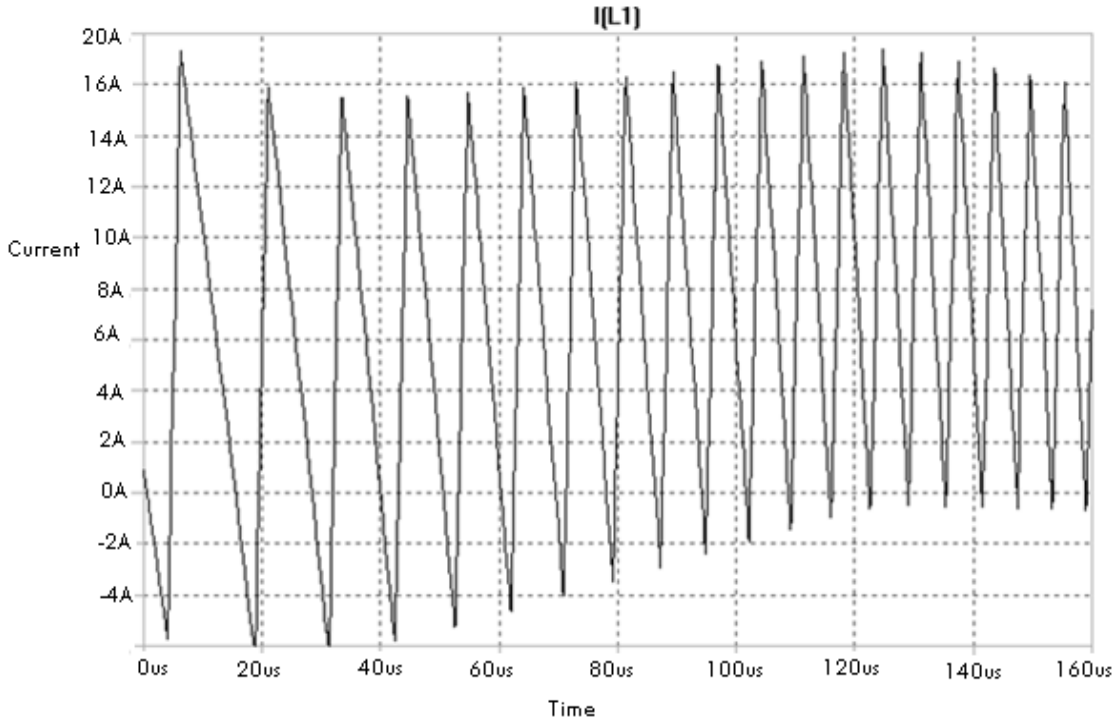


Figure 6.6: Measured current for torque control at 500rpm (cf. Figure 4.17).

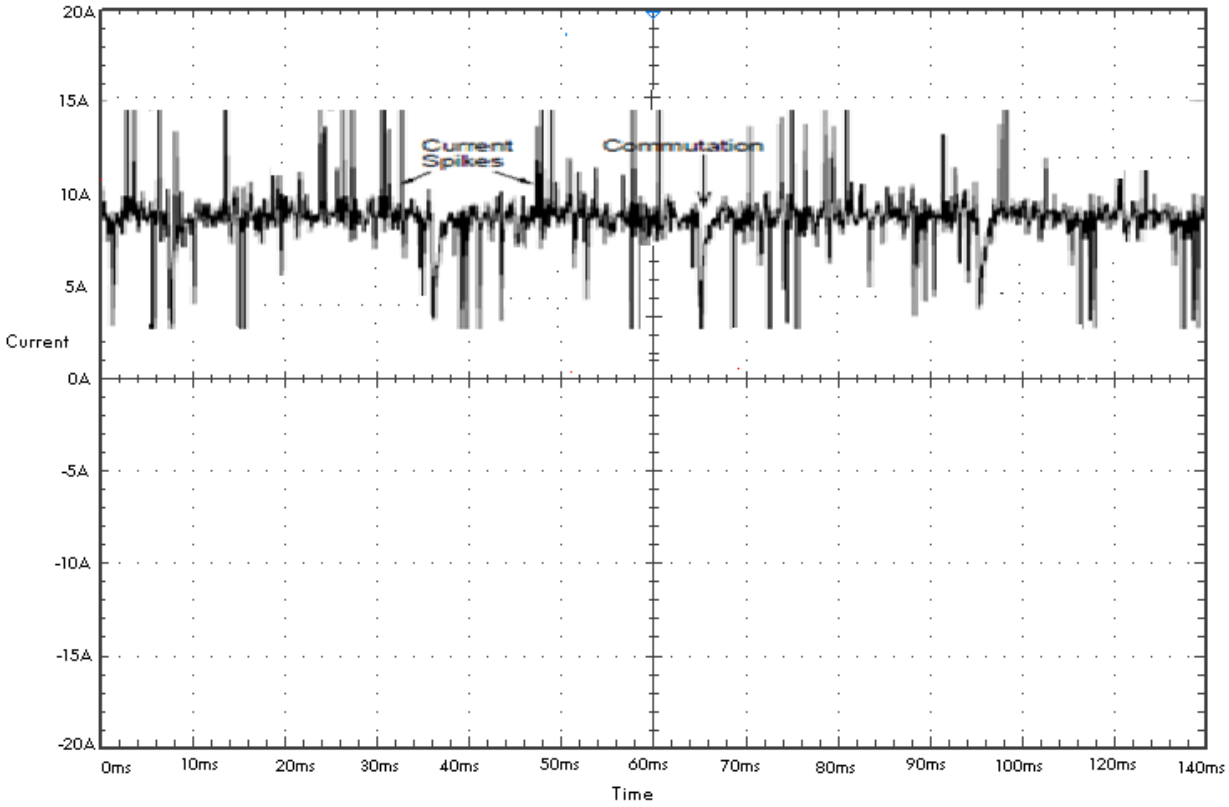


Figure 6.7: Measured motor current (cf. Figure 4.18).

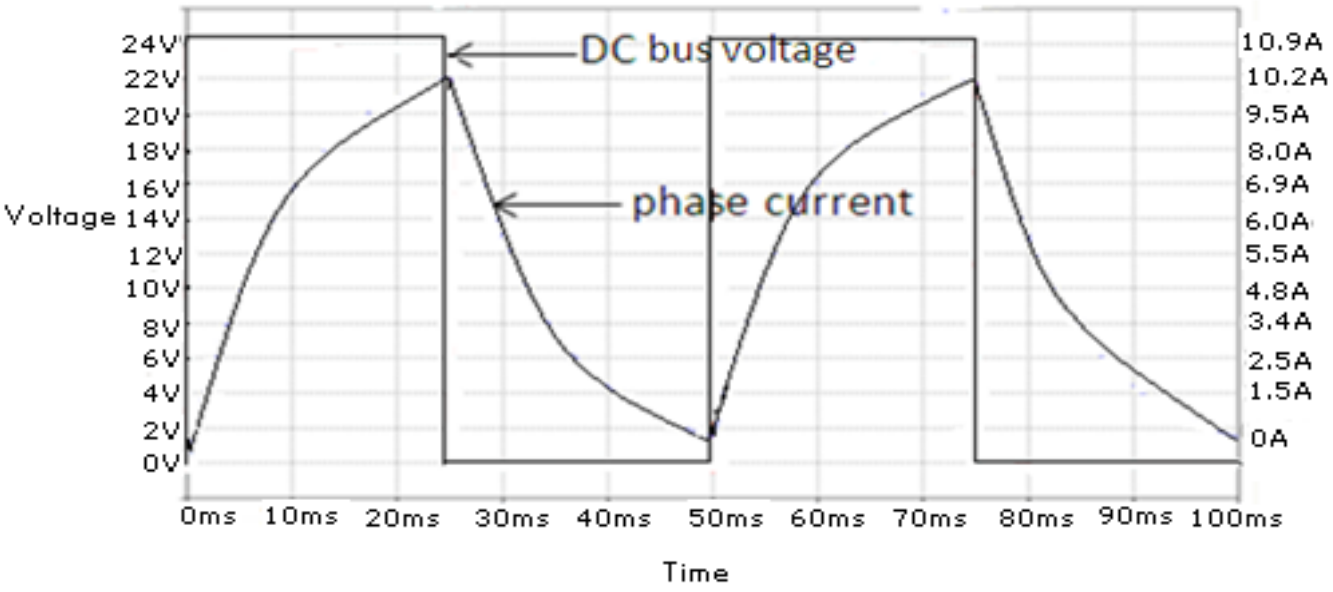


Figure 6.8: Measured phase current and voltage (cf. Figure 4.18).

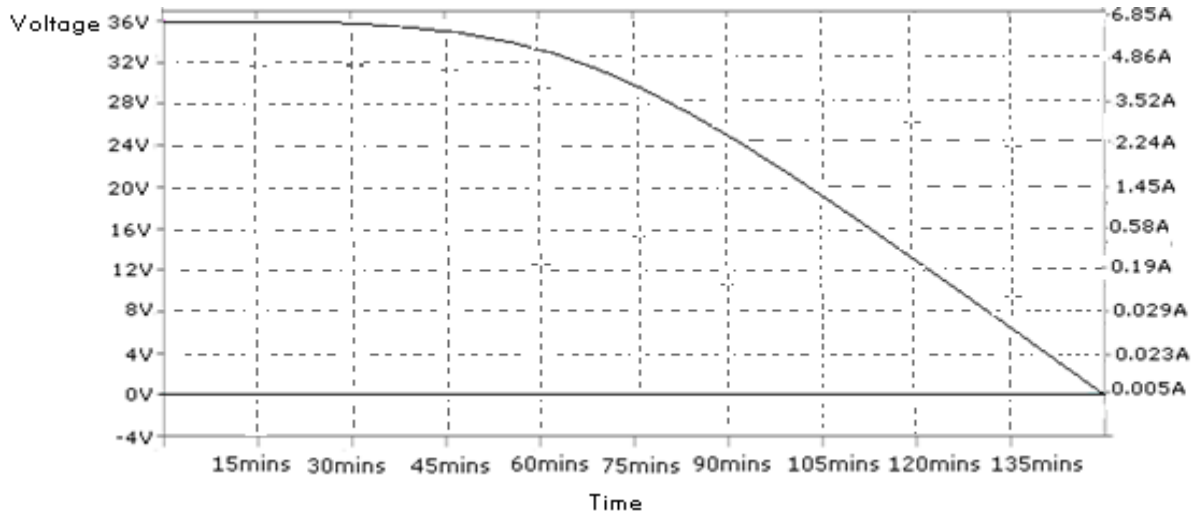


Figure 6.9: Battery discharge without regenerative braking (cf. Figure 4.22 and Figure 2.24).

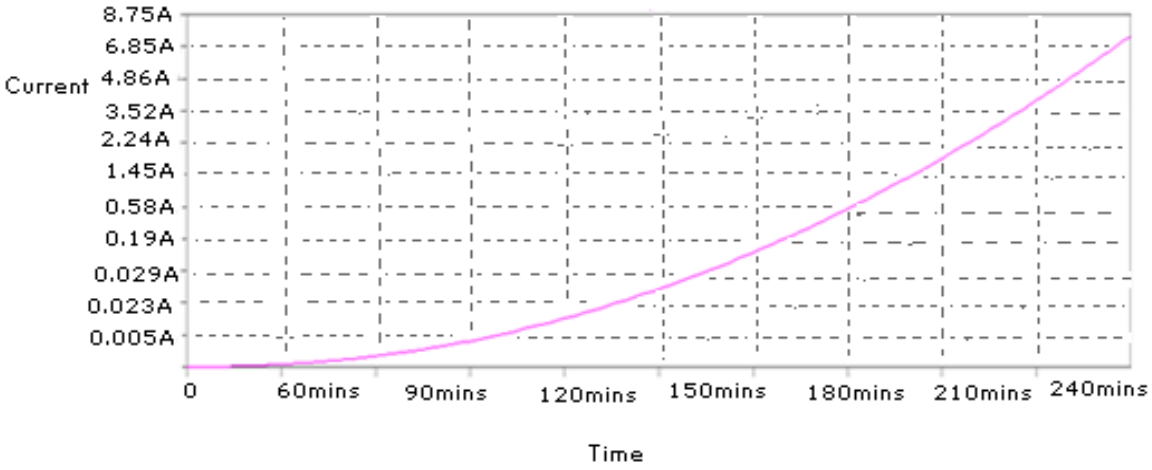


Figure 6.10: Battery charging using regenerative braking (cf. Figure 4.24).

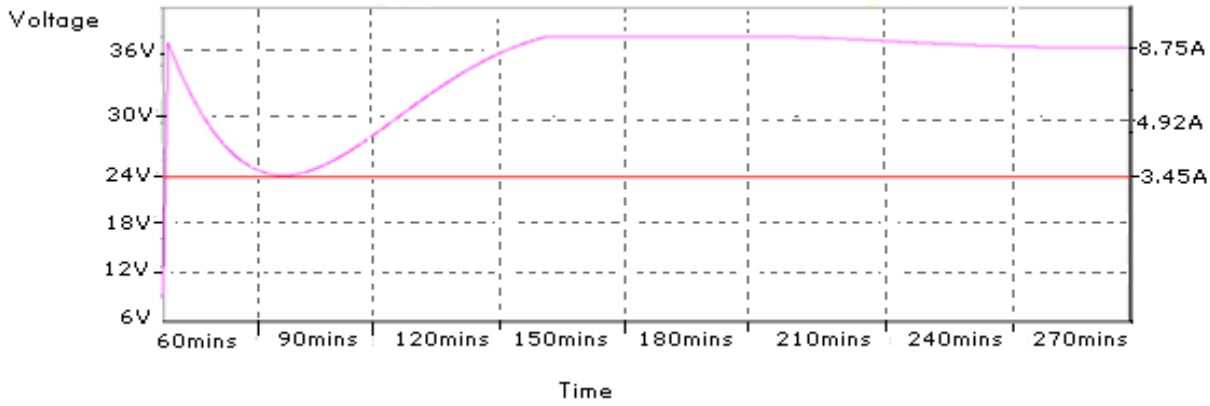


Figure 6.11: Battery discharge and recharge with regenerative braking. The charge threshold is 24V (cf. Figure 4.24 and Figure 4.25).

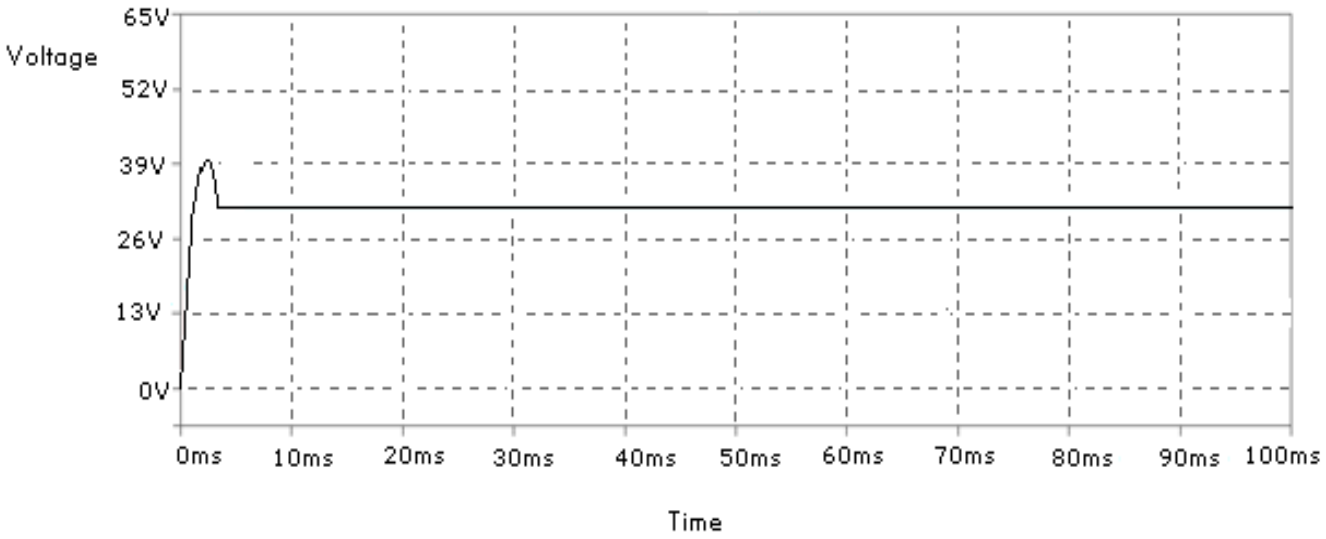


Figure 6.12: Battery voltage which is limited at 36V (cf. Figure 4.22 and Figure 4.24).

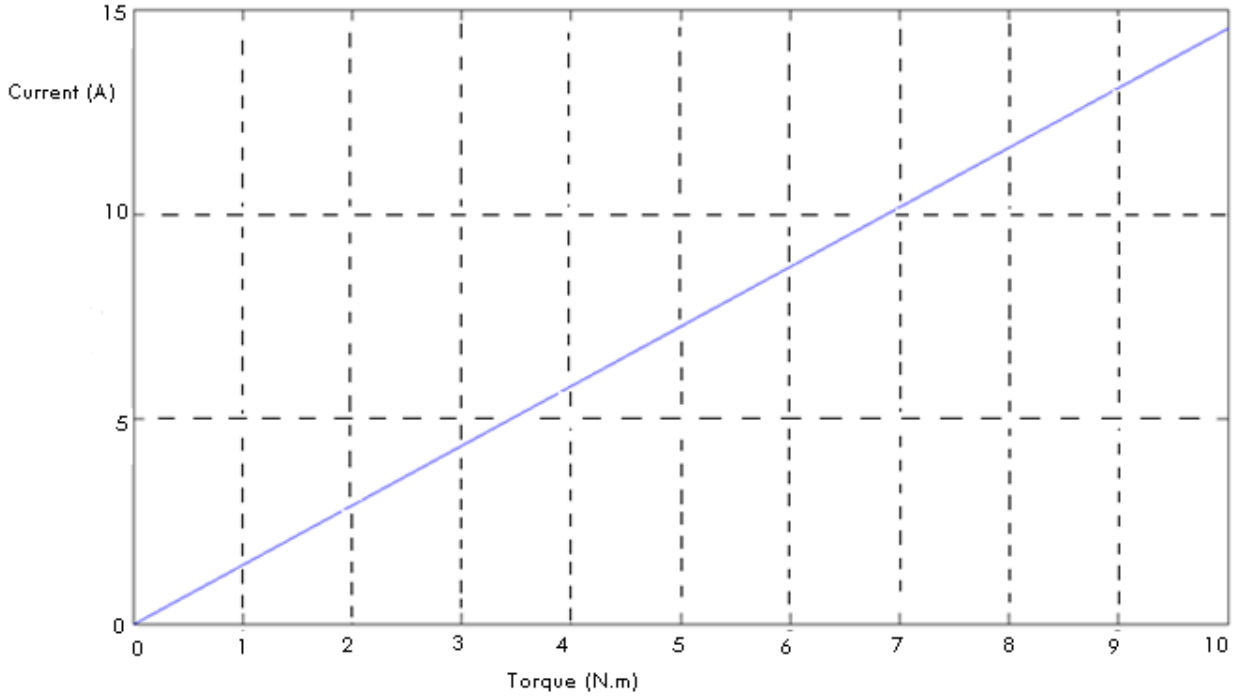


Figure 6.13: Torque versus current characteristic (cf. Figure 4.17).

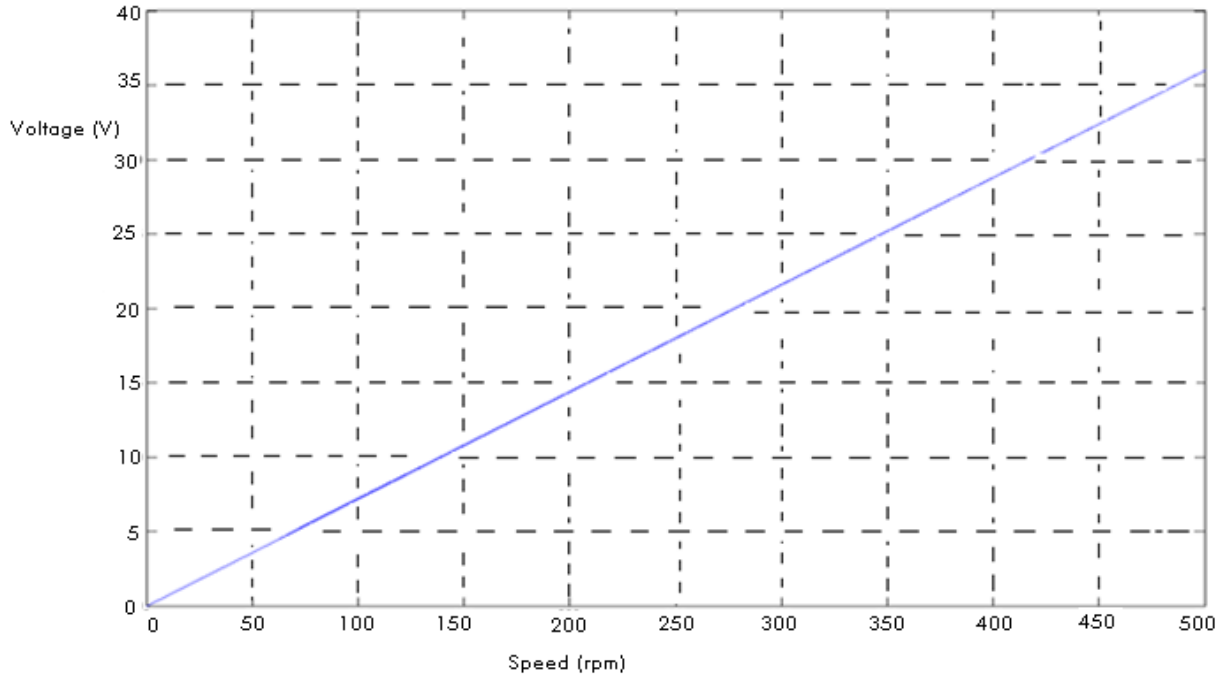


Figure 6.14: Speed versus voltage characteristic (cf. Figure 4.21).

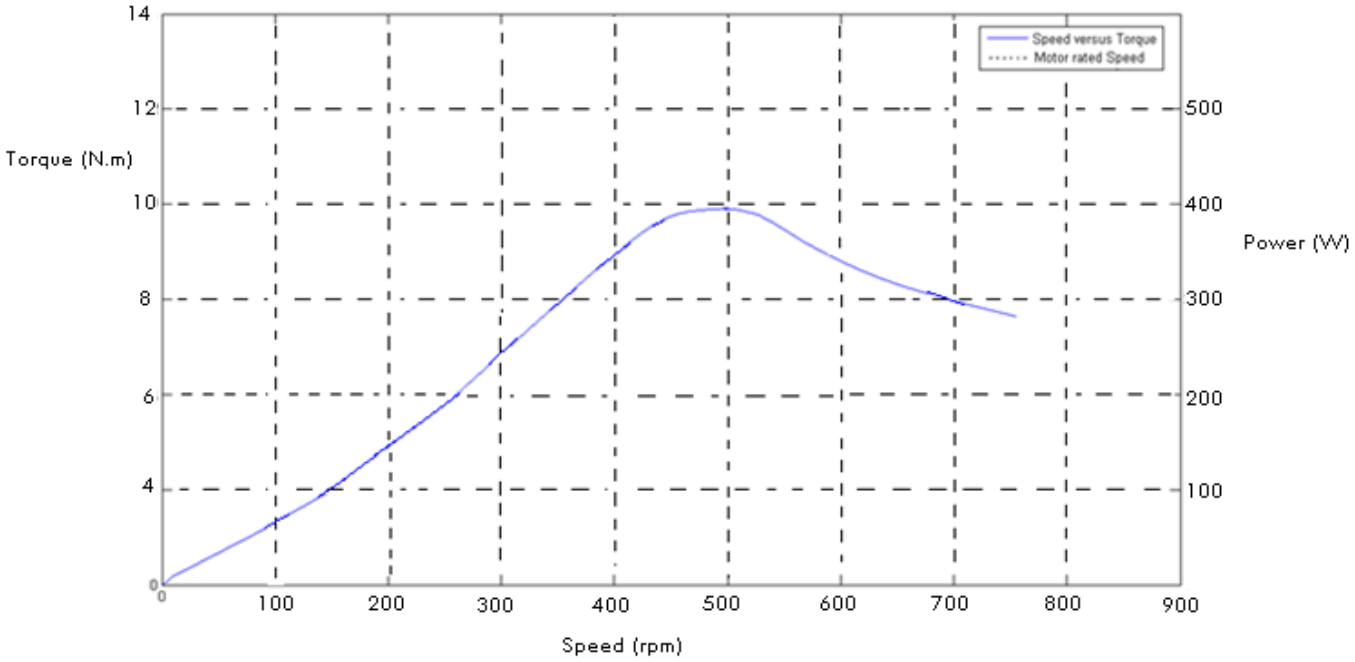


Figure 6.15: Torque versus Speed characteristic (cf. Figure 4.17 and Figure 21).

## 6.3 ANALYSIS OF RESULTS AND DISCUSSION

LTSpice was used for the simulations described in this study. As shown in Figure 6.2 and Figure 6.3, at no time were both the high and low sides MOSFETS switched on at the same time. Reversing the mechanical pedal overrides the position of the throttle and changes the drive to the regenerative braking mode.

Motor speed was monitored by the microcontroller to ensure that the reversing switch is only activated when the PWM signal is off and the motor has stopped. The throttle has to be turned down to zero before the direction can be changed from the forward to the reverse direction and vice versa. Figure 6.2 and Figure 6.5b show the bus voltage and motor current of the PMBLDC motor when a phase change occurs. Figure 6.5a shows the motor current when there is no load on the motor. The motor current decreases when the current from the previously conducting phase freewheels within the phase switcher (cf Figure. 4.8) through the unchanged phase when the next phase is switched on. Figure 6.4a and Figure 6.4b indicate the simulated and measured high side PWM output for each phase which is within the required switching voltage.

The dead-time in the current-mode was difficult to control due to a fast time delay needed to shut down the PWM signal when the motor current exceeded its parameter. The result in Figure 6.6 shows a gradual decay in the current over time. This current decrease indicates a loading effect on the battery. Over time, this load on the battery will cause the speed to gradually decrease. Judging from the rate of change in Figure 6.6, it would take approximately 10μs for the controller to switch the PWM off in the event of an over-speed condition. Figure 6.8 indicates the bus voltage and the motor phase current when operated with a fixed average voltage produced by the PWM having a constant duty cycle. The current reduces to zero at every

commutation because the next connected phase has no current flowing in it and increases during the next conducting phase.

From Figure 6.9 we observe that the battery takes approximately 2 hours to completely discharge without the motor regenerative braking system; Figure 6.10 shows the battery charging characteristics under conditions of regenerative braking. Appendix E indicates the charge/discharge characteristics of the batteries. The regenerative braking system becomes active when the battery discharges to a threshold of 24V (Figure 6.11). This voltage is adjustable (cf. Appendix B) and should be set at a level that avoids the possibility of total discharge before recharging. Figure 6.12 shows that the drive system is operating within the voltage limit of 36V. The torque is directly proportional to the current (Figure 6.13) and the battery voltage is directly proportional to the motor speed (Figure 6.14).

### *6.3.1 Speed and torque measurements*

A MLX90217 speed sensor was used to detect the number of revolutions per minute. Figure 6.15 indicates the torque versus speed characteristic. At maximum system efficiency of 81.5%, the power is 407.5W according to the datasheet in Appendix D, which is close to the actual test results of 400W as shown in Figure 6.15. When the speed exceeds the maximum rating of 500rpm, the torque begins to decline from the maximum rating of 10N.m. The torque continues to decrease as the speed increases. The torque is calculated using Equation 6.1.

$$T = \frac{\mathrm{P} \times 9.554}{\mathrm{n}} \qquad \text{(Equation 6.1)}$$

With regards to equation 6.1, T is the torque, P is the power, n is the speed and 9.554 is the torque constant. The speed of the motor was varied to get a torque measurement. Varying the speed involved adjusting the motor current. The method used to calculate the torque transferred involved the maximum torque rating of the motor with the torque to current ratio. From this we found that our BLDC motor used a current of 2.5A to yield a torque of 1.72Nm. A load was then applied to detect the effect of the torque. The torque was varied by adjusting the positive and negative maximum current in the PMBLDC motor which covers the active braking zones, and also the crossing from motoring into generating zones, which is not possible in the two quadrant operation (cf. 3.3.2). In this test the voltage was varied up to the maximum of ±36V in which the motor current is around ±15A (cf. Figure 6.5a and Figure 6.6) and ±20A in the simulation (cf. Figure 5.1 and Figure 5.3). In the tolerance band scheme, the instantaneous current is not always exactly equal to the average current. The spikes in Figure 6.4b and Figure 6.7 are caused by commutation events and switching of the current comparators.

### *6.3.2 Current commutation*

The current commutation was analyzed to determine the best method for measuring the effective BLDC motor current. The current flow between the BLDC motor and the regenerative braking system uses the open loop voltage control to set the duty cycle, and hence the average value of the BLDC bus voltage as indicated in Figure 5.2. The current is directly proportional to the output torque of the motor as shown in Figure 6.13.

The results in Figure 5.3 illustrate the tolerance band current control of the motor at a constant phase current. Figure 5.1 indicates a modulated DC bus voltage in which the current flowing in

the motor phase decreases and then slowly rebuilds after each step commutation. The current reduces to zero at every commutation because the next connected phase has no current flowing in it. The controller compensates for this, creating a long positive voltage pulse at each commutation which causes a quick buildup of current during the next conducting phase. The open loop voltage control forces the duty cycle to be constant, causing the average value of motor voltage to be smaller than the battery voltage. In the tolerance band scheme, the controller increased the motor voltage to be equal to the battery voltage for a quick commutation (cf. Figure 6.2). The torque ripple of the tolerance band method is half that of open loop voltage control at half the rated speed (cf. Figure 3.24). The current control has the advantage of producing smoother torque since the current is directly proportional to the torque. This makes the control system to achieve smooth torque control (cf. section 3.2.3, section 4.2 and section 4.9).

The design of the current controller uses a single current sensor, positioned after the three phase full bridge or the phase switcher, to senses the effective motor current. The control logic includes a separate single channel half bridge current controller and phase switcher logic. All the three phases are involved in each commutation event. This includes the stable phase which maintains its state during and after commutation, the previous phase which is disconnected after commutation and the next phase which is energized for the next commutation. The current commutation from the previous phase to the next phase takes place in the following three steps:

*Step 1:* The previous and stable phases conduct the motor current.

*Step 2:* The current builds up in the next phase whilst decaying in the previous phase.

*Step 3:* The previous phase current decays to zero and the operation continues.

The current sense resistor signal is being limited to the tolerance band except at commutation events. The phase switcher MOSFET capacitances charge and discharge through the current sense resistor as the motor voltage changes between battery and ground. This causes spikes in the current signal at each transition of the BLDC motor voltage as illustrated in Figure 6.7.

### *6.3.3 PWM and frequency control*

Figure 5.3 shows the phase current and the BLDC motor voltage controlled with a fixed average voltage produced by PWM of the motor voltage with a constant duty cycle ratio. The current takes the motor phase resistance and inductance time constants to settle after a commutation event. This makes the current ripple magnitude large. The phase current and motor voltages were simulated for motoring operation with a tolerance band current controller. When a commutation event occurs, the current controller forces the motor back EMF to battery voltage so that the phase current builds up quickly in the next active phase.

The switching frequency was set to 10 kHz. But the actual system operates with a maximum switching frequency of 25 kHz (cf. Figure 5.2) due to increases in the battery voltage and the maximum frequency when the battery pack is accepting a charge. There is also an increase in the maximum switching frequency as the motor current decreases because the battery voltage which is supplied by a series combination of three sealed lead acid batteries is not steady for all current flow rates. The frequency of operation can be affected by the EMF of the unused phase. The phase inductance of the unused phase experiences a voltage which is equal to its instantaneous back EMF when the motor voltage is forced to ground. This causes current to build up in this phase until the BLDC motor voltage is forced to the battery voltage again. The current in the

unused phase freewheels in the phase switcher through the diodes (cf Figure 4.3). As the rotor of the motor rotates, the phase voltage of the unused phase passes through zero causing the switching frequency to be low (cf section 3.2.1).

### *6.3.4 Motoring mode*

The controller is capable of four quadrant operation as discussed in the hardware design (cf. section 4.2). A BLDC motor current of 15A was instantaneously achieved during the test where the system was accelerated from rest to the maximum no load speed as shown in Figure 6.5b and Figure 6.7. The maximum continuous output power from the tests was 400W as illustrated in Figure 6.15 and 470W in the simulation (cf. Figure 5.5).

The current becomes zero when the current from the previously conducting phase freewheels within the phase switcher through the unchanged phase when the open circuit phase is switched on. The current controller forces the motor voltage to the battery to compensate for this loss of current which is restored in the new phase. At higher currents, the commutation of currents from one phase to the next takes longer. The controller increases the duty cycle of the BLDC motor current to compensate for a commutation and the sensed current restarts from zero at each commutation.

### *6.3.5 Generating mode*

The BLDC motor enters the generating mode when the throttle experiences a negative BLDC motor current. The BLDC motor must be rotating to convert mechanical energy to electrical energy. The battery affected the limits of both the motoring and generating tests by having a

terminal voltage that varied approximately linearly with the current which drained the battery rapidly as shown in Figure 6.8. The maximum power delivered to the battery during the test was 36V x 8.75A = 315W as illustrated in Figure 6.11.

Commutation does not affect the negative current regulation since the body diodes of the MOSFETs in Figure 4.3 always provide a path through the sense resistor. The mechanical torque on the BLDC motor is smoother when generating power, provided the commutation induced phase shift of the phase currents is small. The current spikes from the MOSFET output capacitance are higher when the motor voltage is changing from the battery to ground as shown in the results in Figure 6.7. When the current decays to zero in the unused phase, the phase to phase voltage returns to its open circuit value.

### *6.3.6 Forward/Reverse control*

The reverse control requires a positive voltage and negative current or negative voltage and current. This cannot be achieved using two quadrant control (cf. section 3.3.2). The motor has to completely stop before the direction can be changed from forward to reverse direction. The throttle has to be turned down to zero before the reverse switch can be activated. For automatic direction switching, the throttle input was set at an average BLDC motor current. The speed of the motor was then varied from positive to negative to cause the direction to change from forward to reverse. The direction changed from reverse to forward when the motor speed is varied from negative to positive. The direction of the VSD can be interpreted as forward when the lower comparator of the current controller (cf. Figure 4.17) is high or when the input is above the reference voltage. The comparator changes states when the input voltage is exceeded by the current sensor voltage, therefore putting the controller in reverse direction. A change of the

controller direction bit is needed when the value of BLDC motor voltage and the back EMF changes polarity.

### *6.3.7 Limitation and protection*

The controller was loaded with a set of operating parameters to test the speed, voltage and current limiting. The battery voltage was varied to give an under-voltage and an over-voltage condition in which the power stage was automatically shut down to indicate a faulty condition. The speed was varied to an over speed condition in which the PWM output was disabled until the motor speed was reduced below the speed limit. The battery voltage was limited at 36V as shown in Figure 6.12. The current was limited in all quadrants of operation.

## 6.4 SUMMARY AND CONCLUSIONS

The test was done at different speed levels to obtain a safe operating area for the controller. A step input was applied to the current sense input to indicate an over-current condition. The oscilloscope was set to be triggered by the step input. The DC bus voltage does not change during the set period if the drive operates within its limit. The battery terminal voltage varies with the speed to its maximum value as displayed on the multimeter. The test proved that the controller operated as desired and provided a control system that implements all the required features within adequate response times.

This page is intentionally blank

# CHAPTER 7

# SUMMARY OF STUDY, CONCLUSIONS AND RECOMMENDATIONS

This chapter provides conclusions on the overall design covered in this research study.

## 7.1 SUMMARY AND CONCLUSIONS

The overall result of this study is the design of a simple VSD based on digital logic. Testing of the controller and its associated circuitry has proven that the system can operate safely in all four quadrants. Torque controlled operation was achieved by controlling the path and the magnitude of the current in the BLDC motor. The throttle is used to control the current and therefore the torque within the operating limits of the VSD. The features provided by the VSD system are well suited to an E-bike application. The fully variable parameters of the controller allows for the safe operation of the E-bike during forward and reverse motoring, as well as regenerative braking.

The analog comparators used in the current control system provided accurate thresholds and digital output which makes the current amplification easier. The arrangement of power switches affects the commutation process. The relationship between the measured current in the BLDC motor and the torque is dependent on the speed of commutation. A faster transfer of current between the commutating phases keeps the relationship between the motor current and torque more stable. This can be analysed in the generating or regenerating mode of operation. The

separation of the phase switcher and current controller resulted in a simple current measurement system. The different modules were designed and tested in isolation before assembling the whole system. This approach provided fast detection of faults and quick replacement of faulty components.

Lossless current sensing scheme is required since the sense resistor dissipates power and therefore reduces efficiency. A lossless scheme can also reduce the parasitic inductance introduced into the high power loop to reduce the transient voltages and filtering requirements. The effect of routing the Hall sensor wires away from the phase wires within the motor could not be achieved since all the wires shared the same insulation. Therefore coupling between the Hall sensor signals and the high power signals could not be avoided. This caused a great interference between the signals which affected the position sensors. The VSD operating frequency varied as the rotor position and load changed which decreased the radio interference produced by switching the high power MOSFETs.

The literature review compared other storage methods with their advantages and disadvantages. It revealed that the best solution to the energy storage system would be a combination of technologies, such as an ultra capacitor for high intermittent power and a separate battery for low power high energy density storage as proposed by (Yan and Patterson, 2001) in their novel power management scheme. These types of solutions have the potential to perform much better.

The three phase inverter bridge (cf. Figure 4.8) caused the inactive phase of the three phase brushless DC motor to stop conducting as quickly as possible after each commutation event. The

inverter bridge increased the resolution of the position sensor and changed the switching pattern that forces the motor voltage to ground. The switching pattern ensures that the inactive phase does not conduct by turning on an appropriate pair of top or bottom side switches that will force the BLDC motor voltage to ground. For the three phase motor, the side used to force the BLDC motor voltage to ground would change at $60^0$ intervals but at a point exactly $30^0$ after each commutation. This represents one of the bus clamped space vector pulse width modulation switching schemes implemented by (Narayanan et *al.*, 2006).

All objectives of this project were successfully achieved. The entire control system was designed, constructed and tested together with its associated elements. These include the phase switcher, gate drive circuits, current controller circuits, temperature control circuits, power supplies, protection logic and the associated software for the microcontroller. The control system successfully implements the entire features of four quadrant operation. Most VSD systems for electric bicycles are designed to operate in only two quadrants which do not allow reverse operation and also offer poor regenerative braking. *Regenerative braking can fully be achieved in four quadrant operation.*

The completion of this project has demonstrated the feasibility of using a highly integrated approach to the circuit design. It has also highlighted the benefits of using software to implement many useful features in the design, with minimal cost.

## 7.2 RECOMMENDATIONS

Recommendations to improve the design include the following:

1. *Batteries:* An E-bike or EV motor control can be powered with high technology batteries such as lithium cells or hydrogen fuel cells to make a long distance vehicle. It can also be incorporated with an internal combustion engine to form a hybrid drive train.

2. *Storage Elements:* Use ultra capacitors to improve the energy storage scheme. Ultra capacitors combined with the battery have the potential to improve the performance of the energy storage system for long distance riding. They have the ability to accept and deliver energy quickly and efficiently during acceleration and deceleration.

3. *High Torque Motors:* Use a higher torque motor when carrying out a road test. Appendix F shows a complete system mounted on the bicycle and ready for road testing; Appendix G compares the different BLDC motor models and their respective manufacturers. A load cell can be installed to measure the torque output of the PMBLDC motor. This would enable the observation of torque ripple from the PMBLDC motor and the controller with the parasitic torque from the friction in the system. Install a speed detection sensor on the motor to detect the speed to avoid over-speed. Also implement the four quadrant design for operation in all quadrants to allow reverse and regenerative braking. This allows the controller to be used in electric vehicle systems.

4. *Power Supply:* Design a complete power supply for the different circuits as they all require different voltage levels for activation. Reduce coupling between the Hall sensor

signals and the high power signals. Hall sensor wires should be wrapped separately from the phase wires to avoid signal interference.

# REFERENCES


1. K. Taehyung, L. Hyung-Woo, P. Leila and E. Mehrdad. "Optimal Power and Torque Control of a Brushless DC (BLDC) Motor/Generator Drive in Electric and Hybrid Electric Vehicles." *Energy Conversion and Management,* vol.56, pp.1280-1281, Elsevier, India, 2006.

2. D. Thompson. "Brushless DC Motor Control Made Easy." Internet: www.microchip.com/downloads/en/AppNotes/00857a.pdf, Jun. 18, 2008 [Apr. 20, 2012].

3. A. George and T. William. "Performance evaluation of a permanent magnet brushless DC linear drive for high-speed machining using finite element analysis." *Finite Elements in Analysis and Design,* vol.35, pp. 175-178, 2000.

4. Y. Komatsu, A. Tur-Amgalan, A. Yoshihiko, Z. Syed Abdul Kadir and T. Keita. "Design of the Unidirectional Current Type Coreless DC Brushless Motor for Electrical Vehicle with Low Cost and High Efficiency," *IEEE/SPEEDAM,* 2010, pp.1038-1039.

5. P. Boonyanant, R. Chaisricharoenb and Janpana. "Control of the Brushless DC Motor in Combine Mode." *Procedia Engineering,* vol.32, pp.282-283, 2012.

6. D. Collins. "DOE FE Distributed Generation (DG) Fuel Cells Program," *IEEE Applied Power Electronics Conference,* 2005, pp.832-834.

7. B. Singh and S. Singh. "State of the art on permanent magnet brushless DC motor drivers." *Journal of Power Electronics,* vol.56, pp.9-11, 2009.

8. J. Figueroa, C. Brocart, J. Cros and P. Viarouge. "Simplified simulation methods for polyphase brushless DC motors", *Mathematics and Computers in Simulation,* vol.63, pp.222-224, 2003.

9. J. Faiz, M.R. Azizian and M. Aboulghasemian-Azami. "Simulation and analysis of brushless DC motor drives using hysteresis, ramp comparison and predictive current control techniques," Dec. 1994, pp. 351-353.

10. M.D. Britten, I.D. de Vries and J. Tapson. "Discrete Logic Permanent Magnet Brushless DC Motor Controller," in *Proceedings of the* 16*th Southern African Universities Power Engineering Conference*, January 2007, pp. 132 –134.

11. Toyota Motor Corporation. "Solar car motor and drivetrain." Internet: www.speedace.info, Aug. 13, 2006 [May 11, 2012].

12. Safidrive Technology. "Technical information on motors and drives." Internet: www.sdt-safidrivetechnology.co.uk, Sept. 12, 2009 [May 22, 2012].

13. D. Patterson and R. Spee. "The Design and Development of an Axial Flux Permanent Magnet Brushless DC Motor for Wheel Drive in a Solar Powered Vehicle." *IEEE Transactions on Industry Applications*, vol. 31, pp. 1054 – 1061, Sep. 1995.

14. Y. Padmaraja, Microchip Technology. "Brushless DC (BLDC) Motor Fundamentals." Internet: www.microchip.com, Feb. 2003[April 12, 2014].

15. H. Wang. "Design and Implementation of Brushless DC Motor Drive and Control System," *International Workshop on Information and Electronics Engineering (IWIEE)*, 2012, pp.2220–2223.

16. A. Kasei Microdevices. "Detection of Brushless Motor Rotation." Internet: www.akm.com/akm/en/product/add/magnetic sensors/0027/, Jan. 2011 [Jun. 20, 2014].

17. C.C. Hwang and J.J.Chang. "Design and analysis of a high power density and high efficiency Permanent Magnet DC Motor." *Journal of Magnetism and Magnetic Materials*, vol. 209, pp.233–238, 2000.

18. Fadal Machine Center. "History about AC and DC Servos for Fadal Machines." Internet: www.fadalvmcparts.com, Jun. 2008 [Jun. 20, 2014].

19. EV-INFO. "Electric Bicycle Manufacturers and Models." Internet: www.ev-info.com/electric-bicycle manufacturer/, Nov. 2014 [Jul. 15, 2014].

20. S.T. Microelctronics. "Sensorless BLDC Motor Control and BEMF Sampling Methods with ST7MC," *AN1946 Application Note*, 2007, Rev.2, pp. 3–5.

21. Freescale Semiconductor. "3-Phase BLDC Motor Control with Quadrature Encoder using 56F800/E," *AN1961 Application Note*, 2005, Rev.0, pp. 4–8.

22. B. K. Lee and M. Ehsani. "Advanced BLDC motor drive for low cost and high performance propulsion system in electric and hybrid vehicles," *IEEE electric machines and drives conference,* 2001, pp.246-251.

23. MSK Corp. "30Amp, 75V 3-Phase MOSFET Brushless Motor Controller." Internet: www.DatasheetCatalog.com, Apr. 15, 2011 [Jun. 20, 2013].

24. G. Pavel. "BLDC Motor Control using 8-bit MCU." Internet: www.freescale.com/beyondbits, Aug. 8, 2005 [Jul. 10, 2013].

25. T. Heman and T. Rajesh. "Speed Control of Brushless DC Motor Drive Employing Hard Chopping PWM Technique Using DSP," *Proceedings of India International Conference on Power Electronics*, 2006, pp. 368-375.

26. A. Tashakori and M. Ektsesabi. "Comparison of Different PWM Switching Modes of BLDC Motor as Drive Train of Electric Vehicles." *World Academy of Science, Engineering and Technology,* vol.63, pp. 719-722, 2012.

27. T. Ishikawa and G. R. Slemon. "A Method of Reducing Ripple Torque in Permanent Magnet Motors without Skewing." *IEEE Transactions on Magnetics*, vol. 29, pp. 2027–2030, Mar.1993.

28. C. Zhao and Y. Wu. "The Design of Brushless DC Motor Controller," *in IEEE International Conference on Intelligent Control and Information Processing*, Aug. 2010, pp.729-731.

29. N. Mohan, W.P. Undel and T.M. Robbins. *Power Electronics Converters Application and Design*. USA: John Wiley & Sons Inc, $4^{th}$ ed., 2003, pp. 461–495.

30. IXYS. "GWM100-01X1 Three phase full bridge." Internet: www.Alldatasheet.com, Sep.15, 2009 [Jun. 22, 2013].

31. National Semiconductor. "LM5100A/LM5101A – 3.0 Amp High Voltage High Side and Low Side Driver." Internet: www.national.com, Jun. 2007 [May 11, 2013].

32. Texas Instruments. "LM347 JFET-input Quad Operational Amplifiers." Internet: www.ti.com, Mar. 2005 [July 11, 2013].

33. ATMEL. "ATmega328 AVR 8-bit Microcontroller." Internet: www.Alldatasheet.com, Nov. 2009 [Jun. 7, 2013].

34. G. Narayanan, H.K. Krishnamurthy, D. Zhao and R. Ayyanar. "Advanced Bus-Clamping PWM Technique Based on Space Vector Approach." *IEEE Transactions on Power Electronics,* vol. 21, No. 4, pp. 974 – 984, Jul. 2006.

35. A.M. Legowski and Trzynadlowski. "Minimum-Loss Vector PWM Strategy for Three-Phase Inverters." *IEEE Transactions on Power Electronics*, vol. 9, No.1, pp. 26–34, Jan. 1994.

36. S. Kang and S. Sul. "Direct Torque Control of Brushless DC Motor with Nonideal Trapezoidal Back EMF." *IEEE Transactions on Power Electronics*, vol. 10, No.6, pp. 795 –800, Nov. 1995.

37. Y. Zhang, R. Zane, A. Prodic, R. Erickson and D. Maksimovic. "Calibration of MOSFET On-State Resistance for Precise Current Sensing." *IEEE Power Electronics Letters*, vol. 2, No. 3, pp.100–103, Sep. 2004.

38. J.W. Dixon and I.A. Leal. "Current Control Strategy for Brushless DC Motors Based on a Common DC Signal." *IEEE Transactions on Power Electronics*, vol.17, No.2, pp. 232–240, Mar. 2002.

39. J. Karthikeyan and R. Dhana Sekaran. "Current control of brushless dc motor based on a common dc signal for space operated vehicles," *Electrical Power and Energy Systems*, Aug. 2011, pp.1722-1723.

40. T. Dake and E. Ozalevli. "A Precision High-Voltage Current Sensing Circuit," in *IEEE Transaction on Circuits and Systems*, Jun. 2008, vol.55, No.5, pp.1197–1202.

41. S.H. Kim and C. Doose. "Temperature Compensation of NdFeB Permanent Magnets," in *Proceedings of the Particle Accelerator Conference*, May 1997, vol. 3, pp. 3227 – 3229.

42. Texas Instruments. "SN74LVC1G58 Configurable Multi-Function Gate." Internet: www.ti.com, Feb. 2013 [Jul. 11, 2013].

43. Agilent Technologies. "Application Note 290: Practical Temperature Measurement." Internet: www.agilent.com, Mar. 2008 [Jun. 20, 2014].

44. Texas Instruments. "LM2917 Frequency to Voltage Converter." Internet: www.ti.com, Apr. 2013 [Jul. 11, 2013].

45. Texas Instruments. "LM2576 – 3A, 60V, High-Efficiency, Step-Down Voltage Regulator." Internet: www.ti.com, Apr. 2013 [Sep. 10, 2013].

46. Fairchild Semiconductors. "LM7805 Three-Terminal 1A Positive Voltage Regular."Internet: www.fairchildsemi.com, Aug. 2013 [Sept. 10, 2013].

47. T. Daniel and H. Patrick. "Regenerative Braking of BLDC motors," *High-Performance Microcontroller Division, Microchip Technology*, 2012, pp.3-8.

48. V. Thiyagarajan and V. Sekar. "Controlling of Brushless DC Motors in Electric Bicycles using Electronic Based Circuit with 8-Bit Microcontroller." *International Journal of Engineering Sciences and Emerging Technologies,* vol.4, pp.29 – 32, Dec. 2012.

49. X. Zeng, J. Li and Y. Ren. "Prediction of various discarded lithium batteries in China," in *IEEE International Symposium on Sustainable Systems and Technology (ISSST),* 2012, pp.1–4.

50. E. Manoj, I. Dino and A. Roselinas. "Supercapacitor/Battery hybrid Powered Electric Bicycle via a Smart Boost Convertor." *World Electric Vehicle Journal*, vol. 4, pp.280-284, 2010.

51. B. Andrew, M. Marshall and Z. Hengbing. "Lithium batteries and ultracapacitors alone and in combination in hybrid vehicles: Fuel economy and battery stress reduction advantages," in *The 25th World Battery, Hybrid and Fuel Cell Electric Vehicle Symposium & Exhibition,* EVS-25 Shenzhen, China, Nov. 2010, pp.1–8.

52. A.F. Burke and M. Miller. "Performance Characteristics of Lithium-ion Batteries of Various Chemistries for Plug-in Hybrid Vehicles," *EVS-24, Stavanger,* Norway, May 2009, pp. 256-262.

53. A.F. Burke and M. Miller. "Electrochemical Capacitors as Energy Storage in Hybrid-Electric Vehicles," *EVS-24, Stavanger*, Norway, May 2009, pp.438–446.

54. X. Yan and D. Patterson. "Novel power management for high performance and cost reduction in an electric vehicle." *Renewable Energy*, vol.22, pp. 177–183, Oct. 2001.

55. Panasonic. "Valve Regulated Lead Acid Batteries LC-RA1212P." Internet: www.panasonic.com, Aug. 2011 [Jul. 15, 2014].

56. Maxwell Technology. "BC Power Series BOOSTCAP Ultracapacitors." Internet: www.maxwell.com/esm/, Jun. 2013 [Jul. 15, 2014].

57. Batteryspace. "36V-Nimh-Battery- Pack-Series." Internet: www.batteryspace.com/36V-Nimh-Battery-Pack-Series.aspx, Feb.2013 [Jul. 15, 2014].

58. Dixon Batteries. "Li-Polymer Batteries." Internet: www.dixonbatteries.co.za/leisure-1, Dec. 2013 [Jul.15, 2014].

59. Ebay. "Hydrogen-Fuel-Cells." Internet: www.ebay/bhp/hydrogen-fuel-cell, Jan. 2014 [Jul. 15, 2014].

60. I.D. de Vries and D. B. Jenman. "The Potential of Electric bicycles to provide low cost Transport, Mobility and Economic Empowerment in South Africa," in *Proceedings of the 25th Southern African Transport Conference*, 2006, pp.90–96.

61. Z. Salam. "Power Electronics and Drives," Application note version 3, 2003, pp. 10–20.

62. Advanced Thermal Solutions. "Heat-Sink Types and how they are made." Internet: www.qats.com, Aug. 2013 [Jul. 18, 2014].

63. S. Colton. "3ph Duo: 2 x 1kW Brushless Motor Controller with Field-Oriented Control," Design Notes, 2010, Rev.0, pp.23–30.

64. Q. Wu and W. Tian. "Design of Permanent Magnet Brushless DC Motor Control System Based on dsPIC30F4012," *International Workshop on Information and Electronics Engineering (IWIEE)*, 2012, pp.4224–4227.

65. C. Elmas and O. Ustun. "A hybrid controller for the speed control of a permanent magnet synchronous motor drive." *Elsevier, Control Engineering Practice,* vol.16, pp. 260–270, 2008.

66. A. Namboodiri and S.W. Harshal. "Unipolar and Bipolar PWM Inverter." *International Journal for Innovative Research in Science & Technology*, vol. 1, pp. 237-239, 2014.

67. Agilent Technologies. "Application Note 290: Practical Temperature Measurement," Internet: http://www.agilent.com, Mar. 2008 [Jun. 20, 2014].

# APPENDIX A

## CONTROLLER SCHEMATIC

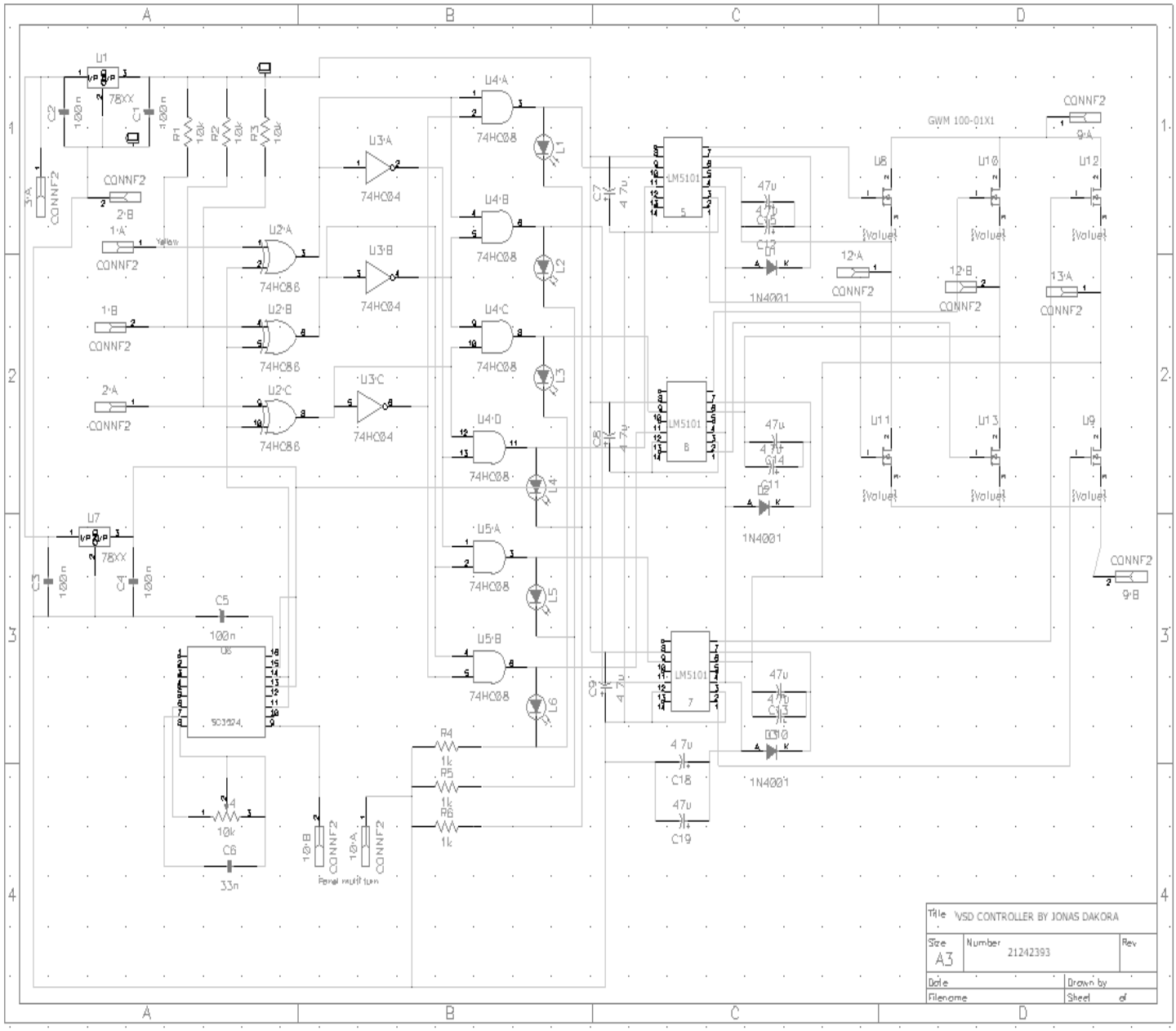

# APPENDIX B

## SOFTWARE CODE

```
'*****************************************************************
'*  Name    : Firmware for 4 quadrant VSD for PMBLDC MOTOR       *
'*  Author  : [JONAS D DAKORA]                                   *
'*  Notice  : Copyright (c) 2014 [select VIEW...EDITOR OPTIONS]  *
'*          : All Rights Reserved                                *
'*  Date    : 10/31/2013                                         *
'*  Version : 1.0                                                *
'*  Notes   :                                                    *
'*          :                                                    *
'*****************************************************************
   program PMBLDC Motor Control
'Define variables and set defaults
'Misc variables
Dim data as BYTE
Dim i as Integer
Dim direction as BYTE
Dim temp as WORD
Dim accel as WORD
Dim decel as WORD
Dim currentlimit as WORD
'Drive parameters
Dim maxbatv As WORD 'Maximum allowable battery voltage
Dim minbatv As WORD 'Minimum allowable battery voltage
Dim maxfwdspd As WORD 'Maximum forward motor speed
Dim maxrevspd As WORD 'Maximum reverse motor speed
Dim maxfwdmoti As WORD 'Maximum forward motoring current
Dim maxrevmoti As WORD 'Maximum reverse motoring current
Dim maxregeni As WORD 'Maximum regeneration current
Dim shuntrating As WORD 'Shunt rating (amps at 50mV)

'Program Subroutines
'Shutdown system
sub procedure Halt
'Stop PWM
Pwm_Stop
'Turn of power stage
PORTC=0
while TRUE
wend
END sub
```

```
'Read EEPROM Parameters
sub procedure ReadParameters
data = Eeprom_Read(0)
maxbatv = (data << 8) + Eeprom_Read(1)
data = eeprom_read(2)
minbatv = (data << 8) + eeprom_read(3)
data = eeprom_read(4)
maxfwdspd = (data << 8) + eeprom_read(5)
data = eeprom_read(6)
maxrevspd = (data << 8) + eeprom_read(7)
data = eeprom_read(8)
maxfwdmoti = (data << 8) + eeprom_read(9)
data = eeprom_read(10)
maxrevmoti = (data << 8) + eeprom_read(11)
data = eeprom_read(12)
maxregeni = (data << 8) + eeprom_read(13)
data = eeprom_read(14)
shuntrating = (data << 8) + eeprom_read(15)
END sub

'Check direction switch and change direction if required
sub procedure CheckDirection
IF PORTB.2 <> direction THEN
direction=PORTB.2
'Turn off PWM
PWM_Change_Duty(0)
PORTC.3=0
PORTC.4=0
'Wait till motor stops spinning
while adc_read(5) > 10
wend
'Change direction
IF direction=0 THEN
PORTC.5=1 'Set reversing direction on
currentlimit=maxrevmoti `Buffer motor current limit FOR this
direction
else
PORTC.5=0 'Set reversing direction off
currentlimit=maxfwdmoti 'Buffer motor current limit for this
direction
END IF
END sub
```

```
'Main Program
main:
'Disable interrupts
intcon=0
'Initialise Ports
'Initialise PWM on port C
  PORTC=0
TRISC=%10000000 'Set input/output ports
T2CON=T2CON 'To fix bug in compiler
Pwm_Init(15000) 'Initialise PWM at 20KHz

'Initialise port B
  PORTB=0
TRISB=%00000110 'Set input/output ports
'Initialise ADC on port A and E
ADCON1 = $82 'Configure analog inputs and Vref
TRISA=%11111111 'Port A is input
TRISE=%00000111 'Port E is input

'Load parameters from EEPROM
ReadParameters()

'Check validity of critical parameters and enter
'programming mode if invalid
IF maxfwdmoti=$FFFF THEN
ProgrammingMode()
END IF
IF maxfwdmoti=0 THEN
ProgrammingMode()
END IF
IF minbatv=$FFFF THEN
ProgrammingMode()
END IF
IF minbatv=24 THEN
ProgrammingMode()
Start regenerative braking
END IF

'Check if programming switch is set
IF PORTB.1=0 THEN
ProgrammingMode()
END IF
```

```
'Test for faults
'Check battery voltage, cancel startup if outside limits
IF ADC_Read(4) > maxbatv THEN
Halt()
END IF

IF ADC_Read(4) < minbatv THEN
Halt()
END IF

'If pedals are pressed, cancel startup
IF ADC_Read(0) > 10 THEN
Halt()
END IF

IF ADC_Read(1) > 10 THEN
Halt()
END IF

'Begin main program
PWM_Start
Pwm_Change_Duty(0) 'Start PWM and set duty cycle to 0
'Begin endless loop
while TRUE
'Clear watchdog timer
ASM
CLRWDT
end ASM
'Check battery voltage
temp=ADC_Read(4)
'If voltage is too high during regen (i.e. batteries fully charged)
then
'skip the cycle
if decel > 20 then 'If in regen mode
if temp>954 then 'If battery voltage > 2.5V per cell then batteries
are charged
  PORTC.3=0
  PORTC.4=0
PWM_Change_Duty(0)
goto skip 'Turn off PWM and skip the cycle
end if
```

```
'Check speed limits
temp=adc_read(5)
select case direction
case 1 'Forward
if temp >= maxfwdspd then
  PORTC.3=0
  PORTC.4=0
PWM_Change_Duty(0) 'If speed limit reached then
goto skip 'Turn off PWM and skip the cycle
end if

case 0 'Reverse
if temp >= maxrevspd then
  PORTC.3=0
  PORTC.4=0
PWM_Change_Duty(0) 'If speed limit reached then
goto skip 'Turn off PWM and skip the cycle
end if
end select

'Check direction switch and change direction if required
CheckDirection()
'Read pedal positions
accel=adc_read(0)
decel=adc_read(1)
'Enter regneration mode if required (Brake takes preference over
accelerator)

'Regeneration mode
temp = adc_read(2)
'If minbatv=24, then turn on regenerative braking
'Current input swings from 1.5V for no current to 0V for max -ve
current
'If the current limit is already exceeded, don't turn on PWM
if temp <= maxregeni then
  PORTC.4=0
  PORTC.3=0
goto skip
end if
```

```
'Select low side
  PORTC.3=0
  PORTC.4=1
'Set PWM duty cycle from pedal position
decel=decel>>2 'Convert to 8 bit number
PWM_Change_Duty(decel)
'Check for current limit during the PWM on time:
while TMR2 < PR2
'Read motor current
temp = adc_read(2)
if temp <= maxregeni then '512=0 current, 0=max current
'Deselect high and low sides to stop PWM
  PORTC.4=0
  PORTC.3=0
break
end if
delay_cyc(10) 'Delay a few cycles so ADC read can work properly
wend
goto skip 'Restart main loop
end if
'Enter motoring mode if required
if accel > 20 then 'Ignore slight pedal movement to combat noise
if decel < 20 then
'Motoring mode
'If the current limit is already exceeded, don't turn on PWM
'Current input swings from 1.5V for no current to 3V for max +ve
current
temp = adc_read(2)
if temp >= currentlimit then '512=0 current, 1023=max current
  PORTC.4=0
  PORTC.3=0
goto skip
end if
```

```
'Select high side
  PORTC.4=0
  PORTC.3=1
'Set PWM duty cycle from pedal position
accel=accel>>2 'Convert to 8 bit number
PWM_Change_Duty(accel)
'Check for current limit during the PWM on time:
while TMR2 < PR2
'Read motor current
temp = adc_read(2)
if temp >= currentlimit then
'Deselect high and low sides to stop PWM
  PORTC.4=0
  PORTC.3=0
break
End.
```

# APPENDIX C

## BLDC MOTOR DATASHEET

**Preliminary Datasheet Brushless DC Motors**

The 500 watt, 36V 409 series motors are the most used motor on commercially available electric bikes. They are popular in Europe and Asia where in many countries there is a 500 watt power limit on E-bikes. Because millions of these motors have been made for the European and Asian Market, the cost to buy them from the factories in China is low, but at the same time it is a motor that is proven to be reliable and efficient. An ultra-affordable 500 watt motor makes it possible for an E-bike manufacturer to sell a decent (but low powered) electric bike, and still make a nice profit.

The 500 watt hub motor comes very close to being a perfect piece of E-bike technology, cool looking, lightweight, reliable, and cheap. It could have been the very best way to make a bicycle into an electric bike.

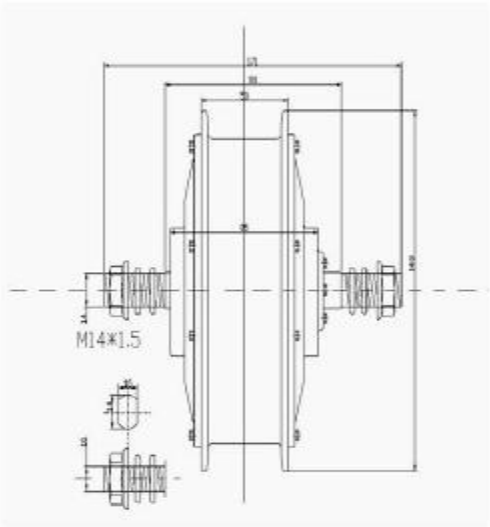


Allied Motion
© Allied Motion Technologies Inc.
Issued: 23 July 2008
www.alliedmotion.com
Specifications subject to change without notice

| | | |
|---|---|---|
| Rated voltage(V) | 36 | |
| Controller matched | 36V limited current 15A controller | |
| No load speed(rpm) | 500±5% | |
| No load current(A) | ≤2 | |
| Rated current(A) | 15 | |
| Max.output power(W) | ≥500(speed≥500) | PowerMARGIN 50% |
| Torque at max. efficiency point(N.M) | 9.75(speed≥500) | |
| Max.torque(N.M) | 10 | |
| Max.efficiency of system | ≥85% | AutomaticTEST |
| Max.system efficiency | ≥81.5%(speed≥500) | Manual loadTEST |
| ColdRESISTANCE(mR) | 75±5% | environmental temperature 20°C |
| Coil copper wire cross-section area(mm.mm) | ≥1.8 | high temperature resistance ≥130°C |
| Life span(h) | ≥5000( on load) | Maintain the initial load characteristics |
| Stator outer diameter(mm) | 100 | Silicon steel D50A470 |
| Diameter of Stator(mm) | 52 | |
| Rotor outer diameter(mm) | 51 | Rubidium iron boron N38H/N40H |
| stack height(mm) | 27 | |
| CERTIFICATION requirements | RHOS,EMC | |

# APPENDIX D

## BATTERY DATASHEET

POWER KINGDOM **Sealed Lead-Acid Batteries** **PS12-12（12V12Ah）**


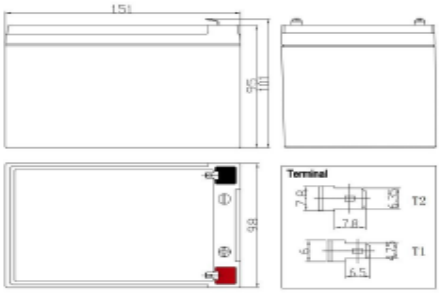


- **Specifications**

| | | |
|---|---|---|
| Nominal Voltage | | 12V |
| Rated Capacity 77°F(25°C) (20HR) | | 12.0Ah |
| Dimensions (mm/inch) | Length | 151 (5.95) |
| | Width | 98 (3.86) |
| | Height | 95 (3.74) |
| | Total Height | 101 (3.98) |
| Approx. Weight (kg/lbs) | | 3.27 (7.21) |
| Terminal | | T1/T2 |

- **Characteristic**

| | | |
|---|---|---|
| Capacity 77°F(25°C) | 20HR (0.60A) | 12.0Ah |
| | 10HR (1.12A) | 11.2Ah |
| | 5HR (2.04A) | 10.2Ah |
| | 1HR (7.32A) | 7.32Ah |
| | 15 min rate (22.2A) | 5.6Ah |
| Internal Resistance | Full Charged Battery 77°F(25°C) | Approx. 18mΩ |
| Temperature dependence of capacity (20HR) | 104°F(40°C) | 102% |
| | 77°F(25°C) | 100% |
| | 32°F(0°C) | 85% |
| | 5°F(-15°C) | 65% |
| Self-Discharge 68°F(20°C) (Capacity after) | 3 months | 90% |
| | 6 months | 80% |
| | 12 months | 60% |
| Max. Discharge Current, 77°F(25°C) | | 180A(5s) |
| Floating design life, 77°F(25°C) | | 5 years |
| Constant Voltage Charge,77°F(25°C) | Cycle | 14.5~14.9V(-24mV/°C) max. current: 3.6 A |
| | Float | 13.6~13.8V(-18mV/°C) |

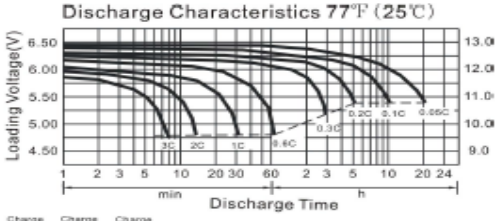


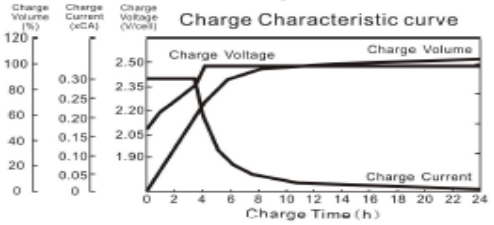


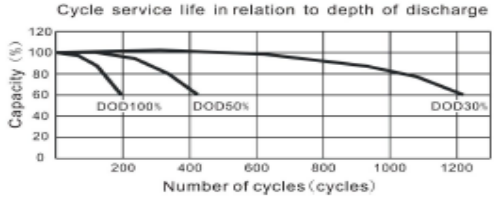


**Constant Current Discharge Characteristics (A), 77°F(25°C)**

| F.V/TIME | 5min | 10min | 15min | 30min | 60min | 2H | 3H | 5H | 8H | 10H | 20H |
|---|---|---|---|---|---|---|---|---|---|---|---|
| 1.60V/cell | 45.6 | 28.8 | 22.20 | 12.00 | 7.60 | 4.28 | 3.13 | 2.12 | 1.41 | 1.15 | 0.62 |
| 1.70V/cell | 43.3 | 27.4 | 21.20 | 11.47 | 7.32 | 4.12 | 3.06 | 2.08 | 1.40 | 1.14 | 0.61 |
| 1.75V/cell | 42.5 | 26.8 | 20.82 | 11.23 | 7.19 | 4.04 | 3.00 | 2.04 | 1.37 | 1.12 | 0.60 |
| 1.80V/cell | 41.6 | 26.2 | 20.45 | 11.02 | 7.06 | 3.97 | 2.95 | 2.01 | 1.35 | 1.10 | 0.60 |

**Constant Wattage Discharge Characteristics (Watt), 77°F(25°C)**

| F.V/TIME | 5min | 10min | 15min | 30min | 60min | 2H | 3H | 5H | 8H | 10H | 20H |
|---|---|---|---|---|---|---|---|---|---|---|---|
| 1.60V/cell | 82.8 | 52.8 | 41.08 | 22.40 | 14.30 | 8.14 | 6.00 | 4.08 | 2.75 | 2.27 | 1.22 |
| 1.70V/cell | 79.4 | 50.6 | 39.58 | 21.60 | 13.91 | 7.88 | 5.92 | 4.04 | 2.74 | 2.26 | 1.21 |
| 1.75V/cell | 78.6 | 49.9 | 39.22 | 21.34 | 13.78 | 7.82 | 5.86 | 4.01 | 2.71 | 2.23 | 1.20 |
| 1.80V/cell | 77.8 | 49.3 | 38.86 | 21.12 | 13.67 | 7.74 | 5.81 | 3.97 | 2.69 | 2.21 | 1.20 |

# APPENDIX E

## CONTROLLER MOUNTED ON E-bike

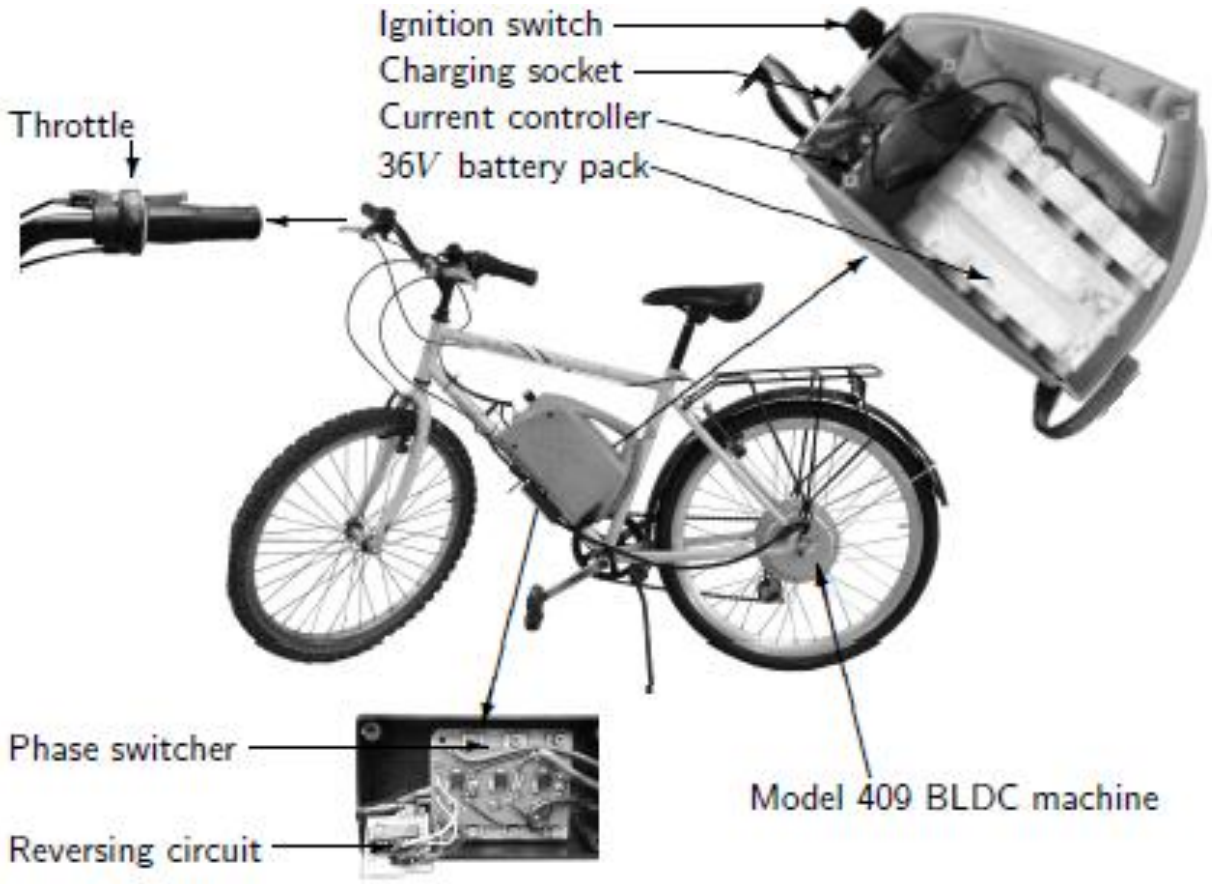

# APPENDIX F

Summary of electric bicycle manufacturers and respective models (Ev-Info, 2014)

| Manufacturer/Brand | Model | Frame Type | Power Control | Battery Type | Motor or Drivetrain |
|---|---|---|---|---|---|
| *50cycles Electric Bikes* Loughborough, UK | Multiple models | Scooter<br>Sport<br>Urban Cruiser | Manual or Pedelec | Li-ion MN | 250W |
| *Belize Bicycle* Lasalle, Quebec, Canada | E-RIDER MTB | Mountain | Manual and Pedelec | 36V-8Ah NiMH | 350 W Hub motor |
| *BikeTec* Kirchberg, Switzerland | Flyer T8 Premium | Touring | Manual | Li-Ion | Panasonic Drive, hub gear |
| *Currie Technologies, Inc.* Chatsworth, CA, USA | eZip Series | Hybrids<br>Urban<br>Mountain<br>Cruiser<br>Scooter<br>Compact | Electro-Drive | Sealed lead-acid, NiMH and Li-Ion | Up to 450W |
| *Eco-Brand Exim* China | Samurai model | Mountain<br>Urban<br>Hybrid<br>Compact<br>Scooter | Pedelec or throttle | 3 x 12 Volt 8Ah Sealed Lead Acid | 250W |
| *EcoBike Medford, USA* | Vatavio<br>Elegance<br>Adventure | Compact<br>Hybrid<br>Cruiser<br>Sport | Throttle | 36V, 8A Li-MnO | 290W -360W Hub motor |
| *eGo Vehicles* International | eGo Cycle SE | Compact | Manual throttle | Lead-acid 24V, 34Ah | 24V Brushed Belt-drive |
| *Electric Motion Systems, Inc. (EMS)* Dulles, VA, USA | E+ Series | Mountain<br>Cruiser | Very high-tech Manual or Pedelec | 36V, 9 Ah NiMH | 750W-1000W Disk motor |
| *Electrik Motion*, USA | *Rayos* | Urban mountain hybrid | Manual | 24V, 14Ah NiMH | 600W or 750W |
| *Euromoto/BinBike* Bornem, Belgium | BinBike Europe | Touring | Pedelec | 24V, 10Ah NiMH | 250W 6-speed |
| *Optibike, LLC* Boulder, Colorado, USA | 400<br>600<br>800<br>OB1 | Monocoque Sport | Manua | 36 V, 25Ah Li-Ion-Cobalt or NiMH | 400W-850W 9-speed drivetrain |